AN ABSTRACT OF THE THESIS OF

Stefan Zauscher for the degree of Master of Science in Materials Science presented on November 9, 1992.

Title: Orienting Lignocellulosic Fibers by Means of a Magnetic Field

Abstract approved: Redacted for Privacy

Dr. Philip E. Humphrey

Controlling the orientation and spatial distribution of discontinuous fibers in composite materials enables product properties to be tailored to anticipated use. Electric fields are already (albeit rarely) used to affect alignment in lignocellulosic (LC) fiber composites. The use of magnetic fields has not, however, been suggested or explored; this is apparently because LC fibers are essentially non-magnetic. The approach may offer, however, some considerable advantages, as long as ferromagnetism may be imparted to the fibers.

In the present research several fiber modification processes were considered and two, electroless nickel plating and spray application of a coating containing nickel in suspension, were investigated in more depth. The latter was chosen to render highly engineered, elongated wood particles responsive to magnetic fields. Individual treated particles were suspended in viscous, newtonian silicone fluids and their rotation under the influence of a controlled magnetic field was video recorded.

The magnetic torque on the particle was, under the

above conditions, directly proportional to the fluid viscosity, to the particle's angular velocity and to a characteristic shape constant. The maximum of the specific magnetic torque (magnetic torque divided by the shape constant) was found to reflect the influence of field strength and particle Ni-treatment on rotation. Results were scaled to an arbitrarily chosen viscosity for comparison.

The dependencies of the magnetic torque found in the present research compare with those theoretically predicted for ellipsoidal and cylindrical bodies. For field strengths ranging from 0.07T to 0.15T (below magnetic saturation) the magnetic torque increased almost linearly with increasing field strength. Magnetic torque was also found to increase nearly linearly with increasing bulk Ni-concentration (5g/kg - 50g/kg).

Rotational motion was sometimes impeded at low field strengths and this was attributed to a permanent magnetic moment obtained by the particle. A coercive field strength of 7600A/m supported this hypothesis. Judiciously switched field polarity increased magnetic torque at small alignment angles.

The present research indicates that orienting LC fibers with magnetic fields is possible and promising. To study dynamics of fiber motion in low viscosity fluids, such as air, a different experimental method is necessary; however, dependencies of the magnetic torque found in the present study still hold true.

Orienting Lignocellulosic Fibers by Means of a Magnetic Field

by

Stefan Zauscher

A THESIS

submitted to

Oregon State University

in partial fulfillment of
the requirements for
the degree of

Masters of Science

Completed November 9, 1992

Commencement June 1993

APPROVED:

Redacted for Privacy

Dr. Philip E. Humphrey
Professor in the Department of Forest Products

Redacted for Privacy

Dr. Robert Ethington
Head of Department of Forest Products

Redacted for Privacy

Dean of Graduate School

Date thesis is presented November 9, 1992

Typed by Stefan Zauscher

ACKNOWLEDGEMENTS

First of all I would like to express my sincere thanks to Professor Philip Humphrey, my advisor. Without his encouragement, enthusiasm and support this project could not have been pursued.

My special thanks are extended to Richard R. Holbo who always had time to discuss electronics and other matters with me. Without his help much of the instrumentation would not have been built.

I am grateful to David LaFever for doing excellent work in the machine shop in the fabrication of parts for the electromagnet. I am also thankful for many discussions with Professor William Warnes and Milo Clauson.

My heartfelt thanks go to the Department of Forest Products and its staff which provided support in every way and created a warm and welcoming environment.

Finally, I would like to thank Elizabeth for her never tiring patience listening to all the little details of this research and for being a very good friend.

The following institutions and companies have generously contributed to the present research:

Paleo-Magnetic Laboratory at O.S.U., Corvallis, OR
Forest Products Laboratory, Madison, WI
Dow Corning Corporation, Midland, MI
Acheson Colloids Company, Port Huron, MI

TABLE OF CONTENTS

LIST OF FIGURES

LIST OF FIGURES

(APPENDIX)

LIST OF TABLES

LIST OF TABLES

(APPENDIX)

ORIENTING LIGNOCELLULOSIC FIBERS BY MEANS OF A MAGNETIC FIELD

Chapter I

INTRODUCTION

1.1 FIBER ORIENTATION IN DISCONTINUOUS FIBER COMPOSITES

Composite materials are well suited to many structural applications where high strength-to-weight and stiffness-to-weight ratios are required (Jones, 1975). To produce a composite, it is normally necessary to combine separated reinforcing fibers, textile preforms (reinforcement on a higher organizational level) or whiskers with a matrix material such as an epoxy polymer. In some cases, however, fibers alone may be arranged in such a way that cohesion can be affected between them without a matricizing agent. Generally, fibers impart localized strength and stiffness to the composite in the fiber direction; this is by improving the shear modulus of the matrix material and by contributing to the work of fracture of the system (Kelly and Davis, 1965). Fibers take part in failure processes by undergoing mechanisms which include fracture, debonding and pull out.

In the manufacture of a fibrous composite it is generally desirable to control the volume fraction,

alignment and spatial dispersion of the fibers. For objects which are to be mechanically stressed in service, orientation of the fibers is important both to achieve maximum reinforcement in the required direction and also because higher packing densities of fibers can be achieved in ordered systems.

Controlling the orientation of individual, discontinuous fibers in three spatial dimensions would allow composite materials which have very complex property distributions and shapes to be produced. This would be of advantage because the spatial distribution of material properties could be tailored to the spatial distribution of anticipated demand. For example, the distribution and orientation of fibers in the composite could be linked to the anticipated stress field (Knoblach, 1989).

1.2 FIBER ORIENTATION IN LIGNOCELLULOSIC FIBER COMPOSITES

Considerable research has been undertaken to affect fiber distribution and orientation for high-performance composite materials containing metal whiskers (Sutton, 1970), carbon (Knoblach, 1989; Yamashita et al., 1989) and other high strength reinforcing fibers. Flow-induced fiber orientation in the injection molding process has been studied extensively. Existing, well established

lignocellulosic (LC) fiber composites could, however, also be improved by affecting fiber distribution and orientation within them (Talbott, 1974; Rowell, 1990). Indeed, this approach could be taken still further and lead to the evolution of entirely new types of products.

Research on orientation for LC fiber composites has, to date, largely concerned electrostatic means which have been used for the production of panel products (Talbott and Logan, 1974; Kawai et al., 1989; Pulido et al. 1990). The few LC fiber composites which have somewhat complex geometries do not presently compete with most of the high performance composites utilizing man-made fibers. This is mainly due to their inferior strength properties and dimensional stability. However, the possibility of manipulating material distribution and properties together with affecting cell-wall modification could make possible a wide range of applications for LC fiber composites (Rowell, 1990). More research is needed to provide methods to control fiber orientation in production processes, such as compression- and injection- molding. Lignocellulosic fibers are already used as reinforcing elements in thermoplastic materials (Michell, 1986; Rowell, 1990). With the ability to control fiber orientation in the thermoplastic matrix, anisotropic strength properties of the composite could be achieved.

At present, many composite materials are made from petroleum based polymers. In contrast to petroleum, a depleting resource, LC fibers are renewable. Furthermore, LC fiber composites could, with judicious design, be recycled and be made biodegradable.

1.3 PURPOSE AND OBJECTIVES OF THE PRESENT RESEARCH

This investigation is a first step toward the goal of controlling the orientation of individual LC fibers during the manufacture of molded composites in a dry system. A review of alternative methods for achieving this goal suggests that magnetic fields may possibly be used to selectively exert torque on magnetically modified LC fibers prior to their being compressed together to form a solid product. This research will address the following objectives:

(1) Render inherently diamagnetic LC fibers responsive to magnetic fields and then to evaluate their magnetic characteristics.

(2) Construct equipment to enable interactions between magnetically modified LC fibers and a magnetic field to be studied.

(3) Develop experimental techniques to explore the dynamics of fiber motion and, in particular, magnetic torque under the influence of several variables (including applied field strength, level of magnetic modification and aspect ratio).

Chapter II

REVIEW OF THE LITERATURE PERTAINING TO FIBER ORIENTATION

2.1 IDENTIFYING SOME MEANS OF ORIENTATION

Before addressing the above objectives, a literature review of fiber orientation in general shall be given. Three methods shall be emphasized because of their relevance to LC fiber composites. These are: (1) hydrodynamic means, (2) the application of electric fields and (3) the application of magnetic fields.

It is not the purpose of this review to explore all possible orientation methods which are employed for discontinuous fibers. However, underlying physical principles shall be identified and classified along with constraints and limitations. In most cases, methods differ in terms of the way that forces or force fields are applied. Actual orientation clearly depends upon affecting rotational motion of fibers about their two minor axes (Figure 2.1).

Three underlying factors influence the rotational motion of the fiber: (1) the medium surrounding the fiber, (2) fiber geometry and (3) sterical hindrance because of fiber-fiber interactions.

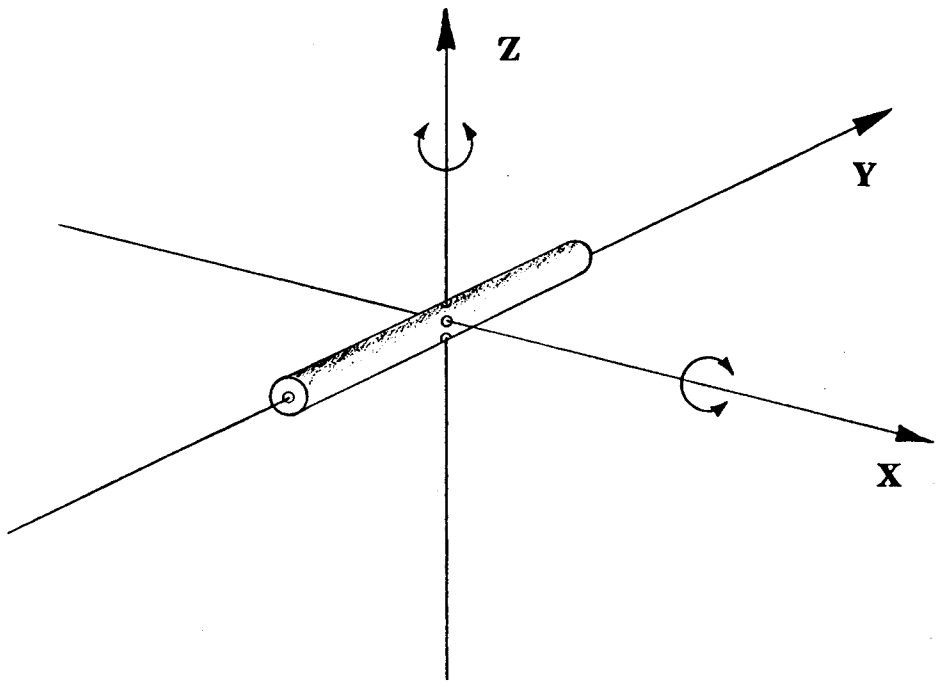

Figure 2.1 Principle of fiber orientation

Properties of fluids surrounding fibers clearly influence fiber motion. The orienting torque, regardless of its origin, is resisted by a hydrodynamic torque. However, with a decrease of fluid viscosity, the damping properties diminish and, in the extreme, rigid fibers oscillate indefinitely about their equilibrium position (Jeffery, 1922; Forgacs et al., 1957; Okagawa et al., 1973; Okagawa and Mason, 1973; Knoblach, 1990;). Fiber density and

geometry determine their rotational moment of inertia; generally a low aspect ratio results in high rotational acceleration for a given torque.

To rotate freely, the fibers need to have space around them -- ideally a spherical volume with diameter equal to the fiber length axis. In other words, assuming a spatially uniform fiber distribution and no translational motion, then the maximal collision-free fiber volume-fraction is determined by the maximum packing density of the spheres (Bibbo et al., 1985; Knoblach, 1990).

Five different approaches to fiber orientation have been identified; these are: (1) mechanical means (Klauditz, 1960), (2) hydrodynamic means, (3) electrophoretic means (Sutton, 1970; Miura and Hosokawa, 1979), (4) electric fields and (5) magnetic fields.

2.2 AFFECTING FIBER ORIENTATION BY HYDRODYNAMIC MEANS

Two different principles of fiber orientation utilizing the motion of an alignment fluid can be distinguished. In the first, fibers are present in the fluid from the onset and the properties and motion of this fluid may affect orientation. Secondly, fibers may be introduced to an already moving fluid and orientation occurs in the flow field while the fibers settle in the fluid (Wolff, 1969).

In planning the current research, the use of composite fluids was given serious consideration before being put aside in favor of magnetic field alignment. Hydrodynamic means will, therefore, be summarized below.

2.2.1 COMPOSITE FLUIDS

Jeffrey (1922) treated the rotation of ellipsoidal bodies in a viscous fluid undergoing laminar shear flow. Low particle Reynolds numbers were assumed so that inertial effects became negligible. The principal conclusions of this study were that the hydrodynamic torque acting on the ellipsoid is linearly dependent upon its geometry and angular velocity, the fluid viscosity, and that rotation is periodic. This analytical treatment formed the basis for many studies concerning the orientation of suspended particles (Demetriades, 1958; Okagawa *et al.* 1973, 1974; Okagawa and Mason, 1973, 1974).

Suspensions of discontinuous fibers are used in manufacturing processes such as injection and compression molding and extrusion. Shear flow can generally be treated separately from extensional flows in such processes. However, in a conduit with varying cross-sectional area, there must always exist a combination of shear and extensional flows.

In extensional flows, fiber alignment is possible in the direction of positive extension. In non-newtonian shear flow (due to the presence of the fibers) this alignment is possible in the flow direction but a balance between viscous and normal stress effects is required -- and this occurs only at relatively high shear rates. Furthermore, non-newtonian fluids in internal flow through non-circular conduits are subject to normal stresses. These normal stresses give rise to a secondary flow superposed on the main axial flow. This phenomenon termed 'cellular flow' (Lockett, 1980) leads to complex fiber orientation patterns.

2.2.2 SUITABILITY FOR LC FIBER COMPOSITES

Generally, means of orientation utilizing flow fields lack precision due to the complex nature of the orienting process. Flow channel geometry and the non-newtonian character of the fluid are only two of the factors involved. The literature indicates that only a very limited number of flow situations can be successfully characterized mathematically.

Interactions of fluid and LC fiber is also problematic. The envisioned LC fiber composites may incorporate little or no matrix material. This means that the carrier fluid is not to become the matrix of the LC

fiber composite but will have to be removed before consolidation and final shaping. In the case of gases, this is generally not a problem. However, when liquid carriers are involved, fluid-fiber interactions become important. Swelling, distortion, plasticizing, capillarity and chemical modification of LC fibers, as well as pollution and energy consumption, are only a few of the problems involved.

The use of flow fields to affect fiber orientation generally aims to control orientation of a volume of fibers simultaneously. Individual fiber control appears fraught with potential problems.

2.3 AFFECTING FIBER ORIENTATION WITH ELECTRIC FIELDS

Dielectric properties of fiber materials dictate their responsiveness to electric fields. These properties may be affected by the presence of polar molecules, dipole polarization and/or surface charge polarization.

Polar molecules have a permanent electric dipole moment that arises from the partial charges on atoms linked by polar bonds. Non-polar molecules may acquire a dipole moment in an electric field due to distortion of electronic distributions and nuclear positions (Atkins, 1990). Fiber torque results from the coulombic forces acting between the external field and the electric dipoles (permanent or

induced) within the fiber. Furthermore, external fields can cause the movement of free electric charges on the surface of particles, and that leads to a charge polarization at the corner nearest to an adjacent electrode. An aligning torque results because of coulombic forces acting between the surface charges and the external field.

All of the above mentioned charge interactions may be present in the alignment of a fiber or fiber bundle. A differential between the dielectric constant of the fiber material and that of the surrounding medium is required for electric orientation. However, if the fiber is electrically conductive, or can be made transiently conductive during orientation, achievable orienting torques are much higher; this is because the dielectric constant for conductors is infinite.

The torque on slender, dielectric bodies can be derived analytically for the case of an axis-symmetric, prolate ellipsoid (Stratton, 1941). The electric torque depends on electric field strength, position of the body relative to the electric field lines, and the geometrical and dielectric properties of the material. An analogy with ellipsoidal bodies is often used to study the rotational behavior of fibers under the influence of an electric field.

Demetriades (1958) investigated the orientation of particles in colloidal suspensions under the combined influence of shear flow and an electrostatic field. Okagawa

et al. (1974) and Okagawa and Mason (1974) extended their studies of rods and discs in shear flow to include electric fields. One central implication of their studies is that above a critical electric field strength the orientation distributions do not oscillate (as found for shear flow alone), but change gradually as each particle moves to a steady orientation. Finally, Knoblach (1989; 1990) presents a method for aligning carbon fibers by means of an electric field; alignment takes place in a liquid.

2.3.1 SUITABILITY FOR LC FIBER COMPOSITES

Klauditz (1960) mentions the possibility of utilizing electric fields for orientation of wood particles in the manufacture of particleboard and strandboard. A patent was issued to the Berol Company (Talbott and Logan, 1974) for a mat forming machine providing parallel alignment of fibers by an electric field. Renewed interest in the electrostatic aligning process was shown by several Japanese researchers (Kawai et al., 1987; Kawai and Sasaki, 1989; Pulido et al., 1990, 1991a, 1991b, 1991c). The modulus of rupture (MOR) of electrostatically aligned medium density fiberboard (MDF), prepared from different fiber sources, is given in Figure 2.2 and shows the strength anisotropy achieved by fiber alignment.

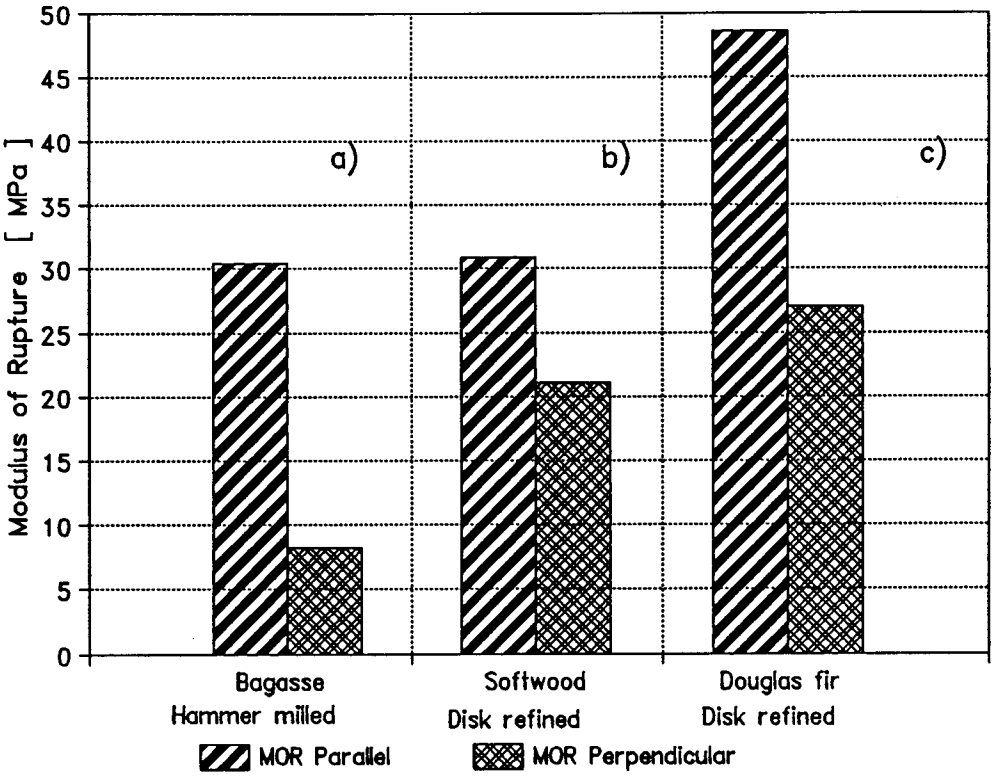

Figure 2.2 Modulus of rupture for electrostatically aligned fiberboard parallel and perpendicular to fiber alignment. (Data a) and b) from Kawai and Sasaki, 1989; c) from Talbott, 1974)

Talbott and Stefanakos (1972) undertook the first fundamental study of the influence of several variables -- such as field strength, moisture content, aspect ratio and field frequency -- on the rotational behavior of wood particles in an electric field. Their findings have been confirmed by Kawai et al. (1987); Knoblach (1990). Some aspects of this study shall be summarized here.

Firstly, the above workers suggest that aligning torque increases as the square of the field strength and has a

maximum at an angle of 45° to the electric field lines. Furthermore, for rotation in air it could be shown that, while the electric torque can be increased by increasing particle dimensions, the inertial torque increases in greater proportion leading to increasingly smaller resultant torques on the fiber. Finally, their work suggested that particles with high aspect ratios experience a higher net torque than wider particles of the same length.

Pulido et al. (1991a, 1991c) showed that orientation of wood particles in an electrostatic field is caused by both dipole and surface charge polarization. Wood is an anisotropic dielectric material with a higher dielectric constant in the direction of the cellulose chains than perpendicular to them (Lin, 1973). Consequently, torque due to dipole polarization orients the particle with the direction of the cellulose chains parallel to the field lines. However, although dipole polarization occurs much faster than surface polarization the latter usually dominates -- tending to align the wood particle with its major axis parallel to the electric field lines.

Because polarization times are usually very short, alternating current fields can be used. Electrophoretic effects causing a translational motion of the fibers towards one electrode can thereby be eliminated. However, the electric torque will decrease when a cut-off frequency is reached. This frequency depends on the charge relaxation

time and occurs when the field frequency exceeds the maximal polarization frequency. Dielectric properties and geometry of the fibers will determine the charge relaxation time (Talbott and Stefanakos, 1972).

The electric torque is a function of particle moisture content (MC). This can be understood by considering the nature of field-particle interactions based on dipole and surface charge polarization. For wood particles at 0%MC the electric torque is at a minimum; only OH-groups of the different wood components can contribute to the dipole polarization. After a linear increase with MC, a maximum of the electric torque is reached with the onset of fiber saturation (cell wall saturation); beyond that region an increase in MC does not significantly affect the magnitude of the electric torque (Kawai et al., 1987).

Charge interactions between fibers can present difficulties. Conducting fiber chains can form and these locally decrease the electric field and thence impede alignment. The associated conductive connection of electrodes can also lead to arcing. The formation of such conductive paths is strongly dependent on the concentration of the fibers in the electric field (Knoblach, 1990). Furthermore, the dielectric properties of the fluid between the electrodes limit the electric field strength and hence torque.

In conclusion, fiber orientation in an electric field can be very suitable for LC fibers; the medium between the electrodes is usually air and therefore no detrimental fluid-fiber interactions occur. If the fibers are separated, orientation control is exerted over fibers individually. Furthermore, no modification of LC fiber properties is normally necessary to achieve responsiveness to electric fields. On the other hand, achievable electric torque on fibers is dependent on MC and is limited by the dielectric breakdown voltage of the medium. Although the orientation process may be relatively simple, problems may arise from insufficient electric insulation which causes arcing and, therefore, a reduction in the achievable field strength. Fire risks may also arise.

2.4 AFFECTING FIBER ORIENTATION WITH MAGNETIC FIELDS

Ferromagnetic fibers or non-magnetic ones which are coated with a ferromagnetic material can be manipulated by exposure to an external magnetic field (Shine, 1982; Yamashita et al., 1989; Knoblach, 1989, 1990). It can be shown (Stratton, 1941) that the functional relationships for torque on a dielectric ellipsoid (discussed above) also hold true for a magnetically linear and uniformly magnetized ellipsoid in a magnetic field.

Ferromagnetic materials have, on occasion, been used because, on a microstructural level, they show large domains of cooperative spin alignment which give rise to relatively large forces. The initial position of a fiber within a field will, however, influence fiber-field interactions because the magnetization depends on the angle between the major body axis and the magnetic field lines.

In their theories of particle behavior in shear flow and electric fields Okagawa et al. (1974) consider the situation where the electric field is replaced by a magnetic one. However, their analysis accounts only for magnetically linear materials (diamagnetic and paramagnetic materials). Shine (1982), on the other hand, studied the motion of a ferromagnetic fiber while it is suspended in a viscous fluid. In this work viscosities of the suspension fluid in the order of 100Pa sec were chosen to emulate zero shear rate viscosities found in injection molding processes. The dynamics of the alignment process for cylindrical fibers in a uniform DC magnetic field were analyzed. Magnetic homogeneity and isotropy, as well as zero coercivity, were assumed for the fiber. Experiments were conducted on cylindrical fibers to verify the analytically predicted dependence of fiber rotation on aspect ratio, applied magnetic field strength and fluid viscosity. Results of these studies will be presented in greater detail in Chapter 6 of the present thesis.

Hatta and Yamashita (1988) and Yamashita et al. (1989) studied the feasibility of orienting magnetically modified carbon fibers in a viscous matrix. In an analytical solution they approximated cylinders by a prolate ellipsoid covered with a thin sheet of ferromagnetic material of constant permeability. The assumption of constant permeability is, however, very crude for the case of non-linear magnetic materials and their solution is only valid for magnetic saturation of the coating. A comparison of electrostatic and magnetostatic alignment torques created on an iron ellipsoid indicates that the magnetic torque (at 1T) is larger than the electrostatic torque (in air) by a factor 10^6 (Knoblach, 1990).

Although the interaction of fibers with electric fields is quite similar to that with magnetic fields, the latter offers some advantages for orientation. High field strengths are possible because a collapse of the field, occurring for electric fields when the dielectric strength of the medium between the electrodes is surpassed, does not occur. Insulation safety problems are not stringent and possible fire risks due to discharge (found in electric fields) do not occur.

In the case of magnetically modified LC fibers, interactions with magnetic fields are assumed to be independent of fiber moisture content. Therefore, magnetic torque can be very selectively applied to only those fibers

which are magnetically modified. This means that control over orientation can be exercised on a fiber to fiber basis. Furthermore, in view of the very much larger magnetic torques, compared with electric torques, orientation should be possible with relatively weak field strengths and/ or low levels of magnetic modification. However, although it is relatively simple and inexpensive to provide weak magnetic fields (using permanent magnets); strong fields, larger than 0.1T for example, require considerable effort and energy to be sustained over time and volume.

The following chapters of this thesis are focused on orienting LC fibers by using magnetic fields. The approach to achieve this goal will be pragmatic; it begins with the magnetic modification of LC fibers. Then, after considering some of the results of studies mentioned above, experimental techniques exploring the dependence of the magnetic torque on important variables such as field strength and magnetic modification, will be outlined. In view of difficulties in the provision of strong magnetic fields in a manufacturing process and with respect to available equipment, focus shall be on fields well below the saturation magnetization of the respective ferromagnetic material.

Chapter III

LITERATURE PERTAINING TO MAGNETIC PROPERTIES OF FERROMAGNETIC AND LIGNOCELLULOSIC MATERIALS

3.1 PROPERTIES OF FERROMAGNETIC MATERIALS

The forces which determine the state of magnetization of a rigid ferromagnetic body are exchange forces, dipole forces and forces due to crystalline anisotropy (Brown, 1962). Dominant among these are the exchange forces which keep neighboring spins aligned and produce spontaneous magnetization below the Curie temperature. Weiss (Brown, 1962; Lee, 1970, Chen, 1977) proposed the existence of a 'molecular' field to account for the phenomenon of spontaneous magnetization. Heisenberg, in his quantum-mechanical approach (Brown, 1962; Lee, 1970; Chen, 1977), later attributed the origin of this field to positive exchange integrals.

Next in importance are the magnetic dipole-dipole forces which dominate at large distances. These forces are dependent on the shape and size of the body.

The crystalline anisotropy forces occupy an intermediate range and determine the direction of the spontaneous magnetization; they are independent of specimen geometry.

3.1.1 MAGNETIC DOMAINS

In a crystallite of ferromagnetic material not only the electrons carry a magnetic moment, but so do small regions in the metal, known as domains. In each domain, the atomic moments are coupled together in a crystallographically preferred direction and the material reaches magnetic saturation in these domains, although no external field is applied. Domains are spontaneously magnetized and the domain structure represents the minimum energy state of the material. In unmagnetized ferromagnetic materials, the orientations of individual domains average out to yield no net magnetization. However, the domain structure changes with the application of a magnetic field (Figure 3.2).

3.1.2 THE MAGNETIZATION PROCESS

Under the influence of an external magnetic field domain boundary displacement increases the volume of domains whose magnetization direction makes an acute angle with the applied field. Boundary displacement requires little energy and this explains why large magnetizations of ferromagnetic materials are achievable with moderate external fields. This process continues until all unfavorably oriented domains in the material are eliminated. Further increase in

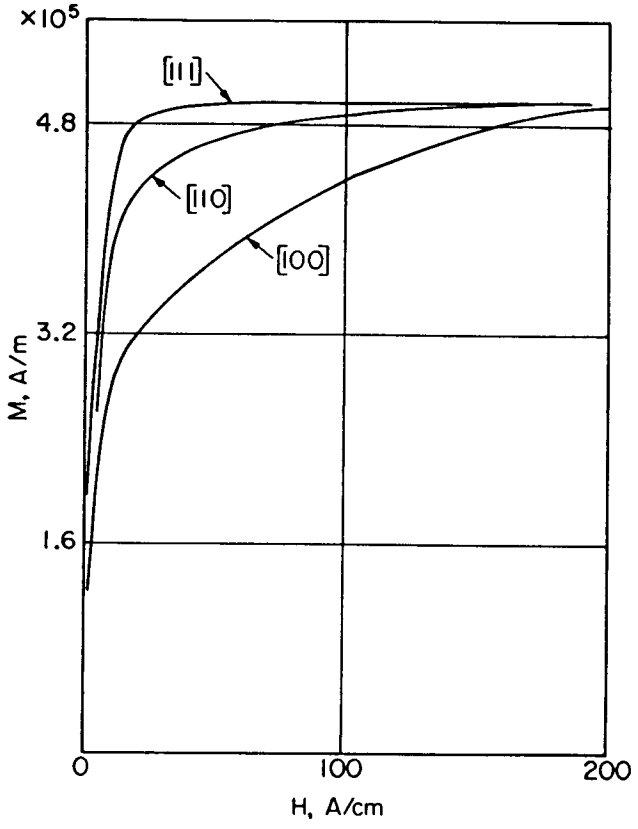

Figure 3.1 Magnetization curves for single crystals of nickel in the [111] easy, [110] intermediate and [100] hard directions (in Chen, 1977; after Kaya, 1928).

the magnetic field strength results in a reversible rotation of the magnetization out of the easy direction into full alignment with the external magnetic field. The anisotropy forces of a crystal cause the magnetization of a domain to be aligned parallel to certain crystallographic axes; called axes of easy magnetization (Figure 3.1). These processes are reflected in the initial magnetization curve for a ferromagnetic material, demonstrated for a single crystal of magnetic material (Figure 3.2).

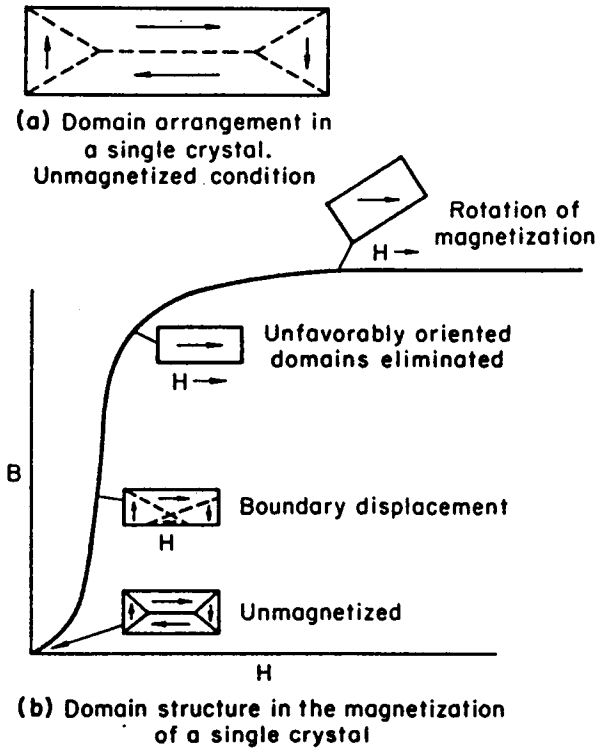

Figure 3.2 Domain structure in an unmagnetized condition and changes produced by application of a magnetic field (in Stanley, 1963).

3.1.3 THE MAGNETIZATION CURVE

Only in the 'toe' region of the initial magnetization curve is the domain boundary displacement reversible -- becoming partially irreversible with increasing field strengths. Consequently, once a material has been magnetized beyond the reversible growth region, the initial

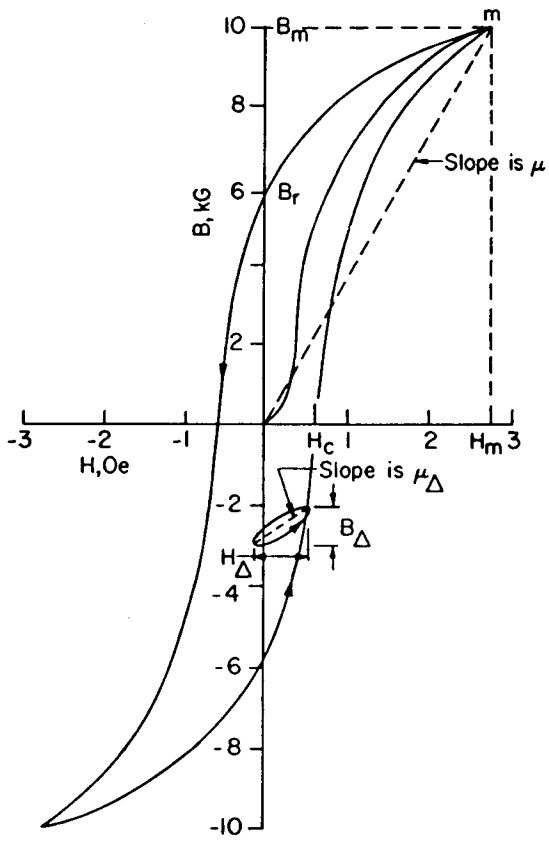

Figure 3.3 Hysteresis loop for 3% Si-Fe featuring the remanence, B_r and the coercive field strength, H_c (in Chen, 1977; after Carr, 1959).

magnetization curve is not retraced upon reduction of the applied field. This situation leads to a hysteresis cycle typical for ferromagnetic materials (Figure 3.3). The residual magnetization, after the applied field has been reduced to zero, is called remanence. The magnetic field necessary to re-attain zero magnetization is called the coercive field strength.

Although all ferromagnetic properties depend upon composition and temperature, not all are sensitive to the metallurgical structure of the material. Variables which influence the magnetic properties are size, shape and orientation of grains, the concentration and distribution of crystal imperfections, and the state of the lattice with regard to impurities, residual stresses and atomic arrangement (Chen, 1977). Magnetic properties shall not be discussed in any detail here; however, a classification of these properties into two groups shall be made.

(1) Intrinsic Properties:
Saturation Magnetization
Curie Temperature
Crystalline Anisotropy

(2) Structure-sensitive Properties:
Coercive Field Strength
Remanence
Permeability

Coercivity is frequently used to determine whether a material is magnetically soft or hard; materials with values below 400A/m are considered to be magnetically soft. The coercivity is linked to other structure sensitive properties such as the initial permeability (Chen, 1977).

Remanence, on the other hand, is often numerically compared with the saturation magnetization. The ratio of remanence to saturation magnetization can be calculated for nickel to be 0.866T. However, in reality lower ratios are found, 0.5 being a typical value (Chen, 1977). Further detail can be found, for example, in Brown, 1962; Stanley, 1963; Chen, 1977; Boll, 1979.

3.2 LIGNOCELLULOSIC MATERIALS

Organic compounds composed of carbon, hydrogen and oxygen are almost invariably diamagnetic (Lee, 1970; Weast, 1985). Diamagnetism is brought about by the precessional motion of the electron charge under the influence of an applied magnetic field. This motion is such, according to Lenzs'law, as to produce a magnetic field opposite in direction to the applied field. This diamagnetic behavior is common to all atoms and materials and is independent of temperature. The susceptibilities of diamagnetic materials are, compared with susceptibilities of para- and ferromagnetic materials, very small, negative and generally independent of the applied field strength.

The magnetic properties of wood were investigated by Nilakantan (1938) with respect to its anisotropy. The mass susceptibility of a powder sample of ground teak wood is

reported to be $-5.47*10^{-9}m^3/kg$ ($-0.44*10^{-6}$cgs-emu). Nilakantan suggests that magnetic anisotropy is due to the highly crystalline alpha-cellulose in wood. The diamagnetic anisotropy of wood is shown to be proportional to its cellulose content and is in the order of $7*10^{-9}$ for alpha-cellulose. The diamagnetic susceptibility is at a maximum in the direction of the wood fiber length axis which coincides roughly with the orientation of the crystalline regions of the cellulose chains. Lignin and hemicelluloses do not show this magnetic anisotropy which is explained with their mostly amorphous structure. A similar anisotropic behavior is also found in the dielectric properties of wood. Lin (1973) describes wood as an orthotropic dielectric material.

Wood specimens having nickel crystallites on their surfaces (30g/kg) showed mass susceptibilities in the order of $+10*10^{-6}m^3/kg$ (refer to Section 9.2.1). Compared with the diamagnetic mass susceptibility of plain wood, this is a difference of more than three orders of magnitude. With regard to the diamagnetic anisotropy and the diamagnetic susceptibility, it is clear that the diamagnetic behavior of wood and other lignocellulosic materials is negligible compared with the ferromagnetic susceptibilities of magnetic surface treatments.

Chapter IV

THE TREATMENT OF LC FIBERS

4.1 LITERATURE REVIEW

Yamashita et al. (1989) did not describe the methods used when dosing carbon fibers with nickel to achieve a thin (0.25 μm) and quite uniform coat of ferromagnetic material. Nagasawa et al. (1990, 1991, 1992) investigated the electromagnetic shielding effectiveness of metalized wood particles electroless plated with nickel. However, the ferromagnetic properties of this coating were not given.

A possible means of applying ferromagnetic materials to LC fibers may be suggested by considering how resin is applied to fibers in the medium-density-fiberboard (MDF) process. In mixers, phenol-formaldehyde (PF) resin is injected in the fiber furnish under high pressure. Transfer of resin is affected by rubbing from one surface to another during rapid agitation of the furnish (Suchsland, 1987). Conventionally, depositions are randomly distributed over the fiber bundles and have a diameter of about 30μm.

Several studies have been undertaken to mix iron powder with PF resin. The intent was to allow for inductive heating of the resin under the influence of a radio frequency electric field. It was, however, found that the

cohesion of the glue was degraded when the iron powder content reached about 10% by weight; the adhesion was not negatively affected (Frühwald, 1992).

Paints which contain nickel powders are utilized in industry for electromagnetic interference (EMI) shielding. After evaporation of the solvent, a thin coat of ferromagnetic nickel is left on the surface of the substrate. This is the approach adopted in the present research; it will be described more fully later in the thesis.

An interesting approach to render LC fibers responsive to magnetic fields is known as lumen-loading. Green et al. (1982) suggested depositing a filler in the lumens of pulp fibers, and they showed that higher retentions with improved fiber-fiber bonding can thereby be achieved. The method was later utilized successfully by Ricard and Marchessault (1990) and Rioux et al. (1992) to prepare magnetically loaded cellulose fibers. Ferrite (eg. Fe_3O_4) loadings of up to 30 % (by weight) have been achieved using lumen-loading and derived multilayered papersheets exhibited bulk magnetic properties comparable to those of data storage media.

4.2 REQUIREMENTS FOR THE MAGNETIC MATERIAL

For the purpose of fiber orientation, materials with: (1) low coercivity (magnetically soft), (2) low remanent magnetization, (3) high permeability rise factor (Boll, 1979) and (4) high saturation magnetization are of advantage.

Low coercivity insures that the material does not become permanently magnetized after removing an external field. The higher the saturation magnetization, the higher is the achievable magnetic torque. The change in field strength required to achieve a certain increase in magnetization is lowest with materials which have a high permeability rise factor.

A wide variety of suitable materials are available and only some shall be mentioned here. Iron reaches a very high saturation magnetization (2.15T) but has to be very pure to attain a low coercivity. Nickel-iron alloys have great technical importance since they combine low coercivity with high permeability at saturation levels between 0.75 and 1T (Boll, 1979). Soft magnetic ferrites feature low coercivities but have also a rather low saturation magnetization (about 0.5T).

Magnetic properties are often given for materials in their bulk form. However, many properties depend greatly on

factors such as the shape and size of the ferromagnetic particles as well as on their spatial distribution (Brown, 1962; Boll, 1979).

4.3 MODIFICATION METHODS

For a symmetric particle geometry such as cylinder or parallelepiped, a uniform distribution of magnetic material will result in magnetic forces which act through or about the geometric center. Therefore, uniformity of the magnetic fiber modification is very important.

Electroless deposition of nickel and spray application of a coating containing nickel powder were the methods explored in this study. Electroless deposition did not, however, prove suitable. A brief discussion of the latter shall be given before considering the more successful spraying method.

4.3.1 ELECTROLESS DEPOSITION

The electroless process whereby some metals and their alloys are deposited on catalytic surfaces is well known. Electroless deposition differs from electroplating in that in the former no external current source is required and the

substrate need not to be electrically conductive. Rather thick and uniform coatings can be achieved with this method.

The metal coating is produced by chemical reduction with the necessary electrons being supplied by a reducing agent present in the solution. The reducing agent determines the alloy formed in the coating. Nickel, for example, can be deposited with sodium-hypophosphite yielding a nickel-phosphor alloy.

It is important to note that electroless nickel deposits exhibit inferior magnetic properties when compared with electrodeposited or elementary nickel (Schwartz and Mallory, 1976). Magnetic properties depend, among other things, on the phosphorous content of the deposit, the pH of the plating solution used and the thermal exposure after coating. Nickel deposits which have a high phosphorous content can even be non-ferromagnetic. This is attributable to the structure of the Ni-P deposits which exhibit both amorphous, liquidlike and very fine polycristalline structures. Deposits from alkaline solutions generally are magnetic, whereas deposits from acid solutions are non-ferromagnetic or only slightly so. However, thermal treatments after deposition can foster ferromagnetic properties. A discussion of the effects of heat-treatments on the magnetic properties of electroless nickel-alloys can be found by Schwartz and Malloroy (1976).

Dielectric (non-catalytic) surfaces must be sensitized and activated prior to deposition and this can be achieved with stannous-chloride ($SnCl_2$) and palladium-chloride ($PdCl_2$). In this way, nucleation sites for electroless nickel, cobalt and silver growth are produced (Schlesinger, 1974). However, the growth of coatings tends to be uneven during the early stages of deposition. Selective deposition is reputedly possible by desensitizing portions of a surface with ultra-violet radiation (Schlesinger, 1974).

The application of the electroless plating techniques to LC fibers has several disadvantages for a practical application. The plating process takes place in an aequous solution and requires long residence times in the treatment tanks (several minutes) as well as washing procedures between the different baths. This interaction of the fibers with water is undesirable because, most probably, subsequent drying is necessary unless a wet mat formation process is used. Furthermore, since the deposition of the metal depends strongly on the physical and chemical surface properties of the substrate, uniform deposition may be difficult to achieve with surfaces as complex as those exhibited by LC fibers; here porosity, the presence of extractives and the occurrence of oxidation are factors.

Several preliminary electroless plating studies have been undertaken by the author. These were done with thin strips of Douglas-fir (Pseudotsuga menziesii (Mirb.) Franco)

veneer. The saturation isothermal remanence magnetization (SIRM) of the coated strips ($115*10^{-9}Am^2$) was found to be about ten times that of the untreated wood. However, compared with SIRM values measured for wood fibers treated with a coating containing nickel particles (this report, $90*10^{-6}Am^2$), these values are small. Overall, even after experimenting with alkaline deposition techniques, non-satisfying ferromagnetic properties of electroless nickel deposits were achieved. The approach, however, may have some future potential if alternative chemical environments were to be explored.

4.3.2 SPRAY APPLICATION OF COATINGS CONTAINING NICKEL POWDER (THE ADOPTED APPROACH)

Several conductive coatings containing nickel particles suspended in a binder are commercially available. The chemical composition of these coatings is selected in light of the substrate being treated; for plastics for example, an acrylic binder system is generally utilized. Spray application using pressure pot systems or suction cup spray equipment is often recommended. After application of the coating and evaporation of the volatile components of the diluent, a conductive coat of nickel particles is left on

the substrate surface and the binder insures its adherence. Containing relatively pure nickel, these coatings exhibit ferromagnetic properties.

The modification process developed for the present research uses a specially manufactured external-mix, single action air spray gun to inject the coating into a rotating tank. This tank contains about 10g of LC fibers which are held in perpetual motion by a chaotic air stream. The motion of the fibers prevents their clustering and sticking while the coating liquid is injected. The randomizing effect of the motion helps to achieve uniform coating distribution on the fiber surfaces. Details of this device and its performance may be found in Appendix B while results of the magnetic modification process can be found in the experimental part of this study (Sections 9.1 and 9.3.6).

Chapter V

THE BEHAVIOR OF PERMEABLE PARTICLES IN STATIC MAGNETIC FIELDS

Before a closer consideration of particle-field interactions, some magneto-static principles shall be explained. After presenting the defining equations for magnetic force and torque on a body, the magnetization of ferromagnetic materials and its mathematical treatment will be discussed. Then, the rotational behavior of ellipsoidal and cylindrical bodies under the influence of an external magnetic field will be considered. Considerations about magnetically inhomogeneous particles of arbitrary shape conclude this chapter.

5.1 MAGNETO STATICS

Maxwell's equations, together with the equation of conservation of charge, govern the behavior of systems under the influence of electric and magnetic fields. The source of an electromagnetic field is a distribution of electric charge and current. This is considered to be continuous and can be specified as a function of time and space by the density of charge ρ, and by the vector current-density $\vec{J}$

(Stratton, 1941; Shine, 1982). The electromagnetic field is the domain of the four finite vectors $\vec{E}$ and $\vec{B}$, $\vec{D}$ and $\vec{H}$. It is postulated that at every ordinary point in space the field vectors are subject to the Maxwell equations:

$$\nabla \times \vec{E} + d\vec{B}/dt = 0 \qquad [5.1]$$

$$\nabla \times \vec{B} - \mu_0\epsilon_0 \, d\vec{E}/dt = \mu_0 \vec{J} \qquad [5.2]$$

The equation of conservation of charge can be written:

$$\nabla \bullet \vec{J} + d\rho/dt = 0 \qquad [5.3]$$

At material boundaries, the transition of the field vectors and their derivatives may not be continuous and hence such surfaces must be considered separately. For the case where the time derivatives in [5.1], [5.2] and [5.3] vanish, these equations reduce to a set describing static electromagnetic fields. Equation [5.2] can be written:

$$\nabla \times \vec{B} = \mu_0 \vec{J} \qquad [5.4]$$

Equation [5.4] is also called Ampere's law. The continuity equation reduces to :

$$\nabla \bullet \vec{J} = 0 \qquad [5.5]$$

It can be shown that the divergence of $\vec{B}$ is equal to zero which can be written:

$$\nabla \cdot \vec{B} = 0 \qquad [5.6]$$

Equations [5.5] and [5.6] must be interpreted such that the fields of vectors $\vec{J}$ and $\vec{B}$ are solenoidal: all field lines close upon themselves. This means, in the case of the magnetic field vector $\vec{B}$, that there are no magnetic monopoles; this stands in contrast to the electric field case. The magnetic boundary conditions at material interfaces must be known in order to solve the partial differential equations governing the static magnetic field at these interfaces. It can be shown that the normal components of the magnetic field vector $\vec{B}$ must be continuous across an interface. However, the tangential component of $\vec{B}$ is discontinuous across the boundary surface by an amount proportional to the total surface current density resulting from free and magnetization currents.

The state of magnetic polarization of a material can be described by the vector quantity $\vec{M}$, which is called magnetization. It represents the magnetic dipole moment per unit volume.

One can show that:

$$\nabla \times \vec{M} = \vec{J}_b \qquad [5.7]$$

where $\vec{J}_b$ is to be interpreted as a bound volume current density. The volume current density $\vec{J}$ consists of two parts in the case of magnetized matter in a magnetic field:

$$\vec{J} = (\vec{J}_f + \vec{J}_b) \qquad [5.8]$$

The free current density is denoted by $\vec{J}_f$.

The effect of magnetization is to establish bound currents within the material and on the surface; the magnetic field due to magnetization is simply the field produced by these bound currents. Ampere's law [5.4] can be rewritten:

$$\nabla \times \vec{B} = \mu_0(\vec{J}_f + \vec{J}_b) = \mu_0(\vec{J}_f + (\nabla \times \vec{M})) \qquad [5.9]$$

and collecting terms:

$$\nabla \times (1/\mu_0 \vec{B} - \vec{M}) = \vec{J}_f \qquad [5.10]$$

The vector term $(1/\mu_0 \vec{B} - \vec{M})$ is designated the letter H and then the magnetization may be written:

$$\vec{M} = 1/\mu_0 \vec{B} - \vec{H} \qquad [5.11]$$

In isotropic, non-ferromagnetic materials the magnetization vector is parallel to the corresponding field vector and is found to be proportional to it. This proportionality is customarily written:

$$\vec{M} = \chi \vec{H} \qquad [5.12]$$

where χ is called the magnetic susceptibility. The metals of the ferromagnetic group (including iron, nickel, cobalt and their alloys) constitute a class of materials with a very large and field dependent susceptibility. The linearity between the magnetization vector and the $\vec{H}$ vector is not given anymore, and to include these materials, the definition of susceptibility is generalized to:

$$\overline{\overline{\chi}} = \partial\vec{M}/\partial\vec{H} \qquad [5.13]$$

5.2 FORCES ON A MAGNETIZED BODY IN A MAGNETIC FIELD

For a magnetized body of arbitrary size it is possible to assign a magnetic moment to each volume element. This is done in such a way that the total force and torque exerted on the body by an external magnetic field can be obtained by replacing the magnetic moment with the magnetization $\vec{M}$ and integrating over the volume of the body. The force and the torque on a magnetized body can then be written respectively (Brown, 1962):

$$\vec{F}^{(m)} = \int_v [\vec{M} \nabla\bullet\vec{B}] \, dv \qquad [5.14]$$

$$\vec{T}^{(m)} = \int_v [\vec{r} \times (\vec{M} \nabla\bullet\vec{B}) + \vec{M} \times \vec{B}] \, dv \qquad [5.15]$$

where $\vec{r}$ is the position vector connecting the center of the magnetic forces with an arbitrary origin.
If the magnetic torque is taken about this center then equation [5.15] reduces to:

$$\vec{T}^{(m)} = \int_v [\vec{M} \times \vec{B}] \, dv \qquad [5.16]$$

It is equation [5.16] which is of interest in this research. The equations for force and torque can be obtained by differentiation of the equation for magnetostatic energy.

5.3 MAGNETIZATION OF FERROMAGNETIC BODIES

The magnetization of a ferromagnetic material is generally a nonlinear function of the magnetic field strength it experiences. The internal field, and the magnetization dependent upon it, vary spatially within a magnetic particle and this is dependent on particle shape, magnetic properties and external field strength. The magnetization is in particular dependent on the orientation of the external field.

The internal field can be expressed formally by a demagnetization tensor.

$$\vec{B}_i = \vec{B}_o - \mu_0 \overline{\overline{D}}\, \vec{M} \qquad [5.17]$$

From equation [5.17] it can be seen that the field inside a magnetized body is smaller than the external field, with $\overline{\overline{D}}$ being a positive, symmetric demagnetization tensor with a trace of unity (Zijlstra, 1967b). Evaluation of $\overline{\overline{D}}$ for elongated bodies indicates that the internal field is influenced by competing effects. One tendency is to lie parallel to the external field, but another is to lie parallel to the long axis of the body. The balance reached between these competing effects, determining the internal field, is influenced by the strength and orientation of the external field, and by particle shape and magnetic

properties. However, the field vectors $\vec{B}_i$ and $\vec{H}_i$ should be considered to have mathematical meaning at internal points in terms of a given magnetization distribution, but no physical meaning should be attributed to them (Brown, 1962). Demagnetization factors are tabulated for bodies of certain geometry such as ellipsoidal and cylindrical ones (Brown, 1962).

The magnetization vector $\vec{M}$, needed in equation [5.16], is in most cases difficult to evaluate. One body amenable to analytical solution is the uniformly magnetized ellipsoid and its limiting cases, the infinite sheet and infinite cylinder. For ellipsoidal geometries it can be shown (Stratton, 1941) that if the external field is uniform and parallel then the resultant field within the ellipsoid will also be uniform and parallel; however it will not necessarily be coincident with the direction of the applied field. Furthermore, if the material is magnetically isotropic and has no coercivity then the magnetization will also be uniform and parallel to the internal field (Brown, 1962; Joseph and Schlömann, 1965). Thus, the theoretically convenient geometry of an axissymmetric ellipsoid is analytically useful in the prediction of features of fiber rotation in a magnetic field. The following paragraphs summarize predictions for the magnetic torque acting on

fibers rotating in magnetic fields based on the analytical study of prolate ellipsoidal bodies. The theory will be extended to include slender cylindrical bodies.

5.4 PREDICTION OF MAGNETIC TORQUE ON ELLIPSOIDAL BODIES

5.4.1 LINEAR MAGNETIC MATERIALS

Diamagnetic and paramagnetic materials have a linear magnetic constitutive equation. Behavior of ferromagnetic materials is considered linear only at very low values of the applied field, corresponding to the 'toe' region of the magnetization curve (Figure 3.2). Under the assumption of colinearity of $\vec{H_i}$ and $\vec{M}$, the magnetization can be expressed:

$$\vec{M} = \chi \vec{H_i} \qquad [5.18]$$

The following dependencies of the magnetic torque can then be shown for in-plane particle rotation (Shine, 1982):

$T^{(m)}$ is proportional to:	the square of the applied field strength
$T^{(m)}$ is proportional to:	the volume of the body
$T^{(m)}$ is proportional to:	$\sin(\alpha)*\cos(\alpha)$
$T^{(m)}$ is maximal:	when α equals 45°

$T^{(m)}$ is a nonseparable

function of: aspect ratio and susceptibility

Where α denotes the angle between the body length axis and field lines.

The magnetic torque increases with increasing aspect ratio and susceptibility. However, in reality there exist limiting aspect ratios because no material may have infinite susceptibility (the electric analogue would be a conductor). The dependencies above are analogous to a dielectric ellipsoid in an electric field (Stratton, 1941; Demetriades, 1958, Knoblach, 1990).

At very high field strengths ($B_0 >> M_s$), ferromagnetic materials reach their saturation magnetization independently of their orientation in the field. It can be shown (Joseph and Schlömann, 1965) that then, even for non-ellipsoidal geometries, the magnetization in a body is uniform and parallel to the internal field. In a first approximation (Shine, 1982), similar dependencies of the magnetic torque, as described above, are found. However, in this case the torque is proportional to the saturation magnetization.

For moderately large fields ($B_0 > M_s$), the magnitude of the magnetic torque does not change as long as saturation is maintained; however, the angular location at which the maximum occurs will shift towards larger angles with decreasing field strength.

5.4.2 NON-LINEAR MAGNETIC MATERIALS

Numerical methods to solve for the equation governing the magnetic torque on ellipsoidal bodies must be used for nonlinear magnetic materials (Shine, 1982). If the material is magnetically saturated, the results above also apply for non-linear magnetic materials. While the body is below the saturation limit, an increase in the magnetic field strength results in higher angular velocities and torques at all angles. For a certain applied field strength there exists an optimal orientation angle at which the magnetic torque is a maximum.

5.5 EXTENSION OF THEORY TO INCLUDE CYLINDERS

Particles of arbitrary geometry will have an internal magnetic field which is a function of position. Joseph and Schlömann (1965) derived an expression in terms of elliptic integrals for a uniformly magnetized cylinder, assuming non-hysteretic particles larger than single domain to fulfill isotropy conditions. Their analysis is valid for large applied fields and long cylinders. Although mathematical analysis is quite difficult, it was confirmed that the

magnetic behavior of a slender, uniformly magnetized cylinder is analogous to an ellipsoid of equal volume (Shine, 1982).

5.6 MAGNETICALLY HETEROGENEOUS BODIES

Analytical solutions for the magnetic torque acting on non-ellipsoidal bodies are difficult to obtain and are only valid for field strengths in the order of the saturation magnetization. The case of magnetically heterogeneous bodies introduces an additional complication. Each magnetic particle will set up a magnetic field on its own when becoming magnetized. However, at the same time, each particle experiences the field influence from all the other particles. Only approximate mathematical treatment of this situation is presently possible. Powder samples, as one example, have been considered by Brown (1962) and fine particle magnetics by Jacobs and Bean (1955); Della Torre (1985).

5.7 CONCLUSIONS

Considering the discussion above, it is clear that analytical determination of the magnetic torque acting on elongated wood particles whose surfaces are uniformly but discontinuously treated with ferromagnetic material is very difficult. Results of such analysis may only be used to provide guidelines.

It is of interest, however, for the development of a suitable orientation process to understand the influence of variables such as external magnetic field strength, amount of ferromagnetic treatment and aspect ratio on the magnetic torque more fully; this is especially so for field strengths below M_s. Experimental work is therefore necessary to investigate these dependencies more satisfactorily.

Chapter VI

PRINCIPLES UNDERLYING THE EXPERIMENTAL APPROACHES

Preliminary experiments in which fibers were agitated in order to free them for orientation will be outlined before embarking upon an outline of the main experiment in which they were suspended in viscous, non-wetting fluids.

6.1 VIBRATIONAL SUSPENSION OF FIBERS: A PRELIMINARY EXPERIMENT

Suspension of LC fibers or particles is difficult to achieve in air. Free fall under the influence of gravity does not allow for a controllable motion because hydrodynamic effects are large and difficult to assess. However, fluidization of the wood particle by means of a vibrating platform was sufficient to reduce static friction between the particle and the supporting platform so that rotation under the influence of a magnetic torque could be detected. Particle motion was observed optically, in a non-intrusive way, by video filming. A schematic view of the experimental setup is given in Figure 6.1.

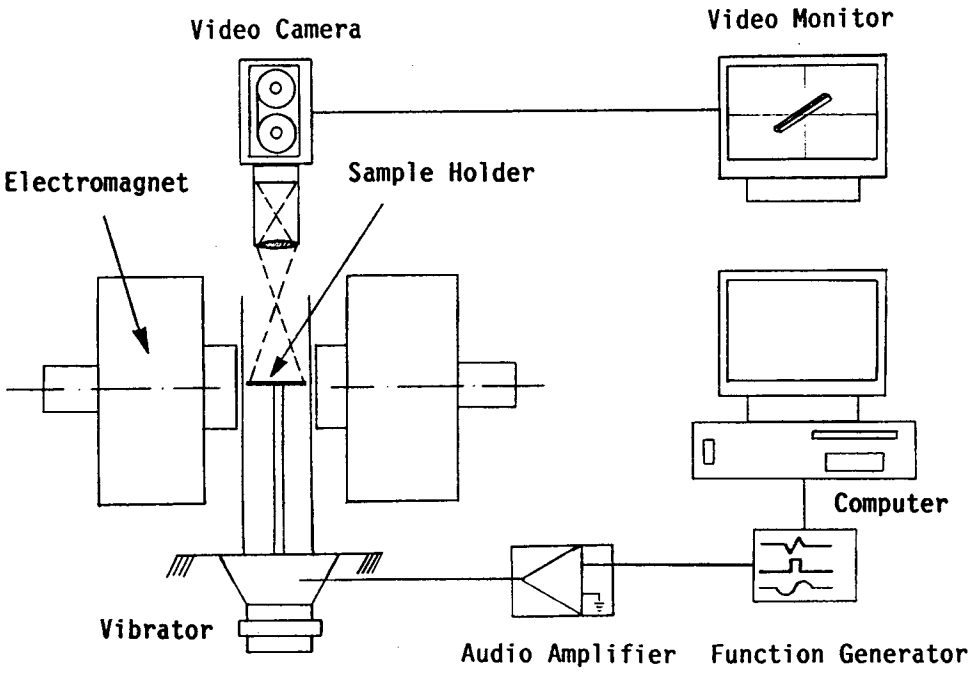

Figure 6.1 Experimental setup for vibrational fluidization.

Frequency and pulse-length of the output signal of the function generator were computer controlled over a wide range. This signal was then amplified by an audio power amplifier and used to excite a loudspeaker. The vibrating platform (30mm diameter) was mounted, at some distance from the magnetic mass of the speaker, on the voice-coil assembly. For high rigidity and surface smoothness, the platform surface was made from glass. Treatment with antistatic fluid was necessary.

Magnetically modified thermomechanical pulp soft-wood fibers (sprayed with the system documented in Appendix B) were investigated over a range of frequencies (100-5000Hz), various amplitudes and several waveforms. It was found that vibrational behavior of these fibers was rather difficult to control. However, under the influence of a magnetic field, rotation resulted for all fibers if agitation exceeded a minimum level.

Under the influence of fluidization alone (no field applied) a precessional motion of some fibers was observed which resulted in orbiting of the fiber on the platform. At constant excitation levels some fibers showed fluidization behavior which was dependent on their position. This can be explained by considering the geometry of TMP fibers which are not perfectly straight. Contact points with the platform change depending on how the fiber settles on the surface and how it has rotated about its length axis since the previous impact.

Observation of particle motion with regular 30Hz video equipment required pulsed excitation so that between vibrational pulses the angular progression of the rotation could be filmed; otherwise the rotation occurred too quickly.

It was observed that fibers sometimes did not settle parallel to the magnetic field lines but rested in an equilibrium position about 10° off-axis. Initially, this

was attributed to a non-uniform distribution of magnetic material over the fiber surface or to some deficiency in the vibrational approach itself. However, in view of experimental results subsequently obtained in the main experiment (liquid suspension), it now seems likely that this behavior can be attributed to a permanent magnetic moment attained by the permeable material on the fiber.

The vibrational approach did not seem ideal for studying fiber-field interactions quantitatively. Besides the difficulties in controlling fiber vibration, the video equipment was not adequate to film the rapid rotational motion. High speed film cameras could, however, be used to overcome this problem.

Such fluidization could well prove appropriate as an actual processing method for multiple fibers. Ultrasonic excitation has been used successfully by Yamashita et al. (1989) to increase the orientable volume fraction of reinforcing fibers in an epoxy matrix.

6.2 ROTATION OF LC-PARTICLES WHILE SUSPENDED IN VISCOUS FLUIDS

6.2.1 EQUATION OF MOTION

The equation of motion, considering rotation only, for a particle under the influence of a magnetic torque has the general form:

$$\vec{T}^{(m)} = \vec{T}^{(h)} + \vec{T}^{(i)} \qquad [6.1]$$

where $\vec{T}^{(h)}$ and $\vec{T}^{(i)}$ are the hydrodynamic- and the inertial-torque respectively. In the present experiments the rotation of an LC particle is to be studied while it is suspended in a viscous, newtonian fluid. Under the assumption that inertial effects of particle and fluid are negligible, the equation of motion takes on the simpler form:

$$\vec{T}^{(m)} = \vec{T}^{(h)} \qquad [6.2]$$

It is the hydrodynamic torque term $\vec{T}^{(h)}$ in [6.2] which is of interest in the following discussion.

The behavior of arbitrary particles undergoing Stokes flow and associated container wall effects were discussed by Brenner (1963, 1962); some results shall be summarized and related to the present work.

6.2.2 HYDRODYNAMICS AT LOW REYNOLDS NUMBERS

The equation of continuity is equal to zero for a fluid of constant density (incompressible fluid):

$$\nabla \bullet \vec{v} = 0 \qquad [6.3]$$

where $\vec{v}$ is the local fluid velocity (Bird et al., 1960). Furthermore, it can be shown that for sufficiently low Reynolds numbers the dynamic equation of motion of a viscous, incompressible fluid is:

$$\rho \, \partial \vec{v} / \partial t + \nabla p = \eta \nabla^2 \vec{v} \qquad [6.4]$$

Equation [6.4] is a simplified form of the Navier-Stokes equation (Bird et al., 1960). The Reynolds numbers N_{Re}, a measure of the ratio of pressure and viscous forces, for translational and rotational motion are, respectively:

$$N_{Re} = |\vec{u}|\ d_c\ \rho\ /\ \eta \qquad [6.5]$$

$$N_{Re} = |\vec{\omega}|\ d_c\ l_c\ \rho\ /\ \eta \qquad [6.6]$$

where $\vec{u}$ is the free stream velocity vector and $\vec{\omega}$ is the angular velocity vector, where d_c and l_c are characteristic particle dimensions, ρ is the fluid density and where η is the fluid viscosity. Dimensional analysis, invoking the magnitude of the Reynolds number, shows that the local acceleration terms, $\rho\ \partial\vec{v}/\partial t$ in [6.4], can be neglected. This even holds approximately true for unsteady flow (again, providing that the Reynolds number is small). Therefore [6.4] reduces to:

$$\nabla^2\vec{v} = \nabla\ p\ /\ \eta \qquad [6.7]$$

It has been shown (Brenner, 1963) that the force $\vec{F}^{(h)}$ acting on a particle translating in a viscous fluid and obeying [6.3] and [6.7] (with the boundary condition of no slip at the particle surface) is:

$$\vec{F}^{(h)} = -\ \eta\ \overline{\overline{K}}\ \vec{u} \qquad [6.8]$$

The term $\overline{\overline{K}}$ is a resistance tensor which is symmetric and depends solely on the shape of the particle; it uniquely characterizes the resistance of the body to translational motion at small Reynolds numbers. In a similar fashion, it

is shown by Brenner (1963) that the hydrodynamic torque acting on a particle rotating in a viscous fluid at low Reynolds numbers can be expressed:

$$\vec{T}^{(h)}_o = -\eta \, \overline{\overline{O}}_o \, \vec{\omega} \qquad [6.9]$$

The term $\overline{\overline{O}}_o$ is a resistance tensor which is again symmetric and is, contrary to $\overline{\overline{K}}$, a function of position.

Similar to the center of mass in the dynamics of rigid bodies, there is a center of hydrodynamic stress. The torque about this point is zero for pure translational motion and a particle rotating about this point will not experience any hydrodynamic force. Having introduced the concept of the center of hydrodynamic stress, [6.9] can be written:

$$\vec{T}^{(h)}_o = \vec{T}^{(h)}_c + \vec{r}^{c}_o \times \vec{F}^{(h)} \qquad [6.10]$$

or equally:

$$\vec{T}^{(h)}_o = - \eta \, (\overline{\overline{O}}_o \, \vec{\omega} + \vec{r}^{c}_o \times (\overline{\overline{K}} \, \vec{u})) \qquad [6.11]$$

where $\vec{T}^{(h)}_o$ and $\vec{T}^{(h)}_c$ are respectively the torques about an arbitrary point o and the torque about the center of hydrodynamic stress. The vector $\vec{r}^{c}_o$ connects these two points.

In addition to the hydrodynamic forces and couples mentioned above, two other forces act upon a particle suspended in a viscous fluid. These are the buoyant and the gravitational forces. The buoyant force acts through the center of buoyancy of the particle, located at the center of gravity of the displaced fluid. The gravitational force acts through the center of mass of the particle. The vector sum of these and the hydrodynamic forces will determine the motion of the particle. If the buoyant force is equal and opposite to the gravitational force, the particle is said to be in a neutrally buoyant state.

In the case of certain symmetrical, homogeneous particles, the centers of mass, buoyancy and hydrodynamic stress coincide. Homogeneous particles possessing three mutually orthogonal symmetry planes (orthotropic) fall into this class (Brenner, 1963). Isotropic particles move in stable position (no rotation) in any starting orientation. Anisotropic particles, however, will move stably under the influence of buoyant and gravitational force only if a principal axis of resistance is collinear with the line of action of these forces. For particles which possess three mutually orthogonal symmetry planes, it is clear from symmetry considerations that the principal axes of resistance lie normal to these planes. Motion normal to a symmetry plane results in a force collinear with the direction of motion.

6.2.3 MOTION OF A RECTANGULAR PARTICLE UNDER THE INFLUENCE OF A MAGNETIC TORQUE

The particle coordinate system is assumed to be located at the geometric center of the particle, with the X, Y and Z axes each coinciding with one of the axes of principal resistance (Figure 6.2). Furthermore, it is assumed that the centers of buoyancy, mass and hydrodynamic stress are coincidently located at the geometric center of the homogeneous particle, and that the magnetic force couple is acting on the particle about the geometric center in the XY-plane only.

The above results in a rotation about the Z-axis. Since no other magnetic force is acting upon the particle and since the rotation is about the center of hydrodynamic stress, no other hydrodynamic force arises. Buoyant and gravitational forces act along the Z-axis on the particle. Ideally for the experiment, the particle is in a neutrally buoyant state and does not translate. But even if this condition is not met, a translational motion will occur only along an axis of principal resistance, not imparting any additional rotation upon the particle; this was the case in our experiments.

Since the equations of motion are linear, one can consider the rotation about the Z-axis and the translation parallel to the Z-axis independently of each other.

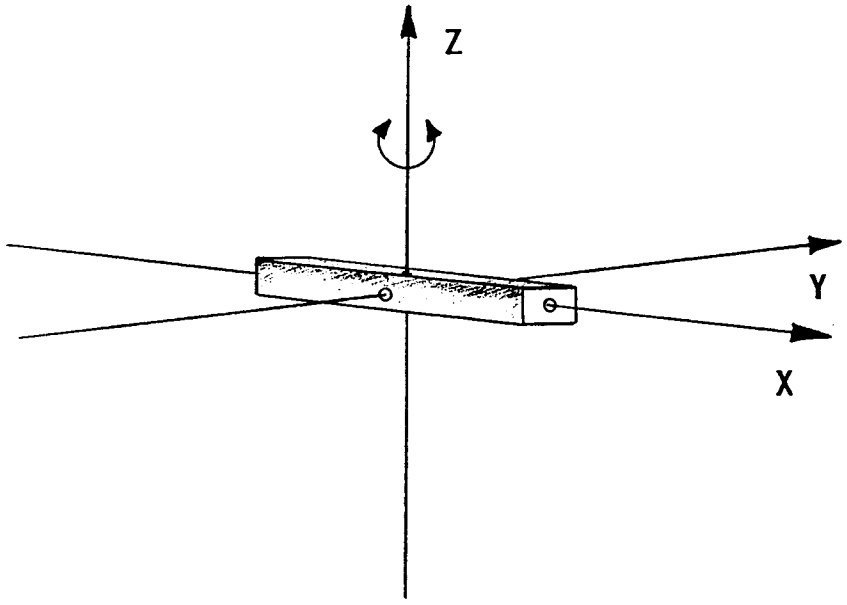

Figure 6.2 The particle coordinate system.

The present study only concerns rotational motion of the particle in the XY-plane and a simplified expression of [6.11] therefore applies:

$$\vec{T}^{(h)}_{o} = \vec{T}^{(h)}_{c} = - \eta \, \overline{\overline{O}}_{c} \, \vec{\omega} \qquad [6.12]$$

Furthermore, by symmetry considerations, the XY-component of [6.12] can be written:

$$T^{(h)}_{xy} = - \eta \, O_{xy} \, \omega_{xy} \qquad [6.13]$$

where O_{xy} is the XY-component of the rotation tensor. The magnitude of this scalar quantity is solely dependent on the geometric properties of the particle and has dimensions of length cubed. It can also be seen that the hydrodynamic torque scales linearly with the fluid viscosity and the particle's angular velocity. The XY-component of the equation of motion [6.2] then takes on the form:

$$T^{(m)}_{xy} = - \eta \, O_{xy} \, \omega_{xy} \qquad [6.14]$$

The components of the rotation tensor are analytically solvable for an ellipsoid (Jeffrey, 1922) and the case of magnetic, ellipsoidal bodies rotating under the influence of a magnetic torque in a viscous fluid has been discussed by Shine (1982). For particles having non-ellipsoidal geometries, the components of the rotation tensor can be obtained experimentally. The magnetic torque can be determined directly, for example, by means of a torsion balance; then [6.14] can be solved for O_{xy} if the fluid viscosity and angular velocity of the particle rotation are known.

In the present research, wood particles in the shape of a rectangular parallelepiped have been used. To facilitate analysis they were highly engineered and therefore varied

little in shape and consequent hydrodynamic behavior. The components of the rotation tensor have not been determined in the present investigation. However, the magnetic torque can still be compared for identical particles by defining a specific torque $T^{(m)}_{xy}{}^{*}$ obtained by dividing the magnetic torque by the corresponding component of the rotation tensor for rotation in the XY-plane [6.15].

$$T^{(m)}_{xy}{}^{*} = T^{(m)}_{xy}/O_{xy} = -\eta\ \omega_{xy} \qquad [6.15]$$

Equation [6.15] has been used throughout this research to describe the magnetic torque acting on the wood particles.

6.2.4 INFLUENCE OF FINITE CONTAINER BOUNDARIES ON PARTICLE ROTATION

For the choice of the proper container size, the influence of finite boundaries on the Stokes resistance of a rotating particle have been considered. In the present situation, an increase in the diameter of the sample container leads necessarily to an increase in pole separation for the electromagnet and hence to a loss in homogeneity and strength of the applied magnetic field. On the other hand, wall effects influencing the motion of a particle decrease the further away the fluid boundaries are.

It is therefore desirable to use the smallest container diameter possible without having disturbing wall effects. In physical arrangements, an analytical solution may readily be found if the torque on the rotating particle in an unbounded fluid is known (Brenner, 1962). In the present case such a solution could not be found and an experimental approach to determine effects of wall proximity was used (see Section 8.6.1).

6.3 RECAPITULATION OF ASSUMPTIONS

The following assumptions have been made studying magnetic torque:

Particle Assumptions

(1) Particles are rigid bodies where centers of gravity, buoyancy and hydrodynamic stress are coincidently located at the geometric center of the particle.

(2) Particle inertia is negligible and equations [6.2] and [6.15] describe rotational behavior.

(3) Particles of identical shape exhibit similar hydrodynamic behavior.

(4) Particle rotation occurs only about an axis of principal resistance; this allows separate consideration of rotational and translational motion.

Hydrodynamic Assumptions

(5) The suspending fluid is newtonian with constant viscosity.

(6) The undisturbed fluid is stagnant and unbounded.

(7) Fluid inertia and Brownian motion are negligible.

Magnetic Assumptions

(8) The external magnetic field is stable, uniform and parallel over the volume in which rotation takes place.

(9) The particle is initially unmagnetized and non-hysteretic.

(10) The magnetic material is uniformly distributed over the particle surfaces.

(11) The particle magnetization adjusts itself instantaneously to its equilibrium value.

Chapter VII

EQUIPMENT USED IN THE EXPERIMENTS

Prior to describing the actual experiments conducted (Chapter VIII) the main pieces of equipment used in the research will be described. An electromagnet and power supply were specially designed and manufactured for the present research. A detailed description and specifications of these devices may be found in Appendix A. The range of relatively standard measurement techniques used in the research are outlined below.

7.1 MAGNETIC FIELD MEASUREMENTS

Field strength was measured with a Hall-effect device (Zijlstra, 1967b). The Hall voltage is a measure of magnetic field strength if the current through the device is maintained constant. In this work, a transverse Hall-effect sensor (Type: LDJ HR-70-CP), calibrated to a standard reference magnet, has been used.

Optimum linearity between Hall-voltage and field strength is obtained only with a certain resistive termination; in the present case a load resistance of 15.4Ω has been provided in the supporting circuitry. Deviations

due to a mismatch in resistive termination become increasingly larger with an increase in field strength; but even with linear matching the relationship between Hall-voltage and control field is not ideal. For the sensor mentioned above, the specified non-linearity is <1% FS. However, the successful and consistent measurement of small fields in the present research (for example Figure A8) provides no evidence that the non-linearity is of the specified magnitude. Accuracy of magnetic field measurements was determined in the present research by a propagation of error analysis where the accuracy for the Hall-sensor was assumed to be ±2% of the measurement. The precision of the field strength measurements is only limited by the resolution of the voltmeter used, the stability of the Hall-current and the precision of the temperature correction. In this research, field differences better than $1*10^{-5}$T were resolved.

In the present study, current was provided by a programmable constant current source (type: Calex 930/MK296HP). The output current regulation of this device is 50μA/V and regulation of ±0.3μA was achieved.

7.2 TEMPERATURE MEASUREMENTS

For temperature measurements a thermistor probe (Type: YSI 44204; Range: 0°C to 38°C) with an accuracy of ±0.27°C was used. This probe was powered by a very stable voltage source (mercury cell, 1.35V) in a full bridge configuration. The thermistor output voltage was monitored using analog to digital conversion and a personal computer.

The A/D conversion (type: Data Translation Board 2801 12-Bit) has a resolution of ±24.4μV in a range from 0 to 100mV. This translates to a temperature resolution of $\pm 2.9 * 10^{-3}$°C. The thermistor voltage was sampled at a rate of 800Hz and averaged, to reduce noise, over 300 readings. This voltage was then converted into a temperature value and displayed with a resolution of ±0.01°C.

7.3 VISCOSITY MEASUREMENTS

Viscosity measurements have been made with a Brookfield spindle viscosimeter (Table 7.1).

Table 7.1 Specifications for the Brookfield viscosimeter.

Model: LVTD (Digital Display)			
Accuracy: 1% Full Scale			
Resolution: 0.2% Full Scale			
Small Sample Adapter: SC4 - 18/13R			
Speed	Shear Rate	Range	Accuracy
[RPM]	[1/sec]	[10E-3 Pa sec]	[10E-3 Pa sec]
60	79.50	50	+/- 0.5
30	39.75	100	+/- 1.0
12	15.90	250	+/- 2.5
6	7.95	500	+/- 5.0
3	3.98	1000	+/- 10.0

7.4 VIDEO EQUIPMENT

Particle rotation was filmed with a NIKON 8mm Video Camera Recorder (Type:VN-700) with a set of magnifying lenses (+7 diopters) attached. To diminish blur a shutter speed of 1/250sec has been chosen. The time between individual frames, composed of two exposures, is 1/30sec, a standard (NTSC) for regular video equipment. This imposes a limit in time resolution of maximal ±1/60sec on the event captured in the video image.

7.5 EXPERIMENTAL SETUP

The arrangement of the components used can be seen schematically in Figures 7.1 and 7.2.

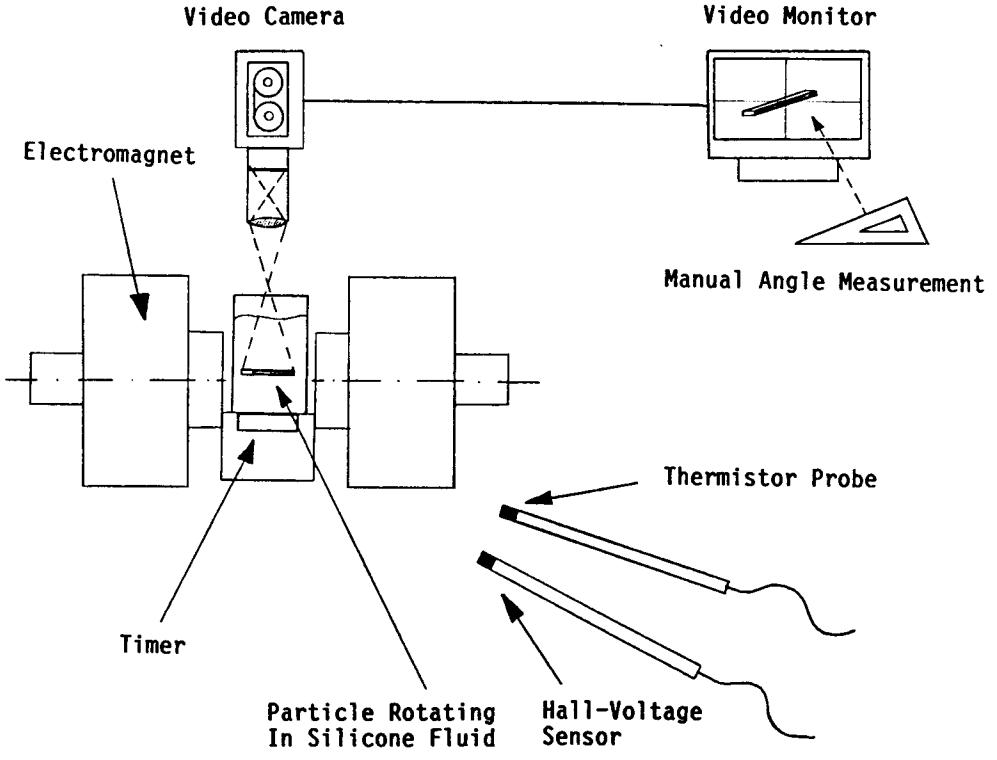

Figure 7.1 Experimental setup for LC particle rotation experiments.

In order to allow determination of the angular velocity (needed in equation [7.15]), both angular position of the particle with respect to the magnetic field lines and the exact time must be known. Video filming of particle rotation proved to be a good, non-intrusive way to obtain

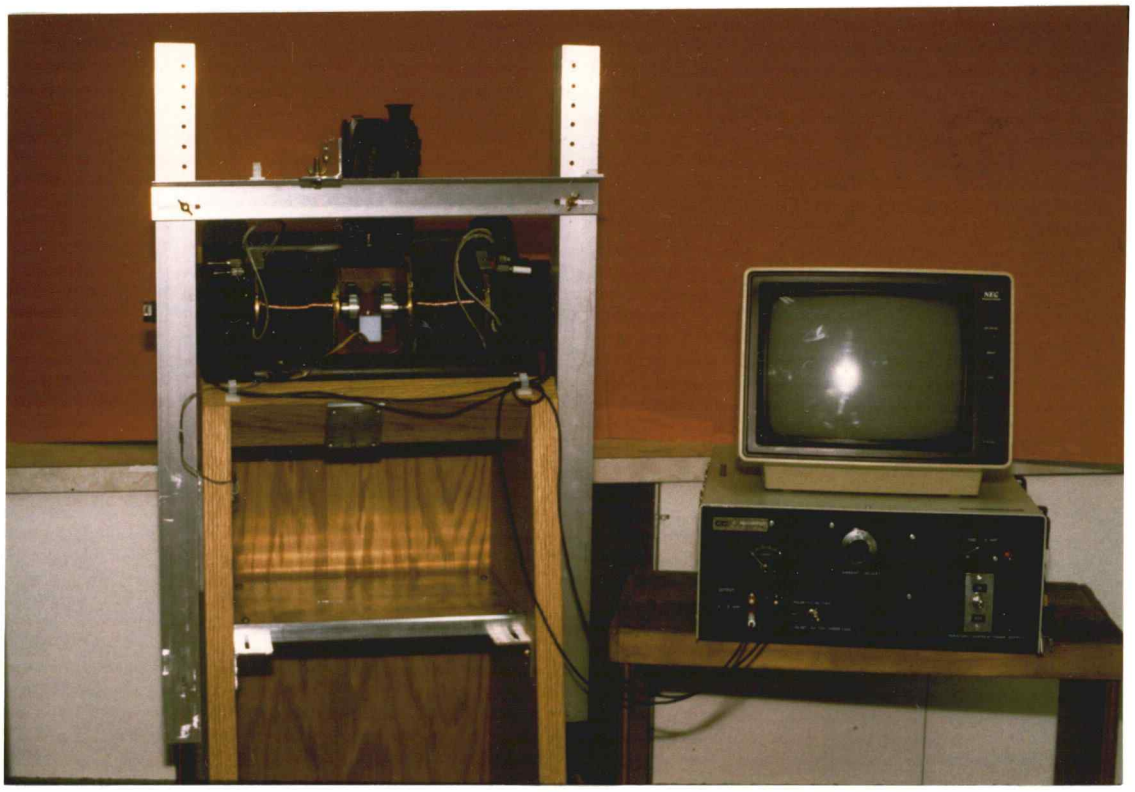

Figure 7.2 Photograph of electromagnet, power supply and video system.

this information. Since the camera did not provide a time signature for each frame, a stop watch with display of 1/100sec was installed beneath the glass sample container located between the magnet pole pieces. The LCD display of this device was filmed through the sample container and therefore time progression from frame to frame could be obtained.

To avoid heating of the fluid in the sample container, caused by resistive heating of the coil windings, the gap region was force cooled by a ventilator.

Chapter VIII

MATERIALS AND METHODS

8.1 LC PARTICLE MODIFICATION

8.1.1 PARTICLE SOURCE

Small, highly engineered strips of aspen (Populus spp.), having the shape of a rectangular parallelepiped (avg. dimensions: 12.9 - 0.8 - 0.5 mm), were selected. These particles were produced at the USDA Forest Products Laboratory (Madison, Wisconsin). The choice for this material was dictated by geometrical constraints necessary to investigate rotation of LC material in a viscous fluid. Although these particles are larger in size than fibers of TMP, their aspect ratio is similar.

8.1.2 NICKEL COATING

A nickel powder-acrylic binder suspension (Electrodag® 440; 59% nickel powder, by weight), provided by Acheson Colloids Company has been used for all fiber surface modifications. As well as providing a medium for conveying the nickel, the binder insures bonding between nickel

particles and also to the substrate. Dilution with SB-10 thinner (1/1, by volume) was necessary for proper application; the viscosity at time of spraying was $45*10^{-3}$Pa sec.

The filamentary nickel powder has a bead-and-chain structure with beads 1μm to 3μm in diameter and chains up to 30 beads long (Figure 9.3e shows this type of nickel powder in an acrylic matrix, 5000X). The bead agglomerations are held together by acrylic binder.

8.1.3 COATING PROCESS

Nine different wood particle target loading levels have been prepared (for a description of the spray coating system refer to Appendix B). The variable influencing the loading level was spray time (Table 8.1). Settings of the spray system may be found in Table 8.2.

In order to maintain the wood particles suspended, the tank volume had to be decreased to $1.44*10^{-3}m^3$ and batch weight had to be limited to about 4g. The particles had an average moisture content of 8.61 ± 0.33% (determined on parallel samples). This is the equilibrium moisture content attained in a climatically controlled environment in which the rotation tests were performed. In a selection process, based on optically inferred uniformity of the coating,

Table 8.1 Spray time for wood particles.

Sample	Spray Time [sec] +/- 0.5sec
1	2
2	5
3	2.5
4	5
5	10
6	7.5
7	15
8	20
9	25

Table 8.2 Settings of the spray system (refer to appendix B).

Spray Nozzle Turns:	2 1/4
Spray Gun Pressure:	275*10E3 Pa
Counterflow Pressure:	620*10E3 Pa
Effective Tank Volume:	1.44*10E-3 m^3
Tank Revolutions:	22.5 RPM
Blower Airflow:	5 m/ sec

candidate particles for the rotation experiments were selected. These and the remainder (about 3g) were each packed in a Zip-lock bag to preserve the moisture content. The remainder was used for magnetic measurements and a 'total nickel' analysis which was performed (according to EPA Method: 249.1) by the laboratories of CH2M-Hill, Corvallis.

8.2 MEASUREMENT OF MAGNETIC PROPERTIES

Mass susceptibility, saturation isothermal remanence magnetization (SIRM) and isothermal remanence magnetization (IRM) measurements after demagnetization in an alternating field were performed at the Paleo-Magnetic Laboratory at Oregon State University.

8.2.1 SAMPLE PREPARATION

Sample apportionment to the different measurements may be seen in Table 8.3.

Table 8.3 Sample apportionment to magnetic measurements.

Type of Measurement	Sample Number										Ni-Powder in Epoxy
	1	2	3	4	5	6	7	8	9	Control	
Mass Susceptibility	**	**	**	**	**	**	**	**	**	**	**
SIRM	**	**	**	**	**	**	**	**	**	**	**
Demagnetization	-	-	*	-	-	-	-	*	-	-	*
Magnetization	-	-	*	-	-	-	-	*	-	-	-

* One Sample
** Two Samples

Powder samples were prepared by mixing about 0.01g of filamentary Ni-powder (INCO, type 255) with an epoxy resin in a sample container. Sub-samples, each having a mass of

about 0.5g, were prepared from each wood particle sample batch. These were then weighed and wrapped in weighing paper before being packed in a sample container having a volume of about $7*10^{-6}m^3$. This procedure resulted in densely packed, randomly oriented wood particles in the container. The weighing paper insured that no shifting of individual particles occurred; this is important in SIRM measurements were only one vector of the magnetization is measured at a time, and shifting of the sample would introduce a considerable error.

8.2.2 MASS SUSCEPTIBILITY

For these measurements a Bartington susceptibility meter (Type: M.S.2; Field Strength: 80A/m (RMS); Accuracy: 1%; Sensitivity: $2.5*10^{-6}$ [Si]) was used. The instrument was calibrated with a known standard prior to being used to make measurements. Measurements were made on samples which had not yet been exposed to magnetic fields (other than that of the earth). For dry materials and for materials of unknown density, mass specific susceptibility measurement is most useful because only the weight of the material is required. The oven dry mass of a sample was determined by assuming an average moisture content of 8.61 ± 0.33%.

8.2.3 ISOTHERMAL REMANENCE MAGNETIZATION

Three types of remanence measurements were undertaken: (1) after excitation to saturation, (2) as a function of applied field strength, and (3) as a function of an alternating demagnetizing field (Table 8.4).

Table 8.4 Magnetization and demagnetization field strengths.

Field Strengths	
Magnetization	Demagnetization
[T] +/- 2%	[mT] Peak
0.00	0.0
0.02	5.0
0.03	7.5
0.04	10.0
0.05	12.5
0.07	15.0
0.09	20.0
0.11	25.0
0.13	30.0
0.15	
0.20	
0.30	

The functional dependency between remanent magnetization and exciting field strength is expected to reflect that of the magnetization and the exciting field (Levi, 1992). To determine the coercivity, the samples were exposed (after being magnetically saturated) to a decreasing

and alternating magnetic field (decay rates 0.4A/m - 0.8A/m per half cycle). The remanence magnetization was measured periodically during this demagnetization procedure. The alternating field required to decrease saturation remanence by 50% is called the medium destructive field; the magnitude of this field is a good indicator of the coercivity of the material (Levi, 1992).

Remanence measurements have been performed with a fluxgate magnetometer (Type: Schoenstedt Digital Spinner Magnetometer, Mod. DSM 1; Accuracy: 1%) which is usually used for geo- and paleo-magnetic measurements.

The isothermal saturation remanence magnetization has been divided by the oven dry mass of the sample to yield the mass-magnetization. Absolute remanence magnetization levels have been normalized to enable comparison among different loading levels. The saturation isothermal remanence magnetization was measured after excitation to 0.3T -- a field strength which assured magnetic saturation.

8.3 SUSPENSION FLUIDS

A viscous and transparent suspending medium was required to enable inertia-free particle rotation to be affected and observed. A balance between several competing effects determines the choice of fluid viscosity and

density. To allow the small magnetic torques resulting from moderate magnetic fields ($B << M_s$) and low particle nickel dosing to be measured, viscosity should be low. On the other hand, the assumption of inertia-free rotation still has to be warranted. In addition, at low viscosities, gravitational and buoyant forces acting on the particle may become important. These forces can lead to a large, disturbing translational motion of the particle.

8.3.1 SILICONE FLUIDS

Silicone fluids (linear polydimethyl-siloxane polymers, Dow Corning 200® Fluid) having viscosities between $20*10^{-3}$Pa sec and $120*10^{-3}$Pa sec were used in this research. These fluids are crystal clear and free from suspended matter and sediment. Their specific gravity at room temperature is about 0.95. By mixing two standard viscosity grades, 10cs and 500cs, intermediate viscosities and densities were obtained.

Chemical and physical interactions with the wood particles are assumed to be minimal since silicone fluids are essentially inert substances. However, the porous wood particles became saturated with the fluid after several hours of exposure. An accompanying change in buoyancy resulted in sinking of the initially buoyant particles in

the fluid. This proved to be advantageous because, with careful time management, particles could be brought to a nearly neutrally buoyant state.

8.3.2 RHEOLOGICAL EVALUATION OF THE SILICONE FLUIDS

Fluid viscosity must be known precisely to solve equation [7.15] for the specific magnetic torque. Temperature influences the viscosity of most fluids significantly and in this research, the range of fluid temperatures was minimized by performing the experiments in a room with tightly controlled temperature (22.5 ±1.0°C). However, heating effects in the gap region of the electromagnet increased the upper limit to about 25°C.

Since measurement of fluid viscosity is impracticable shortly before or after a rotation experiment, a functional relation between viscosity and fluid temperature was developed to enable corrections to be made. A linear dependence was assumed over a temperature range from 22°C to 28°C. This assumption seems justified considering the temperature dependency of these fluids (graphs provided by the manufacturer) and considering the accuracy of the Brookfield viscometer used for all rheological measurements (refer to section 7.3).

Viscosity measurements were performed for five different fluid mixtures at several temperatures after fluid and viscosimeter were brought into thermal equilibrium with the environment. From these data points regression equations were calculated for fluids #1 through #4. For fluid #5, used in the linear scaling experiment (refer to Section 9.6.2), only one measurement was available and for this fluid interpolated values were found using temperature coefficients provided by the manufacturer of the silicone fluids. Table 8.5 lists the interpolated viscosities at 25°C for the five fluid mixtures.

Table 8.5 Interpolated viscosities for mixtures of silicone fluids (@25°C).

Fluid #	Viscosity [10E-3 Pa sec]
1	119.57 +/- 2.51
2	86.21 +/- 1.00
3	49.13 +/- 1.00
4	22.02 +/- 0.50
5	50.26 +/- 1.00

The average measurement precision was 0.16%, 0.06%, 0.08% and 0.11% for fluid #1 through #4 respectively. This indicates that accuracy of the viscosity measurements is not nearly as good as measurement precision.

To test the assumption of newtonian behavior, several viscosity measurements at different shear rates (39.75sec^{-1}, 15.90sec^{-1}, 7.95sec^{-1} and 3.98sec^{-1}; refer to Section 7.3) were performed. Three of these shear rates were higher than the highest shear rate occurring in the particle rotation experiments. Within the limits of accuracy of the instrument, differences in the measured viscosity values could not be attributed to non-newtonian behavior; more accurate instrumentation is necessary to investigate rheological properties at different shear rates in more depth. However, the Dow Corning Inc. claims newtonian behavior for these fluids at the shear rates present and such an assumption will be made in the analysis to follow.

8.4 EXPERIMENTAL PROCEDURE

8.4.1 PARTICLE SELECTION

Particles from each sample batch were selected to fall within a certain dimensional range. The average dimensions and corresponding standard deviations for 36 particles selected for this research are shown in Table 8.6.
The particles were measured with a caliper (Type: Mitutoyo 500; Accuracy: 0.0254mm; Repeatability: 0.0127mm).

Table 8.6 Average dimensions for 36 wood particles.

	Average +/- std
Length [mm]	12.91 +/- 0.03
Width [mm]	0.82 +/- 0.01
Thickness [mm]	0.48 +/- 0.03

8.4.2 STEPS IN THE EXPERIMENTAL PROCEDURE

In early stages of the research it was mistakenly assumed that the magnetically modified wood particles have a low coercivity. However, permanent magnetization after exposure to a magnetic field was subsequently detected. The influence of this remanent magnetization was most noticeable at low field strength. The experimental procedure was therefore modified to include a demagnetization step. Immediately prior to an experimental run the particle was exposed to an alternating magnetic field of decreasing amplitude. This demagnetization field (peak field strength: 0.14T) was generated by an iron-core coil connected to an autotransformer; manual decrease of the voltage output of this transformer resulted in a decrease of field amplitude.

The following sequence was followed when testing particles:

(1) Thermally stabilize all electric and electronic equipment.
(2) Soak particles in silicone fluid to reduce buoyancy.
(3) Determine Hall-voltage offset, including the influence of the local magnetic field.
(4) Conduct alignment check of video camera.
(5) Demagnetize particle (if applicable).
(6) Position particle in sample container, filled with $8*10^{-6}m^3$ of silicone fluid (outside the magnetic field).
(7) Start video camera and timer.
(8) Position sample container in magnetic field in such a way that the particle is close to an unstable equilibrium position (angle α about 90°).
(9) Film particle rotation.
(10) Measure fluid temperature.
(11) Change magnetic field strength (if required) in readiness for next series of tests.

Steps 4) through 11) were repeated for successive experimental runs. In cases where fluids of different viscosity were used, particle surfaces were sponged dry with

filter paper. This minimized cross-contamination and the creation of a boundary layer with differing drag coefficient.

8.5 DATA ACQUISITION AND REDUCTION

Data for each experimental run (about 30 video frames, covering the whole rotational motion) were converted into series of (angle, time) data pairs. This was done by measuring the angle α that the particle length axis made with respect to a reference line parallel to the magnetic field lines. Three video frames of one typical run are shown in Figures 8.1a-c; the vertical line in these images is parallel to the magnetic field lines. These lines were obtained by filming an aligned cross-hair template, located in the gap, and then superposing this image electronically on the video images of the experimental run.

Angle measurements were performed manually using a protractor and a flat plexiglas screen, mounted in front of a video monitor, to support the protractor. The maximal standard deviation of ten measurements at each of five different angular positions was $\pm 0.3°$. The range of angles covered differed from run to run and was dependent on the experimental conditions. The data thus recorded can be plotted directly as angle α vs. time t. A sigmoidal curve

Figure 8.1 A typical sequence of video frames recorded during an experimental run.

Figure 8.1a Frame 1: 73.9° inclination at a reference time of 14.19sec.

Figure 8.1b Frame 2: 47.7° inclination at a reference time of 17.19sec.

Figure 8.1c Frame 3: 16.7° inclination at a reference time of 21.59sec.

was characteristic of all experimental runs (Figure 8.2), except for those in which a change in field polarity was affected. Direct comparison of these curves is possible if a common time is chosen; the angle at which t is chosen to be zero is arbitrary.

A least squares, sixth order polynomial expression was fitted to the data points. In some cases the slope was misrepresented at high and low limits of α and a meaningful extrapolation beyond the range of covered data was therefore not possible. An example of such a polynomial fit is shown in Figure 8.2. The polynomial expression is easily differentiated with respect to time; this yields a function representing the angular velocity.

For the purpose of comparison of experimental runs, the fluid viscosities were temperature corrected and scaled to an arbitrarily chosen reference viscosity of $50*10^{-3}$Pa sec. The angular velocities were then multiplied by these scaling factors and by the reference viscosity to yield the specific magnetic torque $T^{(m)*}$ (Figure 8.2). The maximum of $T^{(m)*}$ provided a useful means of comparing particles. A root finding algorithm provided with the HP48 SX Handheld Calculator (Hewlett-Packard) was used to solve for this maximum. A more refined numerical method is necessary to determine the angular position of max.$T^{(m)*}$ analytically; this has not been attempted in the present research.

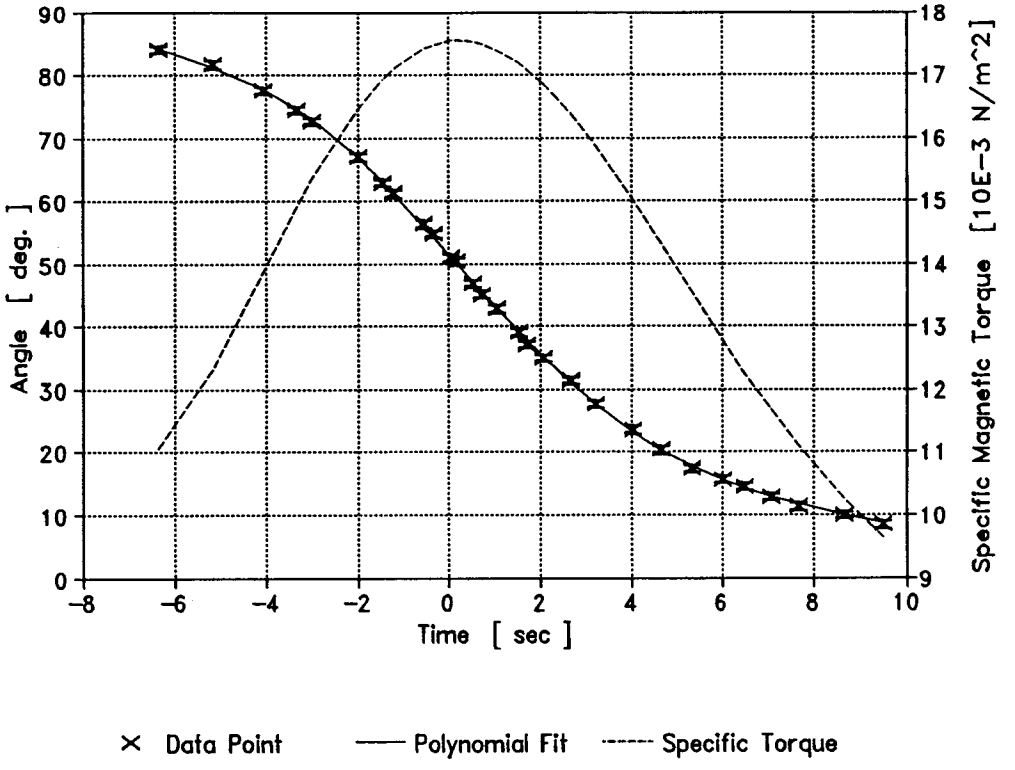

Figure 8.2 Sixth order polynomial fit to data points and its derivative expressed in the form of the specific magnetic torque; all versus time.

A propagation of error analysis was not performed because of considerable mathematical difficulties arising from the polynomial curve-fitting expressions. However, a sensitivity analysis was conducted using a data set from the experiments (Section 8.6.5, sample #6). The influence on max.$T^{(m)*}$ due to shrinking and stretching the time axis by 5% was investigated. The systematic error thus introduced was estimated to be much larger than any combined error in time and angular measurement. This procedure led to a deviation in the magnitude of max.$T^{(m)*}$ of about ±5%.

8.6 SCOPE OF EXPERIMENTS CONDUCTED

In the following set of tables sample apportionment and main experimental conditions for all successfully performed experiments will be given. Gapwidth was always 29.6mm unless otherwise indicated in the tables. The influence of different particle geometries on magnetic torque was not considered because of time constraints.

8.6.1 INFLUENCE OF CONTAINER DIAMETER ON ROTATIONAL BEHAVIOR

The purpose of this experiment was to determine the smallest inner diameter for a sample container to be used in subsequent experiments, without it having disturbing wall effects (Table 8.7).

8.6.2 LINEAR SCALING OF MAGNETIC TORQUE WITH VISCOSITY

This experiment was conducted to verify the assumption that magnetic torque scales linearly with viscosity (equation [7.15]) and to investigate repeatability (Table 8.8).

Table 8.7 Experiment: Influence of container diameter on particle rotation.

Gapwidth: 35 [mm]		
Fluid: #2		
No Demagnetization		
Container Diameter	Replication	Field Strength +/- Accuracy
[mm]		[T]
31.4	1	0.11792 +/- 0.00237
25.4	1	
31.4	1	0.11771 +/- 0.00238
25.4	1	
22.3	2	
20.1	1	

Table 8.8 Experiment: Linear scaling of magnetic torque with viscosity.

Sample:	#5
No Demagnetization	
Field Strength:	0.13080 +/- 0.00263 [T]
Fluid:	#1, #2, #5

8.6.3 VARIABILITY AMONG PARTICLES OF ONE TREATMENT BATCH

This experiment investigated variability in treatment among five geometrically very similar particles extracted from one sample batch (Table 8.9).

Table 8.9 Experiment: Variability among particles of one treatment batch.

Sample: #5					
Fluid: #2					
No Demagnetization					
Particle	Replication	Dimensions			Field Strength +/- Accuracy
		l	w	t	
		[mm]	[mm]	[mm]	[T]
A	2	12.93	0.82	0.45	0.13018 +/- 0.00262
B	2	12.98	0.82	0.47	
C	2	12.88	0.77	0.48	
D	1	12.84	0.82	0.53	
E	2	12.87	0.82	0.51	0.12934 +/- 0.00260

8.6.4 INFLUENCE OF FIELD STRENGTH ON MAGNETIC TORQUE

From both sample batches #8 and #3, one particle was selected and rotation experiments at variable field strengths were then performed (Tables 8.10a and 8.10b). To increase the range of possible field strengths, different fluid viscosities were used.

Table 8.10a Experiment: Dependence of maximum specific magnetic torque on field strength (sample #8, 38.4g/kg nickel).

Sample #8		
Demagnetization		
Field Strength +/- Accuracy [T]	Replication	Fluid #
0.06996 +/- 0.00141	1	2
0.08054 +/- 0.00161	1	2
0.08997 +/- 0.00181	1	2
0.09999 +/- 0.00201	1	2
0.10993 +/- 0.00210	1	2
0.12000 +/- 0.00241	1	2
0.12998 +/- 0.00262	1	2
0.13907 +/- 0.00282	1	1
0.14997 +/- 0.00302	2	1

Table 8.10b Experiment: Dependence of maximum specific magnetic torque on field strength (sample #3, 13.3g/kg nickel).

Sample: #3		
Demagnetization		
Field Strength +/- Accuracy [T]	Replication	Fluid #
0.09001 +/- 0.00181	1	3
0.11000 +/- 0.00221	1	3
0.12001 +/- 0.00241	1	3
0.12995 +/- 0.00261	1	3
0.14003 +/- 0.00281	1	3
0.15002 +/- 0.00302	1	3
0.15500 +/- 0.00312	1	3

8.6.5 INFLUENCE OF NICKEL CONCENTRATION ON MAGNETIC TORQUE

Experiments were conducted at high field strengths and various viscosities to maximize the range of samples. Several particles selected from one sample batch were utilized to detect differences among particles (Table 8.11).

Table 8.11 Experiment: Influence of nickel concentration on magnetic torque.

Sample	Particle	Replication	Field Strength	Fluid #
1	A	1	*	4
2	A	2	*	2
	A	1	**	2
	B	1	**	2
3	A	1	*	2
	A	1	**	3
	B	1	*	2
5	A	2	*	2
	B	1	**	2
	C	1	**	2
6	A	1	*	2
	B	1	*	2
	C	1	**	1
	D	1	**	1
8	A	1	*	1
	B	1	*	1
	C	1	**	1
	D	1	**	1
9	A	1	*	1
	A	1	**	1
	B	1	*	1
*	0.15492 +/- 0.00311 [T]			
**	0.15501 +/- 0.00312 [T]			
Demagnetization				

8.6.6 INFLUENCE OF CHANGE IN FIELD POLARITY ON MAGNETIC TORQUE

One control run was performed without changing the polarity of the external magnetic field. Following this, another run was performed where the field was switched shortly before the particle reached its final equilibrium position (Table 8.12).

Table 8.12 Experiment: Influence of change in magnetic field polarity on magnetic torque.

Sample:	#6
Demagnetization	
Field Strength:	0.07922 +/- 0.00159 [T]
Fluid:	#2

Chapter IX

RESULTS AND DISCUSSION

9.1 PARTICLE TREATMENT

The nine nickel dosing levels ranged between 5.3g/kg and 49.7g/kg (Method detection limit: 500mg/kg @ 10000X dilution; Repeatability: about ±7%)(Table 9.1).

Table 9.1 Nickel concentrations found for treated wood particles.

Sample	Nickel Concentration [g/ kg]	Sample	Nickel Concentration [g/kg]
Control	0.0 + 0.5	5	20.1 +/- 1.5
1	5.3 +/- 0.6	6	27.2 +/- 2.0
2	11.6 +/- 1.0	7	28.4 +/- 2.0
3	13.3 +/- 1.1	8	38.4 +/- 2.7
4	16.7 +/- 1.3	9	49.7 +/- 3.5

The amount of nickel deposited on the particle surfaces for each of the samples is shown in Figure 9.1 as a function of the coating time; numbers in the graph indicate the order of the consecutive spray batches.

Cleaning of the spray equipment was necessary prior to coating of batch numbers 6 through 9. Considering the first five batches, a near linear relationship between coating

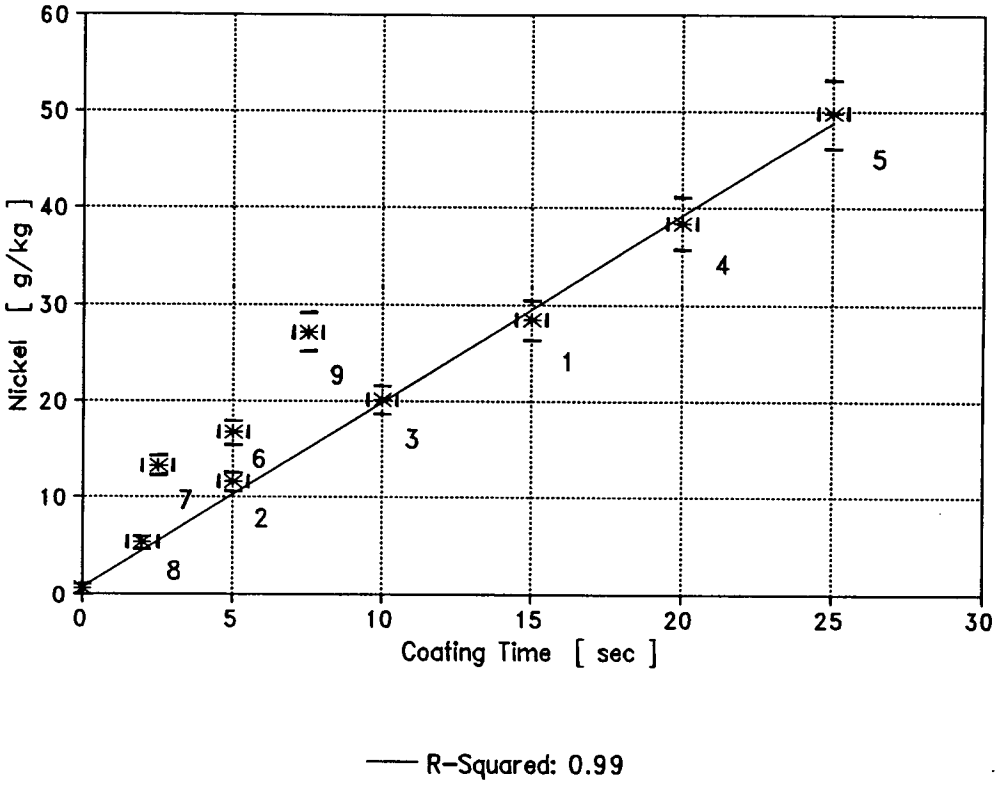

Figure 9.1 Nickel concentration found for the wood particles as a function of spray time (numbers indicate consecutive spray batches).

time and amount of nickel deposited can be seen (r-squared: 0.99). For batches 6 through 9 this trend is not as clear and can be partly explained by the use of slightly dissimilar settings of the spray system following cleaning. Reproducibility of loading levels with the spraying system has not been investigated in this study.

Uniformity of dosing was evaluated using a scanning electron microscope equipped with an X-ray detector. Element maps of nickel (1000sec exposure time) of a particle surface for dosing levels of 5.3g/kg; 11.6g/kg and 38.4g/kg

(2 particles each) are presented in Figures 9.2a through 9.2c. These images (20X), taken over about 50% of total fiber length, indicate rather uniform surface coverage. A sequence of micrographs (50X - 5000X), showing the surface of a particle selected from sample #8, can be seen in Figures 9.3a through 9.3e. Diameters of the deposits range between 70μm and smaller than 2μm (measured from micrograph, 9.3b). Uniformity in surface coating among fibers of one batch was evaluated considering max.$T^{(m)*}$ (Table 9.5; refer to Section 9.3.3 for a discussion thereof).

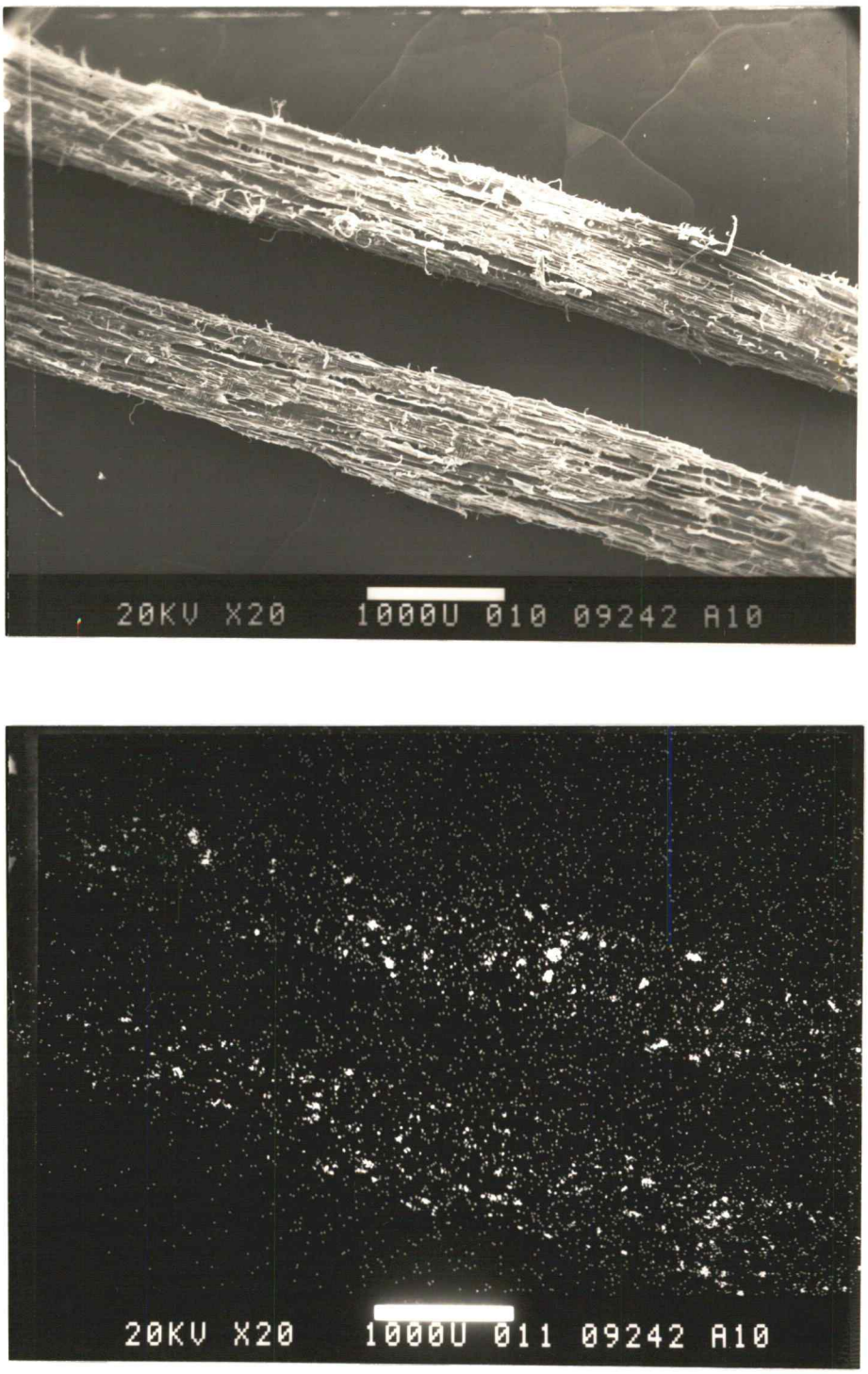

Figure 9.2 Element maps of nickel on particle surfaces for three different concentrations.

Figure 9.2a Sample batch #1, 5.3g/kg nickel, 20X (top: image; bottom: Ni-map).

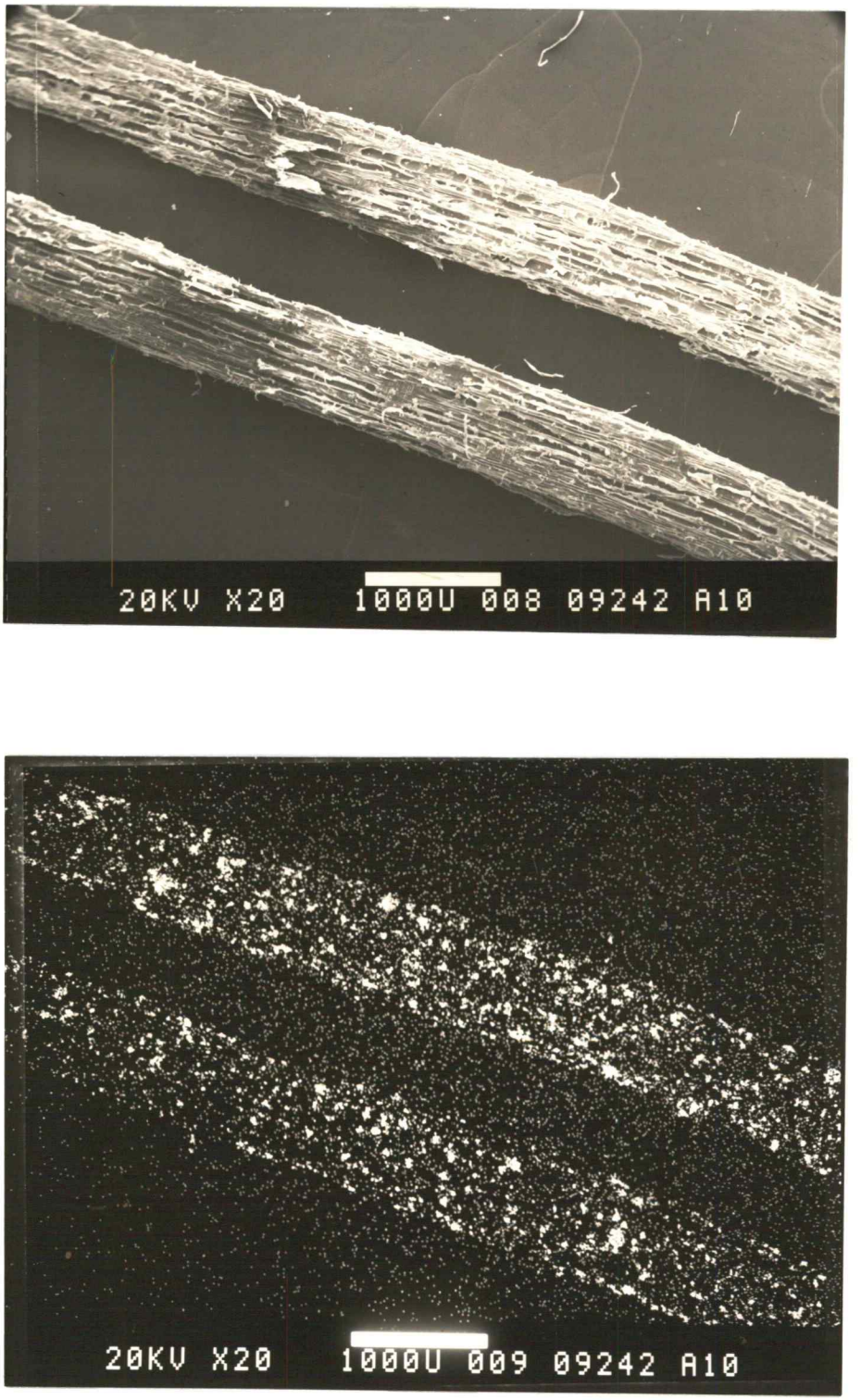

Figure 9.2b Sample batch #2, 11.6g/kg nickel, 20X (top: image; bottom: Ni-map).

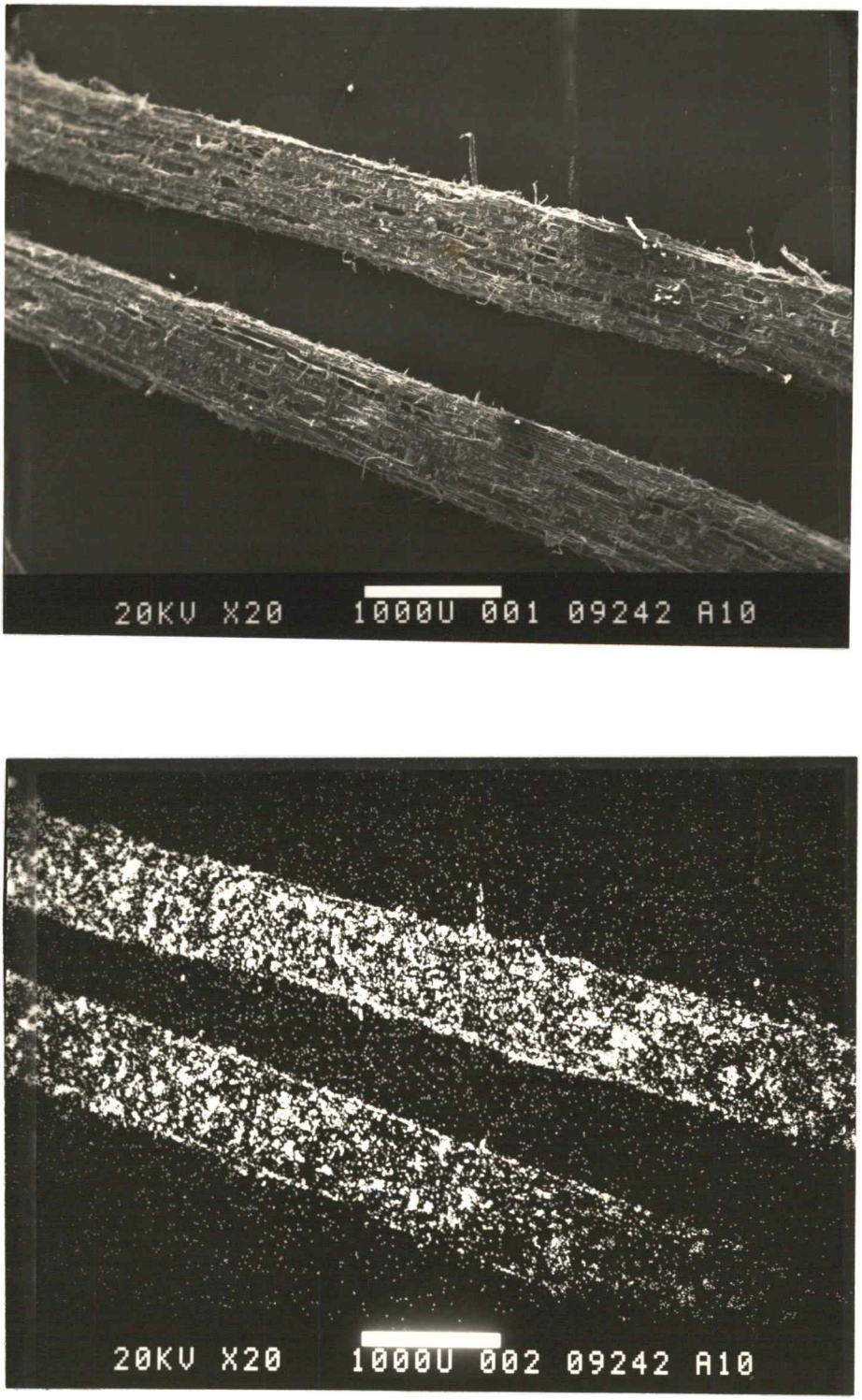

Figure 9.2c Sample batch #8, 38.4g/kg nickel, 20X (top: image; bottom: Ni-map).

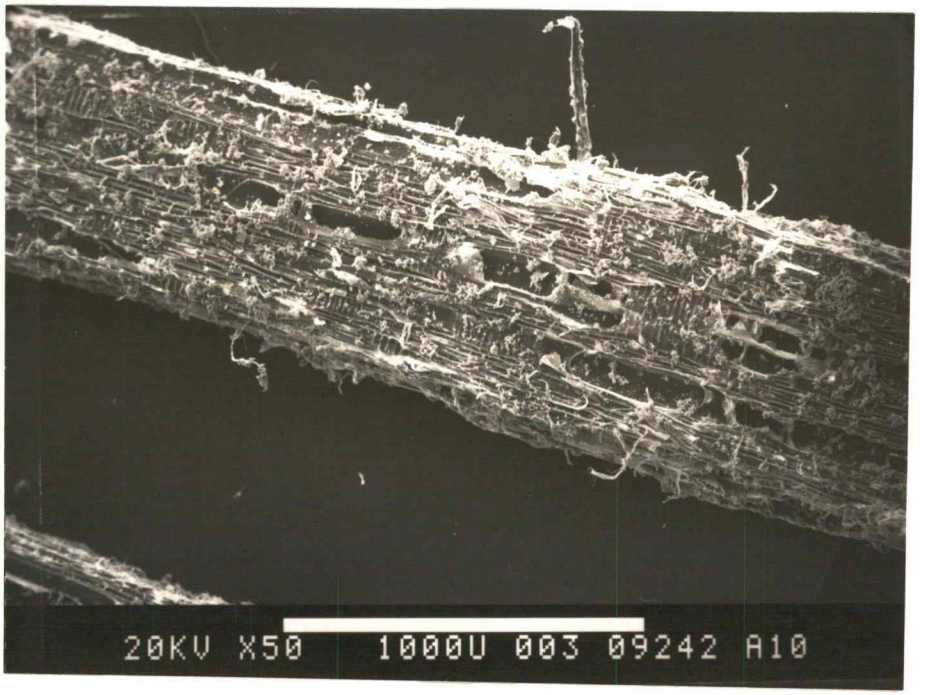

Figure 9.3 A sequence of micrographs showing the surface of a particle extracted from sample batch #8.

Figure 9.3a 50X

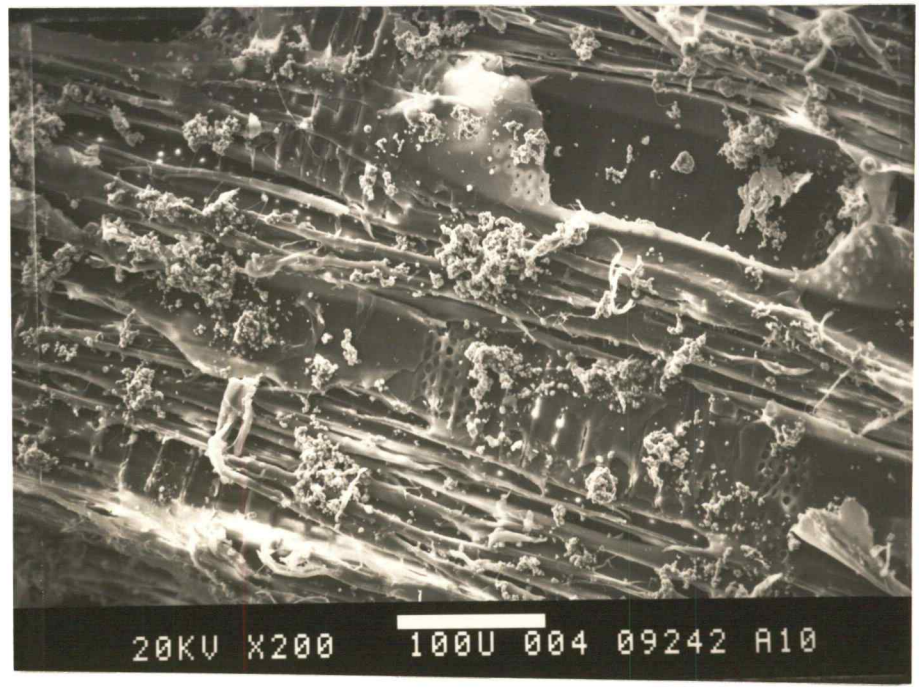

Figure 9.3b 200X

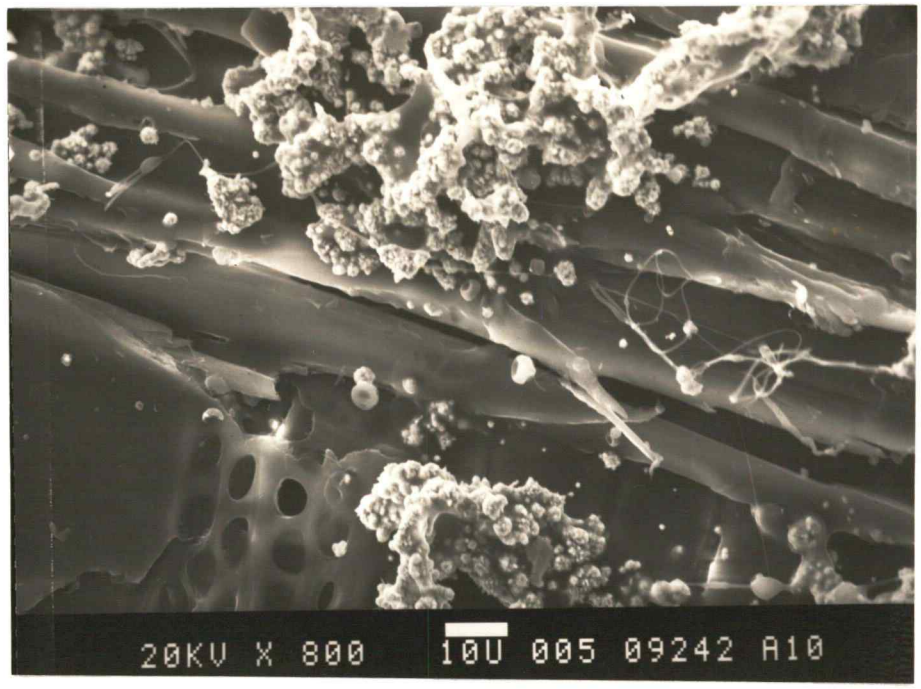

Figure 9.3c 800X

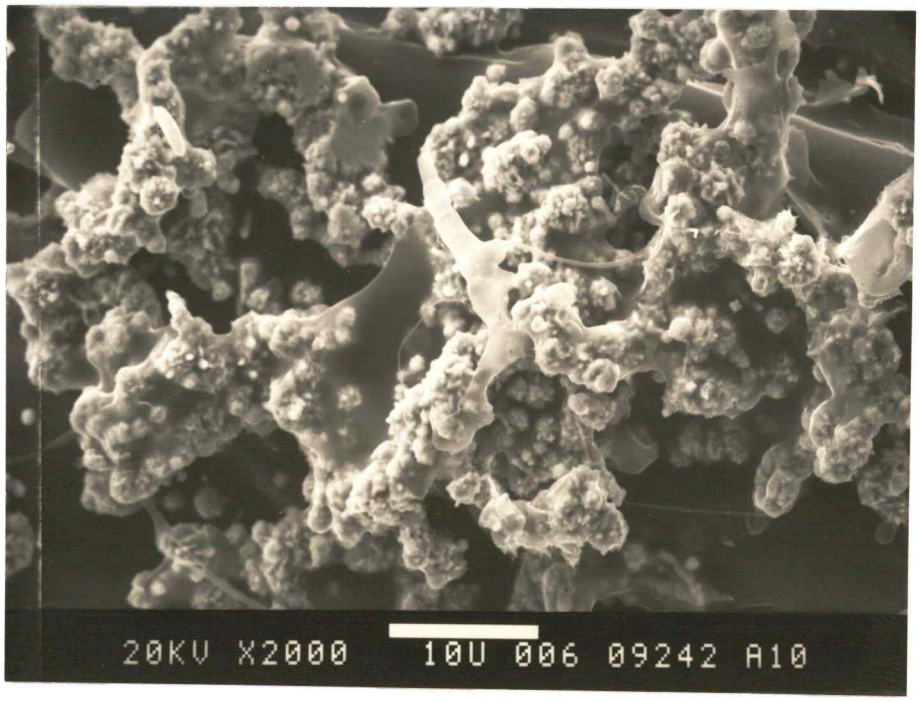

Figure 9.3d 2000X

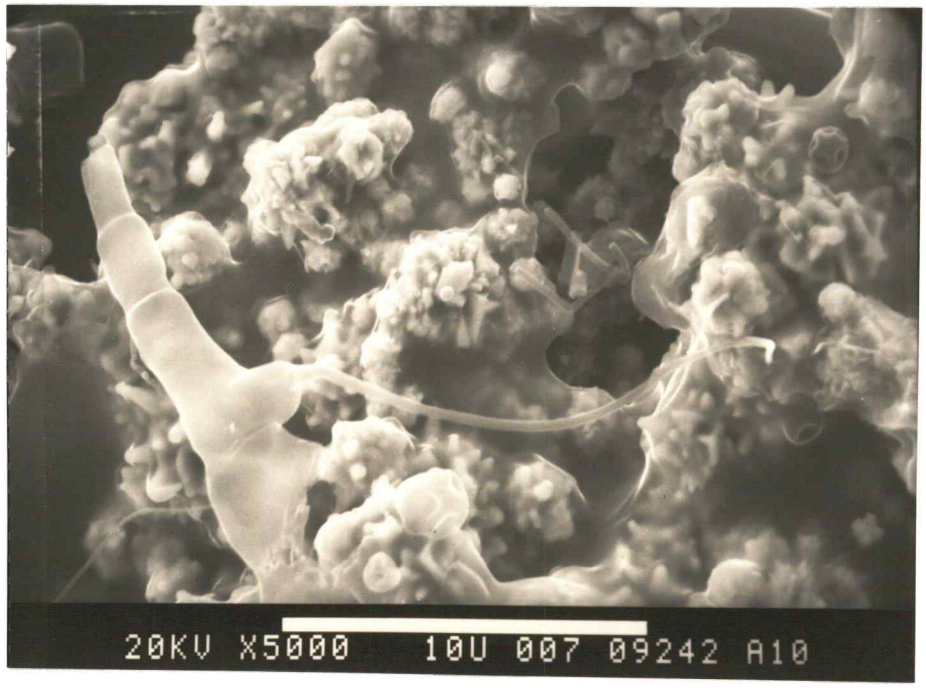

Figure 9.3e 5000X

9.2 MAGNETIC CHARACTERISTICS

9.2.1 MASS SUSCEPTIBILITY

Averaged values of mass susceptibility are found in Table 9.2. The mass susceptibility scales nearly linearly with the nickel loading of the sample (Figure 9.4).

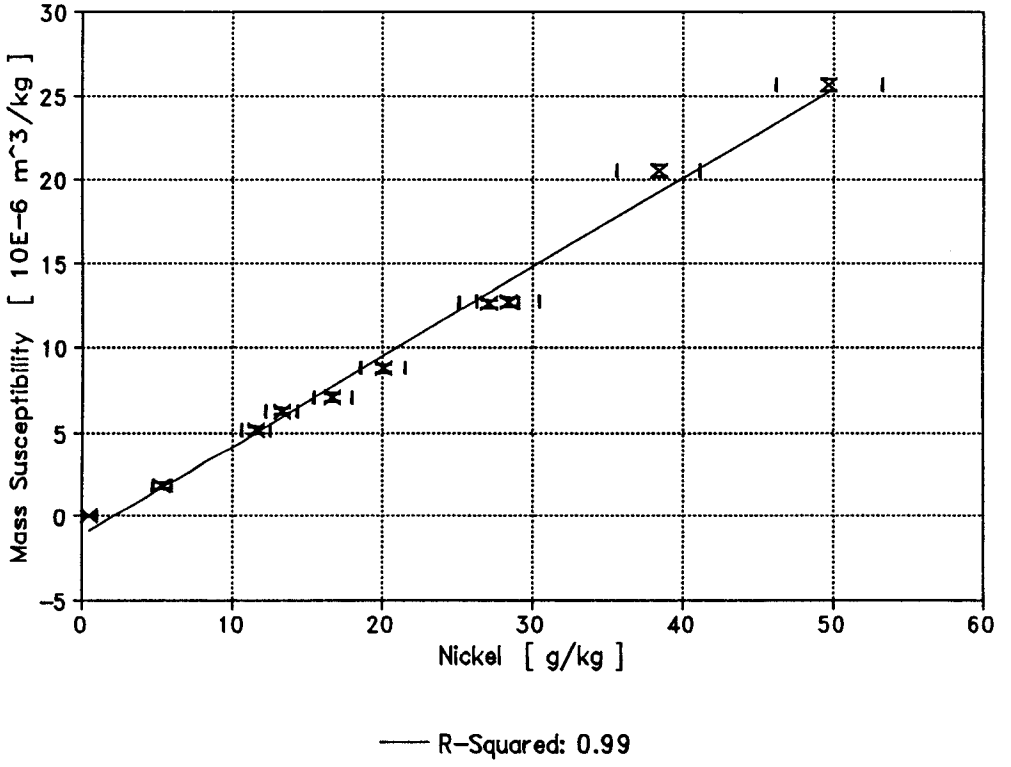

Figure 9.4 Mass susceptibility as a function of nickel concentration.

Table 9.2 Mass susceptibility.

Sample #	Mass Susceptibility [10E-6 m ^ 3/kg]
1	1.80 +/- 0.22
2	5.16 +/- 0.21
3	6.28 +/- 0.19
4	7.08 +/- 0.23
5	8.80 +/- 0.25
6	12.6 +/- 0.25
7	12.7 +/- 0.25
8	20.6 +/- 0.32
9	25.7 +/- 0.34
Control	-0.001 +/- 0.02
Ni-powder	459 +/- 15

9.2.2 SIRM MEASUREMENTS

Averaged values of the remanence mass-magnetization after excitation with 0.3T may be found in Table 9.3. Figure 9.5 shows the SIRM as a function of nickel loading of the samples; this exhibits a near linear relationship.

The SIRM of nickel on the wood particles can be inferred by combining SIRM data for the wood particles with the known nickel concentration of each sample; a value of 5.4 ± 0.5A*m^2/kg results. This compares well with the average SIRM value of 5.8Am^2/kg obtained for the two Ni-powder samples. Using this value, and assuming the bulk

density of nickel to be 8860kg/m^3, then a remanent magnetization field strength of 0.06 T is obtained. This value is one order of magnitude smaller than the saturation magnetization for pure nickel and is smaller than the theoretically expected factor of about 2 (Chen, 1977).

Table 9.3 Saturation isothermal remanence mass magnetization (SIRM).

Sample #	SIRM
	[10E-3 Am^2/kg]
1	24.3 +/- 0.5
2	58.7 +/- 1.2
3	75.8 +/- 1.5
4	85.3 +/- 1.7
5	104.0 +/- 2.1
6	147.9 +/- 2.9
7	146.8 +/- 2.9
8	250.2 +/- 5.0
9	300.5 +/- 6.5
Control	-0.2 +/- 0.0
Ni-powder	5804.3 +/- 165.3

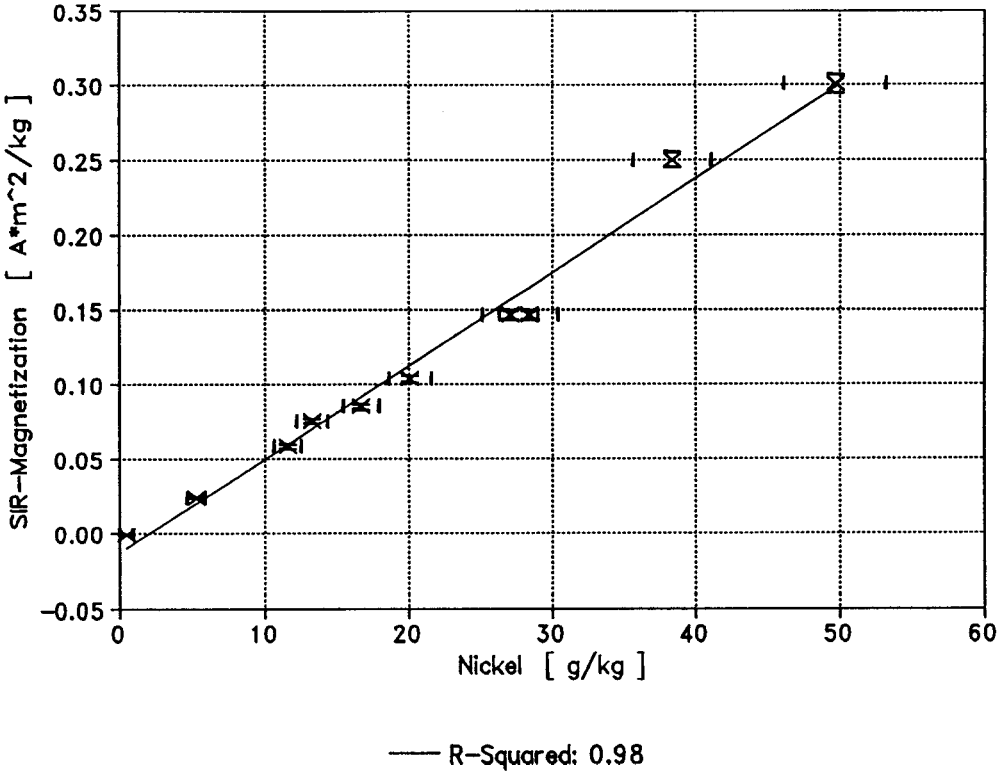

Figure 9.5 Saturation isothermal remanence (SIR) magnetization as a function of nickel concentration (expressed as mass magnetization).

9.2.3 COERCIVITY

A medium destructive field of 9.5mT is obtained by graphical interpolation from Figure 9.6.

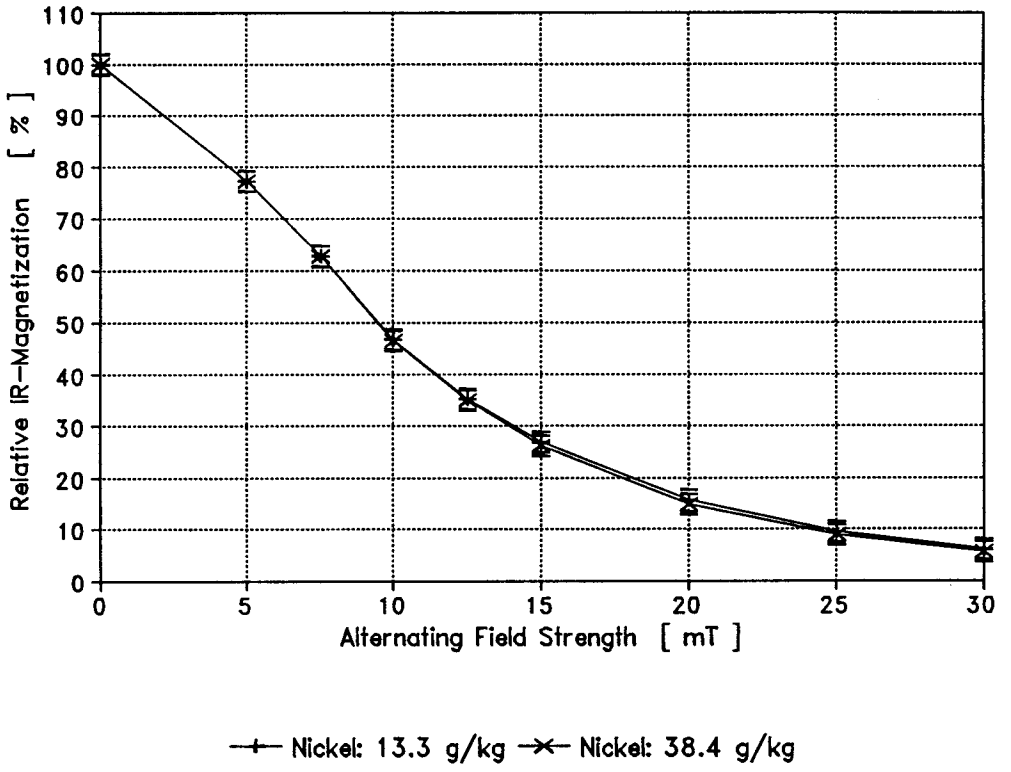

Figure 9.6 Relative isothermal remanence (IR) magnetization as a function of an alternating demagnetization field (sample #3, 13.3g/kg Ni and sample #8, 38.4g/kg Ni).

This value corresponds to about 7600A/m which indicates that the nickel coating can not be considered a magnetically soft material; a value in this order is found, for example, for semi-hard Cr-Co-Fe alloys (Boll, 1979).

Remanence and coercivity are expected to differ from values found for pure nickel in a homogeneous sample. Firstly, particle size of the nickel (2-3μm) used in the coating will influence magnetic behavior and, although single domain size is about one order of magnitude smaller, the small particle size increases coercivity (Brown, 1962). Secondly, impurities are present in the nickel powder. These impurities are expected to hinder domain wall movement which, in turn, leads to increased coercivity. The saturation magnetization is, however, not affected; it is expected to have a value of 0.6T which is approximately that for the element nickel (Chen, 1977).

A high coercivity means that the wood particles act like permanent magnets after exposure to a magnetic field. This permanent magnetism was, in the course of the rotation experiments, found to be consequential and this led to a change in the experimental procedure (refer to Section 8.4.2). Figure 9.6 indicates that, within experimental error, there is no difference in the demagnetization behavior of particles having quite different Ni-concentrations on their surfaces.

Figure 9.7 shows the demagnetization behavior for the two Ni-powder samples and the wood particle samples. It can be seen (Figure 9.7) that the powder samples demagnetize with slightly smaller fields than the wood particles; however, the overall trend is very similar. The difference

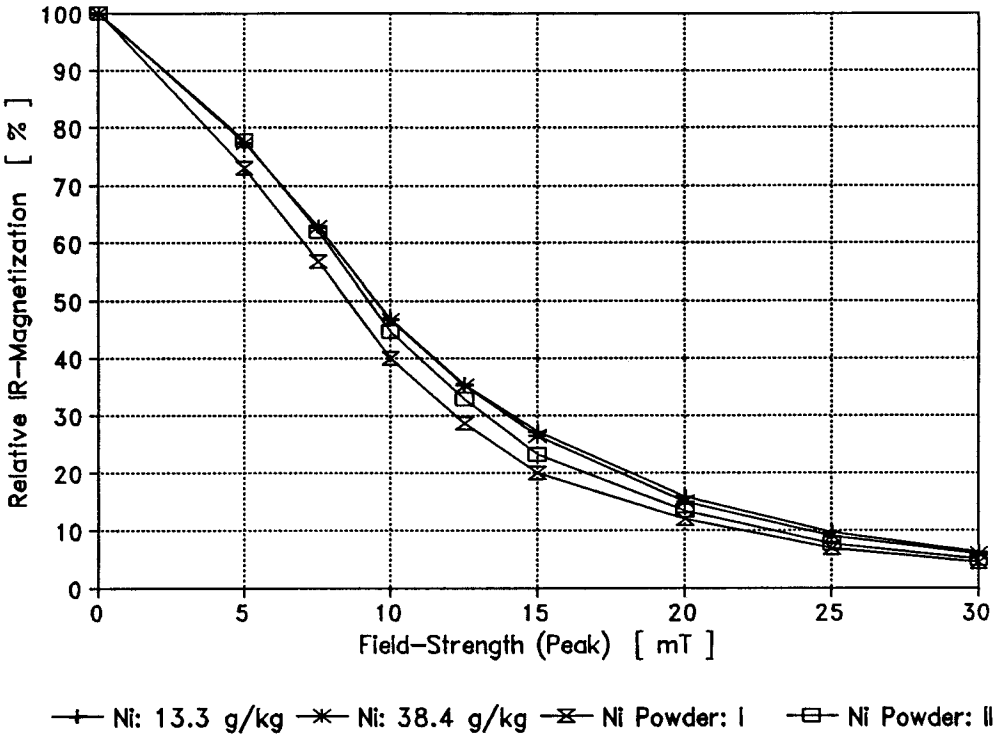

Figure 9.7 Relative isothermal remanence (IR) magnetization versus demagnetization field strength for Ni-powder samples and wood particle samples.

can be explained by considering the packing density of the Ni-powder in each of these samples; generally coercivity decreases with increasing density of the material.

These samples were prepared by suspending Ni-powder in a matrix of epoxy. However, the volume of the sample container was only partially filled with this suspension and this led to a considerably higher Ni-density compared with that of the modified wood samples.

9.2.4 MAGNETIZATION BEHAVIOR

The magnetization behavior is nearly identical among specimens with differing surface concentrations of nickel (Figure 9.8). A slight irregularity occurring at about 0.135T for both samples was confirmed by repeated remanence measurements. Interestingly, this irregularity is also apparent in published initial magnetization curves for nickel (Chen, 1977; Shine, 1982). Over 90% of saturation is reached at a field strength of 0.1T.

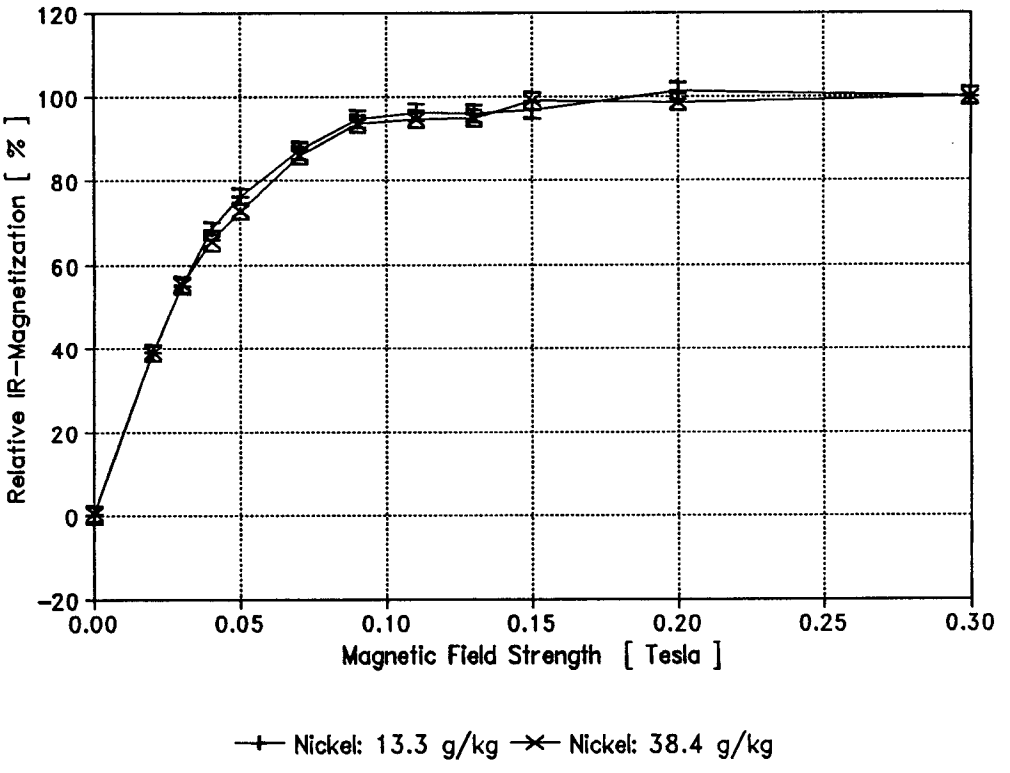

Figure 9.8 Relative isothermal remanence (IR) magnetization as a function of field strength (sample #3, 13.3g/kg Ni and sample #8, 38.4g/kg Ni).

9.3 RESULTS OF THE ROTATION EXPERIMENTS

9.3.1 MAXIMUM SHEAR RATE AND MAXIMUM REYNOLDS NUMBER

The assumption of newtonian fluid behavior is justified considering a maximum shear rate of $4.2 sec^{-1}$ (refer to Sections 7.2 and 9.3). This value was calculated using equation [9.1] (Shine, 1982),

$$(\partial\gamma/\partial t)_{max} = \omega_{max}\ l_{max}/\ 2\ d_{min} \qquad [9.1].$$

A maximal Reynolds number (refer to equation [6.6]) of $17*10^{-3}$ supports the assumption of negligible particle and fluid inertia (refer to section 6.2). Both values are the maximum found considering all experimental runs.

9.3.2 CHOICE OF CONTAINER DIAMETER

A decrease of $max.T^{(m)*}$ with decreasing inner diameter (ID) of the sample container was found (Table 9.4). However, variability among repeated runs increased with decreasing diameters; this may have been due in part to inaccurate particle centering. Considering this, and the limited number of data points, the choice of 23.9mm ID was a compromise.

Table 9.4 Dependence of maximum specific magnetic torque on container diameter.

Diameter [mm]	Maximum Specific Torque [10E-3 N/m^2]
31.4	14.87
	15.24
25.4	15.36
	14.35
22.3	12.89
	15.25
20.1	13.31

9.3.3 REPEATABILITY OF EXPERIMENTAL RUNS AND VARIABILITY AMONG PARTICLES OF ONE TREATMENT

It was found (using linear regression, section 9.3.5) that an uncertainty in field strength of ±0.0001T leads to a variability of ±0.2% in max.$T^{(m)*}$. Slight differences in the field strengths of some experiments were therefore neglected to enable results to be combined. Table 9.5 summarizes results of three different experiments (refer to sections 8.6.2, 8.6.3 and 8.6.5) analyzed with respect to repeatability and variability among particles.

The percent change in max.$T^{(m)*}$ for repeated runs of one particle is based on the average value and calculated using the standard deviation. For comparison of max.$T^{(m)*}$ among different particles, repeated runs have been averaged.

Table 9.5 Repeatability of experimental runs and variability among particles of one treatment batch.

		Variability of Maximum Specific Magnetic Torque [%]			
Experiment	Sample	Repeated Runs	Replication	Among Particles	# of Particles
*	1	-	-	-	-
	2	+/- 3.5	3	+/- 4.3	2
	3	+/- 1.4	2	+/- 57.9	2
	5	+/- 0.9	2	+/- 24.1	3
	6	-	-	+/-16.8	4
	8	-	-	+/- 10.1	4
	9	+/- 1.3	2	+/- 0.1	2
**	5 Avg.	+/- 1.2	8	+/- 23.4	5
***	5 Avg.	+/- 1.0	6	-	-

* Influence of Ni-concentration on maximum specific torque. (8.6.5)
** Variability among samples of one treatment batch. (8.6.3)
*** Linear scaling of magnetic torque with viscosity. (8.6.2)

It can be seen that differences among particles are very much larger than the uncertainties exhibited among repeated runs for the same particle. This suggests that there is variability in the content, distribution or nature of nickel on the particles.

Variability in size among particles is assumed to have only a very minor influence. However, a systematic study of this influence has not been undertaken in the present research. The repeatability error increases for low loading levels at constant field strength. This can be explained by the increasing likelihood of particle misalignment (out of XY-plane) and resulting changes in hydrodynamic behavior due

to increasing rotation times caused by low loading levels. A more thorough statistical evaluation was not performed because of the small number of data points available.

9.3.4 LINEAR SCALING OF MAGNETIC TORQUE WITH VISCOSITY

A range of unscaled but fitted data curves for rotation versus time are compared in Figure 9.9a. A scaling factor was calculated by correcting fluid viscosity for temperature and adjusting it to an arbitrarily chosen viscosity of

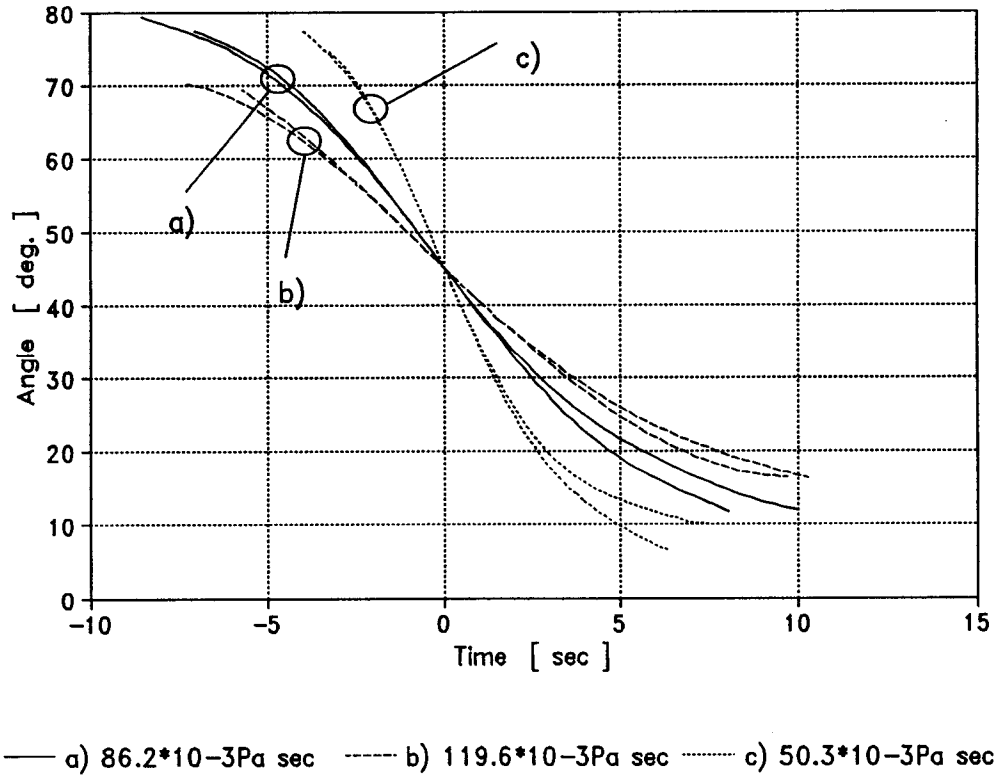

Figure 9.9a Fitted angular displacement versus time for a range of viscosities.

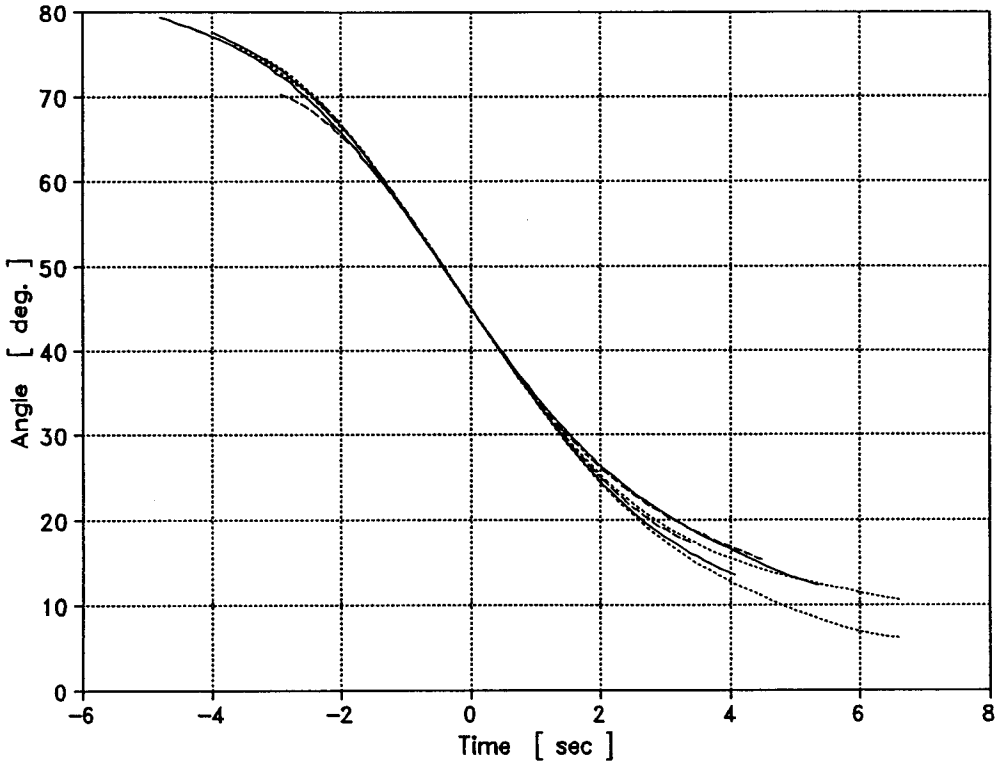

Figure 9.9b Fitted angular displacement versus time for the range of fluid viscosities shown in figure 9.9a, but <u>after</u> correction to a common viscosity of $50*10^{-3}$Pa sec.

$50*10^{-3}$Pa sec. The time axis for each single curve was then multiplied by its corresponding factor (Figure 9.9b). These figures illustrate that particle rotation scales almost linearly with viscosity. The values of max.$T^{(m)*}$ obtained by this procedure may be seen in Table 9.6; they indicate that equation [7.15] describes the specific magnetic torque adequately.

It can be seen (Figure 9.9a) that the slopes of repeated runs [a), b) or c)] differ at angles below about 30°. This discrepancy can only be explained partly -- in

Table 9.6 Maximum specific magnetic torque at three viscosities after scaling.

Fluid #	Maximum Specific Torque After Scaling [10E-3 N/m^2]
1	10.00 10.01
2	9.95 10.17
5	10.12 10.31
Avg. Torque:	10.10 +/- 0.14

terms of variations in the fluid viscosity -- and are believed to have their origin in a permanent magnetization obtained by the particle (refer to section 9.3.8). This observation prompted the demagnetization procedure discussed in section 8.4.2. However, considering the slopes in Figure 9.9b, the magnitude of max.$T^{(m)*}$ is not affected.

9.3.5 FIELD STRENGTH DEPENDENCE OF SPECIFIC MAGNETIC TORQUE

Max.$T^{(m)*}$ is plotted as a function of field strength for samples #8 and #3 in Figures 9.10a and 9.10b respectively. The maximal error about each data point is estimated to be approximately ±2% for sample #8 (Figure 9.10a) and ±4% for sample #3 (Figure 9.10b).

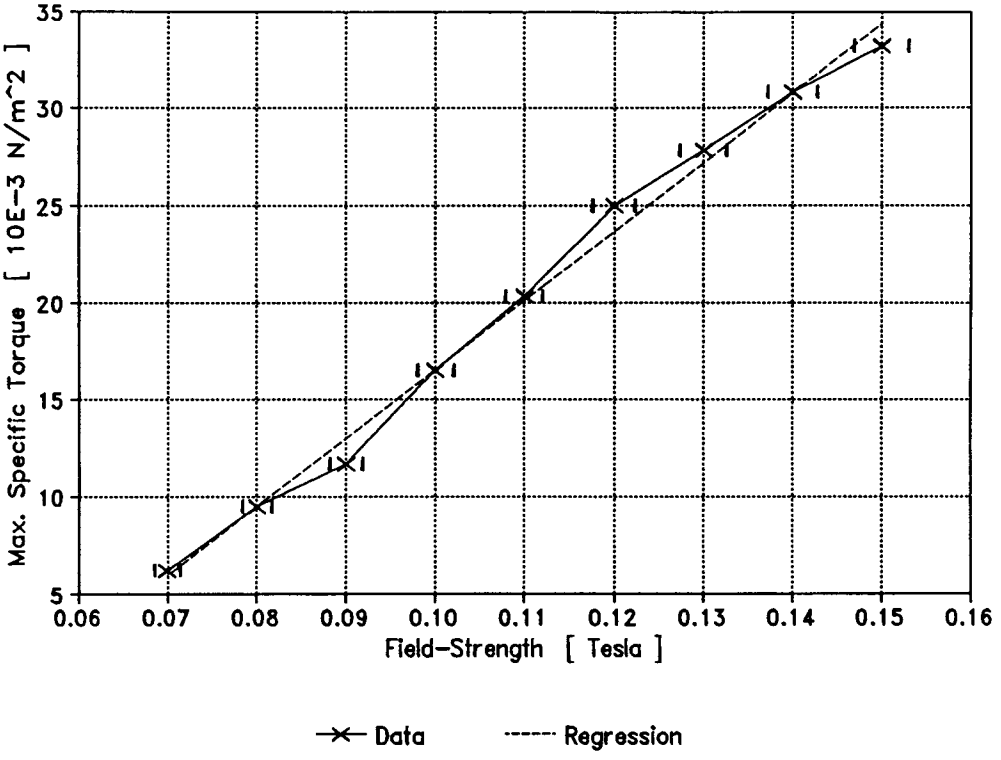

Figure 9.10a Specific magnetic torque maxima as a function of magnetic field strength (sample #8, 38.4g/kg Ni).

The magnetic torque may be seen to increase nearly linearly with increasing field strength from 0.08T to 0.14T (Figure 9.10a). A similar trend is seen for sample #3; however, a depression at field strengths of 0.12T and 0.13T is evident (Figure 9.10b). The slopes of both samples seem to be very similar, with the exception of sample #3 at 0.12T and 0.13T (Figure 9.11). Although no replication is available at these two field strengths, their magnitude is believed to be correct. With further increases of field strengths, asymptotic approach to a maximum torque value,

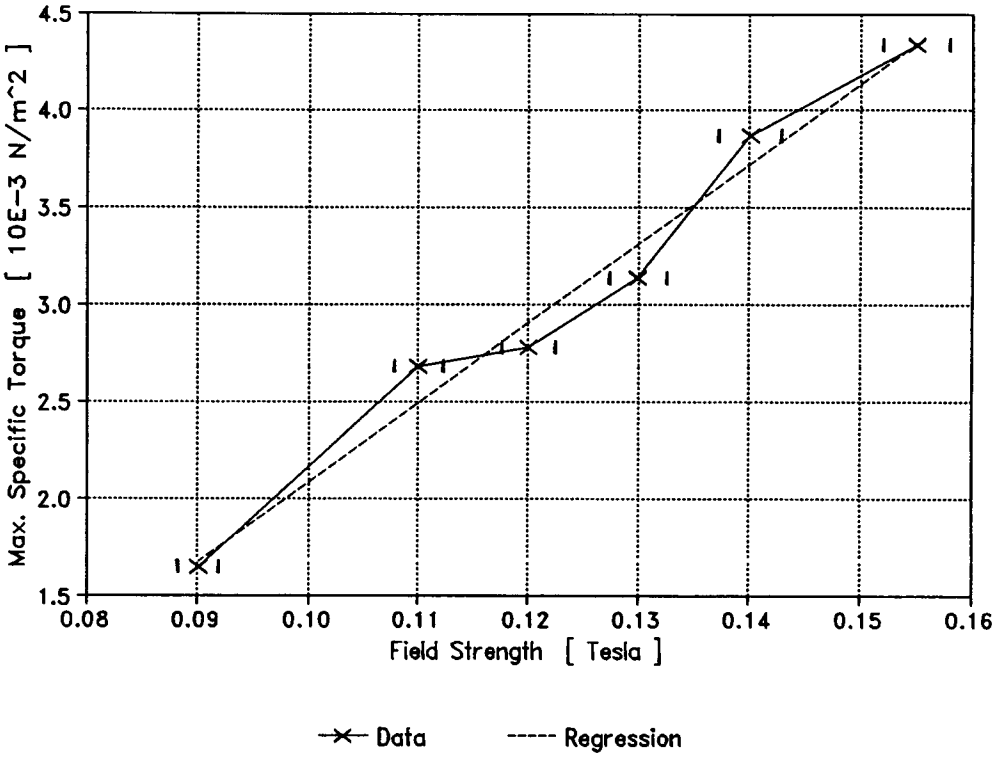

Figure 9.10b Specific magnetic torque maxima as a function of magnetic field strength (sample #3, 13.3g/kg Ni).

reached when the material is magnetically saturated, is expected. This is reached when the material becomes magnetically saturated and this trend is indicated in Figure 9.11. A flat 'S'-curve for the magnetic torque is predicted and this is because, with decreasing field strengths, the torque must approach zero.

Torque increases with increasing field strength and the maximum occurs at angles larger than 45°. Furthermore, angles at peak torque wander towards 45° with increasing

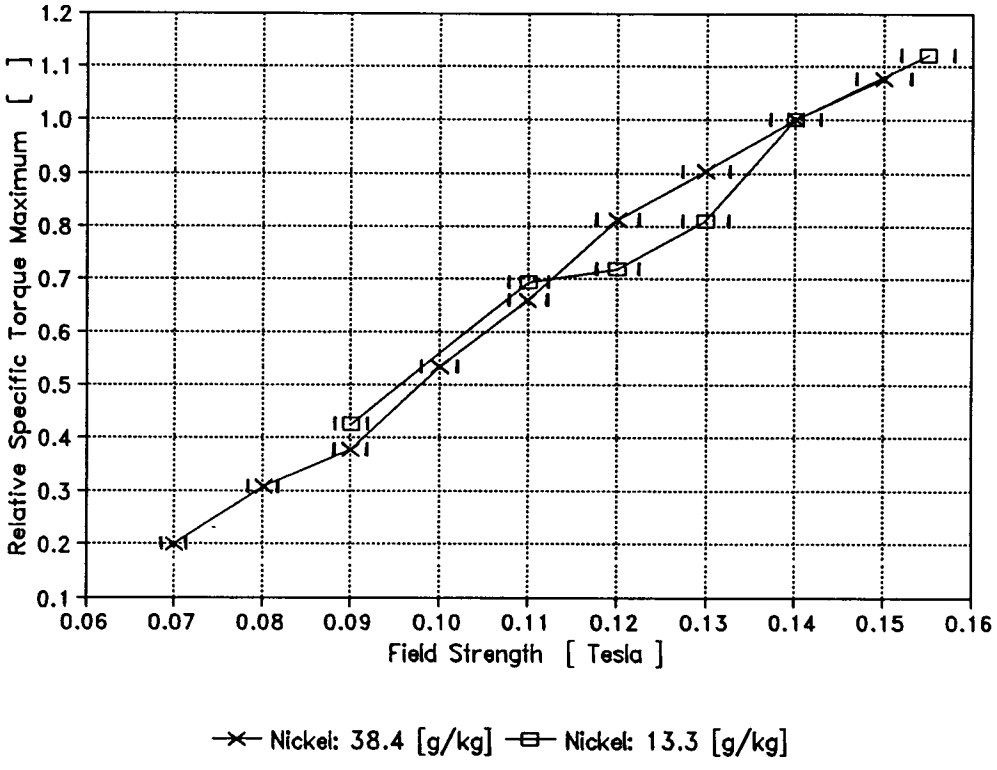

Figure 9.11 Relative specific magnetic torque maxima as a function of magnetic field strength (sample #3, 13.3g/kg Ni and sample #8, 38.4g/kg Ni).

field strengths (Figure 9.12). The increase in the angular position of max.$T^{(m)*}$ for the uppermost curve in Figure 9.12 (field strength of 0.15T) could not be explained satisfactorily. It may, however, be related to discontinuities in the bulk magnetization of nickel at a field strength of about 0.135T (Figure 9.8). The still increasing trend for max.$T^{(m)*}$ at field strengths above 0.1T suggests that the wood particles are not close to being magnetically saturated. This observation qualitatively

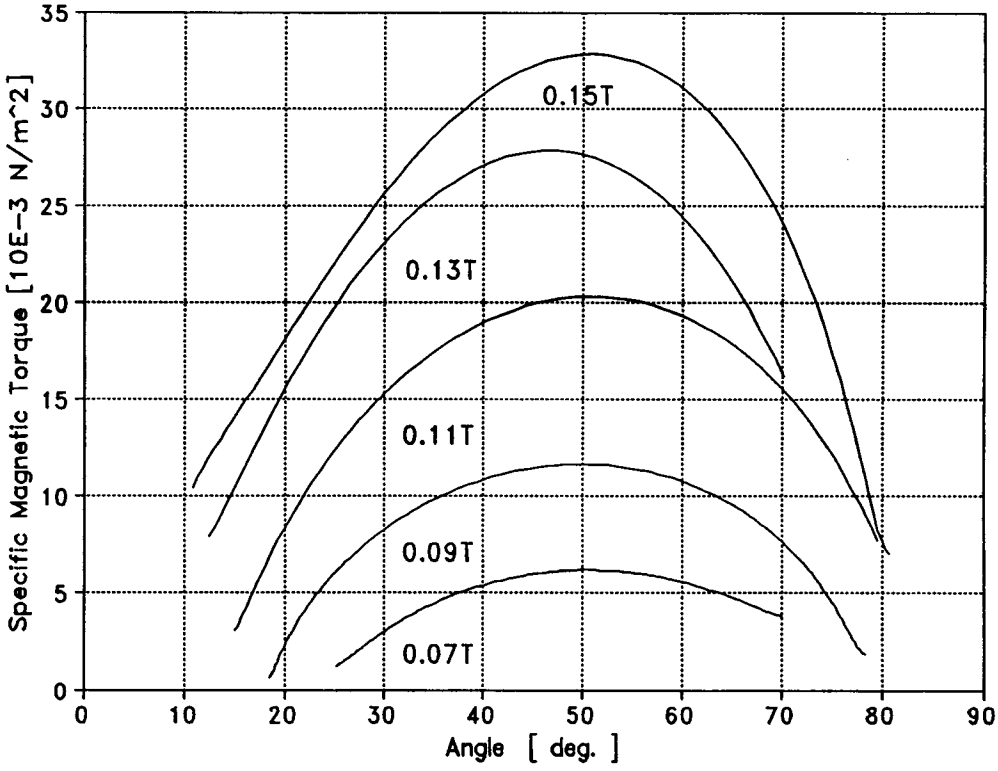

Figure 9.12 Specific magnetic torque as a function of angular position for a range of field strengths (sample #8, 38.4g/kg Ni).

confirms the existence of a demagnetizing field, requiring larger magnetic fields for magnetic saturation of the particles than for the material in bulk (refer to Section 5.3).

The range of field strengths used in the present experiments were limited by certain constraints. The upper bound was a maximum of 0.155T, above which stable fields could not be maintained with the magnet system developed for the research. Decreased field strengths led to longer rotation times and a balance between fluid viscosity and

disturbing, translational particle motion had to be found. Successful experimentation was therefore not possible below a certain limiting field strength.

9.3.6 DEPENDENCE OF MAGNETIC TORQUE ON PARTICLE TREATMENT

Results are summarized in Figure 9.13.

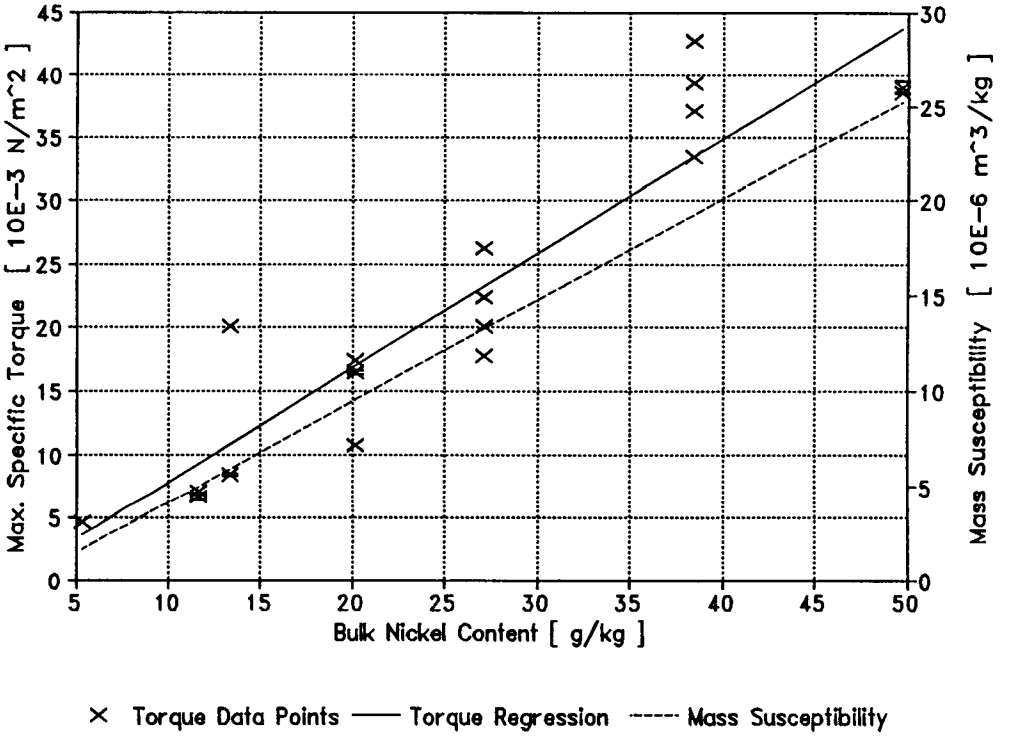

Figure 9.13 Dependence of the maximum specific magnetic torque on particle nickel treatment.

For repeated runs, max.$T^{(m)*}$ was averaged and plotted with error bars indicating the standard deviation from the mean.

Max.$T^{(m)*}$ is plotted as a function of the Ni-concentration found for each sample in bulk. Clearly, similarly treated particles exhibit considerable variability in their surface nickel concentrations (refer to section 9.3.2). A first order linear regression fit (r-squared: 0.87) to the data points does however suggest, to a first approximation, that max.$T^{(m)*}$ increases linearly with increasing Ni-loading. The linear first order regression found for the dependence of mass susceptibility is plotted for comparison. The similarity of the slopes for these curves suggests that a measurement of mass susceptibility may be used to predict the magnetic torque. This is of great practical importance and usefulness, since susceptibility measurements are relatively easily performed.

9.3.7 INFLUENCE OF CHANGE IN FIELD POLARITY ON MAGNETIC TORQUE

All preceding experiments were performed in static magnetic fields. It was found, however, that changing field polarity can increase magnetic torque and improve particle alignment. This phenomenon was most effective at alignment angles below 45°. Figure 9.14 demonstrates these effects by comparing two experimental runs using one particle. Polarity

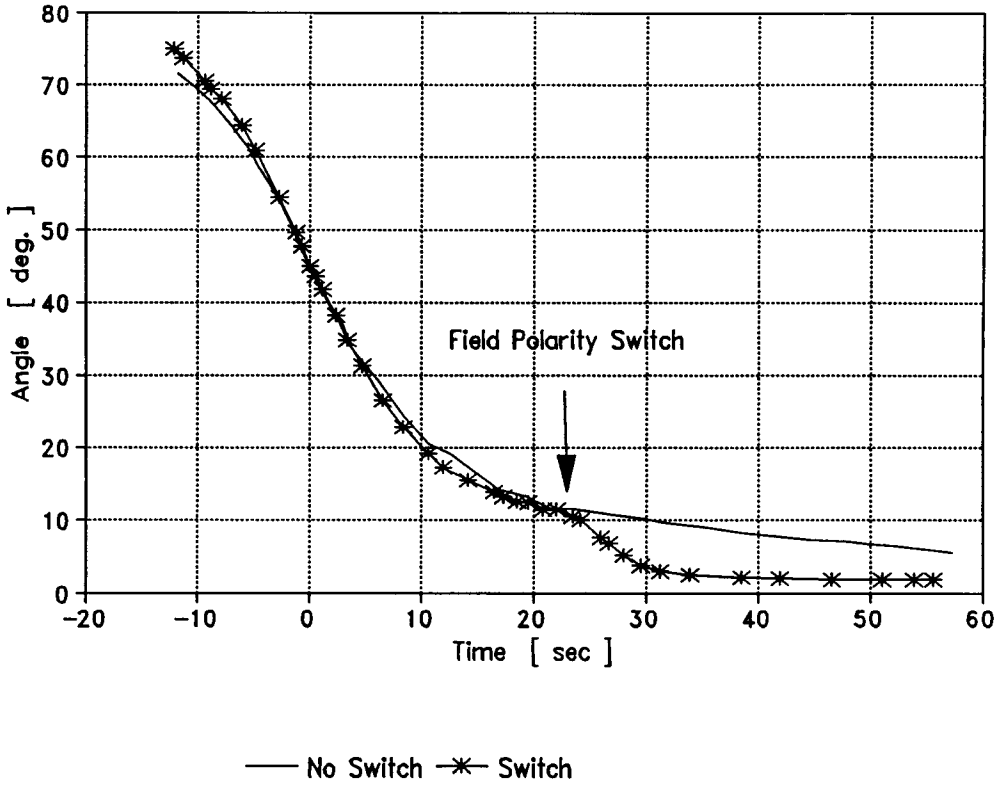

Figure 9.14 Angular displacement versus time for two runs using the same particle -- one in which the field was held constant and one where the field was switched.

was switched after the particle started to drift towards its final equilibrium position (about at 22 seconds).

The Hall-voltage, indicating magnetic field strength, was monitored with an oscilloscope during field switches. As expected on physical grounds, no surges in the magnetic field occurred; such surges could possibly have explained the increased torque. On the other hand, the state of magnetization of the magnetic material must have been profoundly changed. A possible explanation may therefore be

associated with some form of remagnetization process which could destroy unfavorably directed remanent magnetization which otherwise may prevent full alignment.

The increasing effectiveness of polarity switches with decreasing alignment angles may be explained in terms of magnetic shape anisotropy. The internal magnetic field governing magnetization increases with decreasing demagnetization fields, and these, in turn, become smaller the more the particle length axis aligns with the magnetic field lines. This effect, combined with a complete remagnetization after a change in polarity, could well cause an increase in magnetic torque with decreasing alignment angle. Even compared with anticipated particle orientation times, which are in the order of tenths of seconds, remagnetization times are very much smaller.

The use of alternating or judiciously switched magnetic fields may have great practical importance since shorter rotation times and higher torques are achievable. Inductive heating of the magnetic material could even be used to accelerate adhesive curing. However, frequency limits may arise depending on inductance of the magnet windings and physical construction of the yoke. The use of permanent magnets would, of course, be precluded.

9.3.8 INFLUENCE OF PERMANENT MAGNETIZATION ON PARTICLE ROTATION

It was found that rotation depends on the magnetic history of the particle. Scenarios for low and high fields will be considered in turn:

(1) Low Fields

A particle which was never before magnetized rotated under the influence of a magnetic field and came to rest in a stable equilibrium position. If this particle was repositioned in its initial location (nearly perpendicular to the magnetic field lines) and then released, then three possible responses were observed. In some cases rotational motion was merely retarded, in others it did not take place at all and occasionally reversal in the direction of rotation even occurred.

(2) High Fields

At high fields, rotation always took place -- irrespective of prior history. However, if the particle, after it reached its final equilibrium position, was further rotated manually to full alignment with the field lines and then released, it rotated back into its former misaligned

position. This indicates that it is energetically more advantageous for the particle to rest in a not fully aligned equilibrium position.

The above behavior may possibly be the consequence of unfavorably oriented permanent magnetization which impedes particle rotation. This hypothesis seems justified considering the high coercivity found for the particles (refer to Section 9.2.3).

Some experiments were performed without particle demagnetization (refer to Section 8.4.2). However, the field strengths used in these experiments were high enough so that discrepancies due to permanent magnetization were observable only for alignment angles below 30°. The magnitude of max.$T^{(m)*}$ seemed not to be influenced in these cases.

Chapter X

CONCLUSIONS OF THE RESEARCH

10.1 THE NATURE OF PARTICLE-FIELD INTERACTIONS

LC-particle orientation under the influence of a magnetic field has been shown to be feasible if the particles are magnetically modified. Modification can be achieved by a spray coating process. An experimental method, developed in the present research, enabled the magnetic torque as a function of several influence variables to be studied. This was achieved in a simple, non-intrusive way by video filming particle rotation. The characteristic maximum of the specific magnetic torque is a sensitive variable for comparison of experimental results. Repeatability error for this method is about ±2%. However, mismatch between particle buoyancy and fluid density imposes a lower bound on the range of observable particle modification - field strength combinations.

Analytically derived predictions for the magnetic torque on magnetically homogeneous particles of ellipsoidal shape were qualitatively confirmed.

In the present research it was, more specifically, demonstrated that:

(1) The maximum magnetic torque increases nearly linearly with field strengths below particle saturation in the range from 0.07T to 0.14T.

(2) The magnetic torque has its maximum at a characteristic angle somewhat above 45°.

(3) The maximum magnetic torque increases nearly linearly with increasing concentration of magnetic material and the easily measurable mass susceptibility can be used to predict its magnitude.

(4) A permanent magnetic moment within the particle may interfere with alignment at low field strengths.

(5) Magnetic field reversal during particle rotation increases magnetic torque, decreases alignment time and improves (reduces) ultimate static alignment angles.

(6) The concentration of ferromagnetic material (nickel) used in the research has no effect on the magnetic characteristics of the wood particles.

(7) Magnetic torque on LC-particles may, for practical purposes, be assumed to be independent of MC.

(8) The successful orientation of LC-particles in a viscous fluid suggests that fiber orientation in polymer melts using LC fibers as reinforcing materials is feasible.

10.2 APPLICABILITY OF RESULTS TO LC FIBER ORIENTATION IN LOW VISCOSITY FLUIDS

The equation of motion for particle rotation in low viscosity media may be augmented by a term accounting for the inertial torque. Furthermore, the hydrodynamic torque term is changed to account for pressure drag. However, the magnetic torque and its dependencies discussed above remain unchanged.

For practical LC fiber alignment, short orientation times are an objective. In this case, the inertial torque term is important and increases more rapidly with increasing aspect ratio compared with the hydrodynamic torque. When low viscosity media are used, lower magnetic loading levels and/or magnetic fields may be used to obtain the desired alignment. However, more experimental work and a different experimental method than that proposed in this research is needed to investigate these interdependencies further.

10.3 APPLICABILITY OF THE EXPERIMENTAL METHOD TO FIBER ORIENTATION IN VISCOUS FLUIDS

The proposed experimental method may prove to be very useful for the evaluation of magnetic torques achievable in viscous media, such as polymer melts. This is because, with higher viscosities the mismatch between fiber buoyancy and fluid density is further reduced. However, elevated field strengths or nickel loading levels (or a combination thereof), will be necessary to achieve rotational motion. Furthermore, the approach is not limited to particular types of fibers. Indeed, it is likely that torque on nearly any magnetically modified or inherently magnetic fiber or particle could be investigated by the techniques developed in the present research.

BIBLIOGRAPHY

Anonym.. 1971. National Semiconductor Linear Brief 15: High Stability Regulators. National Semiconductor Corporation, Santa Clara, CA.

Atkins, P. W. 1990. Physical Chemistry, 4th ed.. W. H. Freeman and Company, New York, NY.

Bibbo, M. A., S. M. Dinh and R. C. Armstrong. 1985. Shear Flow Properties of Semiconcentrated Fiber Suspensions. Journal of Rheology 29(6):905-929.

Bird, B. R., W. E. Stewart and E. N. Lightfoot. 1960. Transport Phenomena. John Wiley & Sons, Inc., New York, NY.

Bloom, A. L. and M. E. Packard. 1955. Magnets and Magnetic Field Measurements. Science 122(3173):738-741.

Boll, R., editor. 1979. Soft Magnetic Materials. Siemens AG, Berlin and München; Heyden & Son Ltd, London.

Brenner, H. 1962. Effect of Finite Boundaries on the Stokes Resistance of an arbitrary Particle. Journal of Fluid Mechanics 12(1):35-48.

_____. 1963. The Stokes Resistance of an Arbitrary Particle. Chemical Engineering Science 18(1):1-25.

Brown, W. F. 1962. Magnetostatic Principles in Ferromagnetism. In: Selected Topics in Solid State Physics, Vol. I. Wohlfarth, E. P., editor. North-Holland Publishing Co., Amsterdam.

Chen, C. 1977. Magnetism and Metallurgy of Soft Magnetic Materials. In: Selected Topics in Solid State Physics, Vol. XV. Wohlfarth, E. P., editor. North-Holland Publishing Co., Amsterdam, New York, Oxford.

Della Torre, E. 1985. Fine Particle Micromagnetics. IEEE Transactions on Magnetics 21(5):1423-1425.

Demetriades, S. T. 1958. Effect of Electrostatic Fields on the Orientation of Colloidal Particles Immersed in Shear Flow. Journal of Chemical Physics 29(5):1054-1063.

Ewing, J. A. 1894. Magnetic Induction in Iron and Other Metals, 2nd ed.. The D. Van Nostrand Company, New York, NY.

Forgacs, O. L., A. A. Robertson and S. G. Mason. 1958. The Hydrodynamic Behaviour of Papermaking Fibres. In: Transactions of the Symposium held by the Technical Section of the British Paper and Board Makers' Association at Cambridge, September 1957. Bolam, F., editor. The British Paper and Board Makers' Association Inc., Kenney, Surrey, UK. 447-487.

Frühwald, A. 1992. Personal communication. Ordinariat für Holztechnologie, Universität Hamburg, Hamburg, FRG.

Green, H. V., T. J. Fox and A. M. Scallan. 1982. Lumen-loaded Paper Pulp. Pulp & Paper Canada 83(7):39-43.

Habermehl, S., D. C. Jiles and C. M. Teller. 1985. Influence of Heat Treatment and Chemical Composition on the Magnetic Properties of Ferromagnetic Steels. IEEE Transactions on Magnetics MAG-21(5):1909-1911.

Hatta H. and S. Yamashita. 1988. Fiber Orientation Control by Means of Magnetic Moment. Journal of Composite Materials 22(5):484-500.

Jacobs, I. S. and C. P. Bean. 1955. An Approach to Elongated Fine-Particle Magnets. Physical Review 100(4):1060-1067.

Jeffery, G. B. 1922. The Motion of Ellipsoidal Particles Immersed in a Viscous Fluid. Proceedings of the Royal Society of London, Series A 102(A715):161-179.

Jones, R. M. Mechanics of Composite Materials. 1975. Hemisphere Publishing Corporation, New York, NY.

Joseph, R. I. and E. Schlömann. 1965. Demagnetizing Field in Nonellipsoidal Bodies. Journal of Applied Physics 36(5):1579-1593.

Kawai, S., H. Sasaki and M. Norimoto. 1987. Aligning Torque Generated on Wood Particles by an Electrostatic Field I.. Mokuzai Gakkaishi 33(11):872-878.

_____, H. Sasaki. 1989. Oriented Medium-Density Fiberboard Produced with an Electrostatic Field I.. Mokuzai Gakkaishi 35(3):218-226.

Kelly, A. and G. J. Davies. 1965. The Principles of Fibre Reinforcement of Metals. Metallurgical Reviews 10(37):1-75.

Klauditz, W., H. J. Ulbricht, W. Kratz and A. Buro. 1960. Herstellung und Eigenschaften von Holzspanwerkstoffen mit gerichteter Festigkeit. Holz als Roh- und Werkstoff 18(10):377-385.

Knoblach, G. M. 1989. Using Electric Fields to Control Fiber Orientation during the Manufacturing of Composite Materials. SAMPE Journal 25(6):9-16.

_____. 1990. Processing, Electric Fields for Fiber Orientation. In: International Encyclopedia of Composites, Vol. 4. Lee, S. M., editor. VCH Publishers, New York, NY. 413-424.

Lee, E. W. 1970. Magnetism - an Introductory Survey. Dover Puplications, Inc., New York, NY.

Levi, S. 1992. Personal communication. College of Oceanography, Oregon State University, Corvallis, OR.

Lin, T. R. 1973. Wood as an Orthotropic Dielectric Material. Wood and Fiber Science 5(3):226-236.

Lockett, F. J. 1980. Report: Predictions of Fibre Orientation in Moulded Components. National Physical Laboratory, Teddington, Middlesex, UK. NTIS Access Number: PB 83211250XSP. pp38.

Michell, A. J. 1986. Composites containing Wood Pulp Fibres. Appita 39(3):223-229.

Miura, Y. and J. Hosokawa. 1979. The Electrochemical Process in the Molding of Nonwoven Structures. Textile Research Journal 49(12):685-690.

Nagasawa, C., Y. Kumagai and K. Urabe. 1990. Electromagnetic Shielding Effectiveness of Particleboard Containing Nickel-Metalized Wood-Particles in the Core Layer. Mokuzai Gakkaishi 36(7):531-537.

_____, Y. Kumagai and K. Urabe. 1991. Electroconductivity and Electromagnetic Shielding Effectiveness of Nickel-Plated Veneer. Mokuzai Gakkaishi 37(2):158-163.

_____, Y. Kumagai, N. Koshizaki and T. Kanbe. 1992. Changes in Electromagnetic Shielding Properties of Particleboards, made of Nickel-Plated Wood Particles Formed by Various Pre-Treatment Processes. Mokuzai Gakkaishi 38(3):256-263.

Nilakantan, P. 1938. Magnetic Anisotropy of Naturally Occurring Substances. Proceedings of the Indian Academy of Sciences, Series A 7(1):38-49.

Okagawa, A., R. G. Cox and S. G. Mason. 1973. The Kinetics of Flowing Dispersions - VI. Transient Orientation and Rheological Phenomena of Rods and Discs in Shear Flow. Journal of Colloid and Interface Science 45(2):303-329.

_____ and S. G. Mason. 1973. The Kinetics of Flowing Dispersions - VII. Oscillatory Behavior of Rods and Discs in Shear Flow. Journal of Colloid and Interface Science 45(2):330-359.

_____, R. G. Cox and S. G. Mason. 1974. Particle Behavior in Shear and Electric Fields - VI. The Microrheology of Rigid Spheroids. Journal of Colloid and Interface Science 47(2):537-567.

_____ and S. G. Mason. 1974. Particle Behavior in Shear and Electric Fields - VII. Orientation Distributions of Cylinders. Journal of Colloid and Interface Science 47(2):568-587.

Pulido, O. R., S. Kawai, Y. Yoshida and H. Sasaki. 1990. Oriented Medium-Density Fiberboard Produced with an Electrostatic Field II.. Mokuzai Gakkaishi 36(1):29-35.

_____, Y. Yoshida, S. Kawai and H. Sasaki. 1991a. Aligning Torque Generated in Wood Particles by an Electrostatic Field IV.. Mokuzai Gakkaishi 37(2):135-141.

_____, H. Sasaki, S. Kawai and Y. Yoshida. 1991b. Oriented Mat-Former with High Voltage Electrode System II.. Mokuzai Gakkaishi 37(12):1167-1176.

_____, Y. Yoshida, Q. Wang, S. Kawai and H. Sasaki. 1991c. Aligning Torque Generated in Wood Particles by an Electrostatic Field V.. Mokuzai Gakkaishi 37(8):711-718.

Ricard, S. and R. H. Marchessault. 1990. Preparation of in situ Magnetically Loaded Cellulose Fibers. In: Materials Research Society Symposium Proceedings, Vol. 197. Materials Research Society, Pittsburgh, Pa. 319-325.

Rioux, P., S. Ricard and R. H. Marchessault. 1992. The Preparation of Magnetic Papermaking Fibres. Journal of Pulp and Paper Science 18(1):J39-J43.

Rose, M. E. 1938. Magnetic Field Corrections in the Cyclotron. Physical Review 53(5):715-719.

Roters, H. C. 1941. Electromagnetic Devices. John Wiley & Sons, Inc., New York, NY.

Rowell, R. M. 1990. Materials Science of Lignocellulosics. In: Materials Research Society Symposium Proceedings, Vol. 197. Materials Research Society, Pittsburgh, Pa. 3-9.

Schlesinger, M. 1974. The Basic Principles of Electroless Deposition. In: Science and Technology of Surface Coating. Chapman, B. N. and J. C. Anderson, editors. Academic Press, London and New York. 176-182.

Schwartz, M. and G. O. Mallory. 1976. Effect of Heat-Treatments on Magnetic Properties of Electroless Nickel Alloys. Journal of the Electrochemical Society 123(5):606-614.

Shine, A. D. 1982. The Rotation of Suspended Ferromagnetic Fibers in a Magnetic Field. Ph.D. Thesis, Massachusetts Institute of Technology, Cambridge, MA.

Stanley, J. K. 1963. Electrical and Magnetic Properties of Metals. American Society of Metals, Metals Park, OH.

Stratton, J. A. 1941. Electromagnetic Theory. Mc Graw-Hill Book Company, Inc., New York, NY.

Suchsland, O. and G. E. Woodson. 1987. Fiberboard Manufacturing Practices in the United States. Agriculture Handbook no. 640. U.S. Department of Agriculture, Forest Service, Washington, D.C..

Sutton, W. H. 1970. Principles and Methods for Fabricating Whisker-Reinforced Composites. In: Whisker Technology. Levitt, A. P., editor. Wiley-Interscience, a Division of John Wiley & Sons, Inc., New York, NY. 273-342.

Talbott, J. W. and E. K. Stefanakos. 1972. Aligning Forces on Wood Particles in an Electric Field. Wood and Fiber Science 4(3):193-203.

_____. 1974. Electrically Aligned Particleboard and Fiberboard. In: Proceedings of the 8th Particleboard Symposium. Maloney, T. M., editor. Washington State University, Pullman, WA. 153-182.

_____ and J. D. Logan. 1974. U.S. Patent 3,843,756 to Berol Corporation.

Weast, R. C., editor-in-chief. 1985. CRC Handbook of Chemistry and Physics, 66th ed.. CRC Press, Inc., Boca Raton, FL.

Wolff, E. G. 1969. Hydrodynamic Alignment of Discontinuous Fibers in a Metal Matrix. Fibre Science and Technology 1(4):307-323.

Yamashita, S., H. Hatta, T. Sugano and K. Murayama. 1989. Fiber Orientation Control of Short Fiber Composites: Experiment. Journal of Composite Materials 23(1):32-41.

Yoshida, Y., S. Kawai, O. R. Pulido and H. Sasaki. 1989. Production of Oriented Particleboard I.. Mokuzai Gakkaishi 35(3):227-233.

_____, O. R. Pulido, S. Kawai and H. Sasaki. 1988. Aligning Torque Generated in Wood Particles by an Electrostatic Field II.. Mokuzai Gakkaishi 34(5):401-408.

_____, O. R. Pulido, S. Kawai and H. Sasaki. 1990. Aligning Torque Generated on Wood Particles by an Electrostatic Field III.. Mokuzai Gakkaishi 36(7):523-530.

Zijlstra, H. 1967a. Experimental Methods in Magnetism - 1. Generation and Computation of Magnetic Fields. In: Selected Topics in Solid State Physics, Vol. IX. Wohlfarth, E. P., editor. North-Holland Publishing Co., Amsterdam; American Elsevier Publishing Company, Inc., New York, NY.

_____. 1967b. Experimental Methods in Magnetism - 2. Measurement of Magnetic Quantities. In: Selected Topics in Solid State Physics, Vol. IX. Wohlfarth, E. P., editor. North-Holland Publishing Co., Amsterdam; John Wiley & Sons, Inc. (Interscience Publishers Division), New York, NY.

APPENDICES

APPENDIX A

DESIGN OF A RESEARCH ELECTROMAGNET AND POWER SUPPLY

A.1 ELECTROMAGNET DESIGN

An electromagnet was specially designed and manufactured for the present research.

A.1.1 DESIGN APPROACH

A widely used type of magnet has cylindrical poles with coils immediately facing the air gap (Figure A1). The volume of high field uniformity depends, in part, upon the ratio of pole face diameter to gap width (Bloom and Packard, 1955; Zijlstra, 1967a). The magnitude of the field is determined by the overall size and effectiveness of the core as well as by the number of coil-windings and the current passing through them.

Scaling, using a well established design as a starting point, is the usual way in which large electromagnets are developed because leakage flux is difficult to calculate. For the estimation of the magnetic field between the poles by calculation, a magnetic potential approach is useful (Zijlstra, 1967a), and magnetic circuit calculations

(Roters, 1941) serve for the overall design of the core (consisting of yoke and pole pieces). These calculations often have to be solved by numerical or graphical methods since the magnetization characteristics of ferromagnetic materials are non-linear. In the design concept, the magnetic circuit can be considered separately from the coil design.

The coil provides the necessary magnetomotance (ampere-turns) to create and sustain a certain magnetic flux in the core material and across the air gap. The yoke and the pole pieces convey this magnetic flux in a fashion very similar to that operative in the transfer of electrons in an electric circuit. However, the magnetic circuit is not ideal and leakage flux occurs at material boundaries, especially in the gap region.

Generation of the largest possible magnetic flux in the gap under the constraint of available winding space and heating effects is the main objective in coil design.

A.1.2 PHYSICAL LAYOUT

DC electromagnets commonly used in research feature a double yoke construction which is mechanically very stable and has the additional advantage of providing symmetry in the magnetic circuit (Figure A1). In general, the pole gap

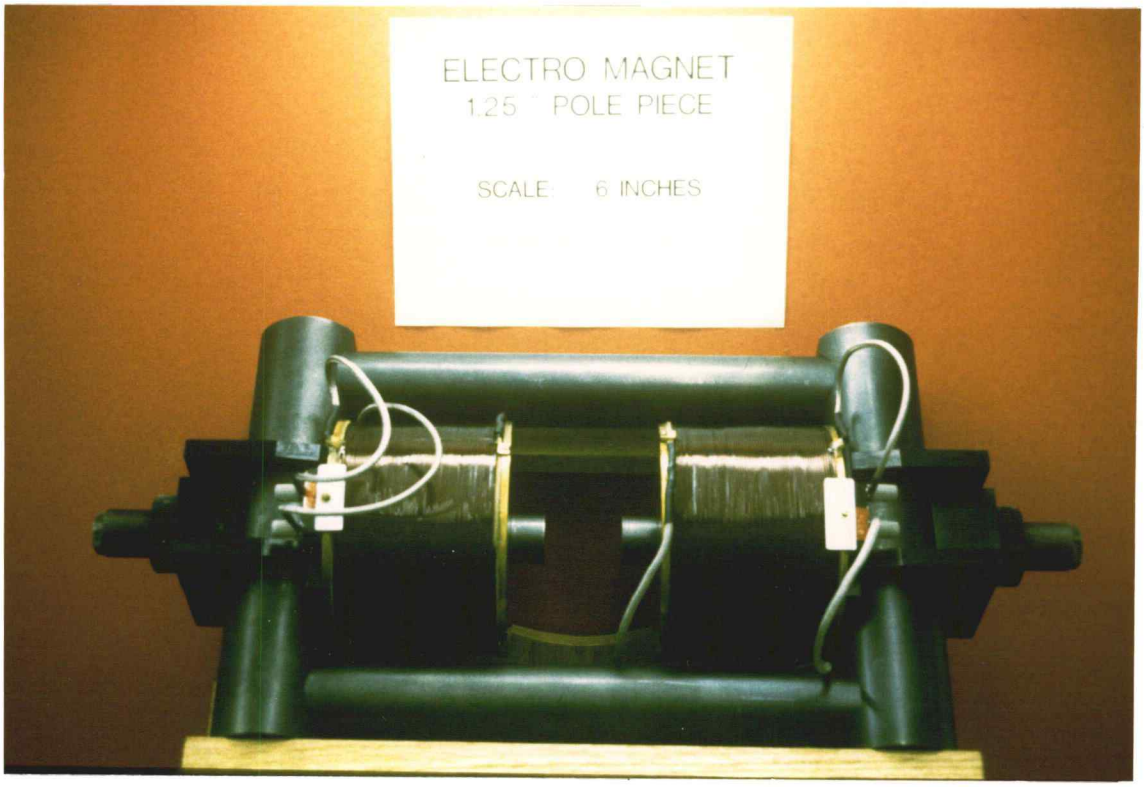

Figure A1 Electromagnet manufactured for the present research (pole piece diameter: 31.8mm).

is variable which requires the pole pieces to be moveable. To insure field uniformity, the pole faces must be absolutely parallel and of high surface quality (ground and polished). The material for the core, and especially for the pole pieces, is chosen so that a very high magnetization at negligible remanence is achievable. Heat-treatments are generally required to enhance these material properties.

In magnets were field uniformity is of importance, ring shims are used to supplement the field at the edges of the gap (Rose, 1938; Bloom and Packard, 1955).

Current requirements depend upon the size of the magnet and its projected gap field strength. When large currents are required, the coil assemblies must be force cooled to avoid electrical breakdown of the wire insulation and subsequent melting. The following section will describe the design of the electromagnet used in the present study and, in a separate section, the design of the associated power supply.

A.1.3 MAGNET REQUIREMENTS

(1) Performance

A uniform DC magnetic field across a variable gap (0 to 50mm) with a maximum field strength of about 0.2T at maximum gap width. Fields of 0.2T are sufficient to achieve saturation of many magnetically soft materials in bulk.

Yoke and pole pieces must be made of materials having a very small remanence and a high saturation magnetization. This requirement enables high field strengths to be achieved and minimizes the effects of residual magnetization at low field strengths.

(2) Physical Size

The overall dimensions of the magnet must be kept as small as possible so that access to the gap and transportation are facilitated.

(3) Power Requirements, Coil Cooling

The coils must be designed so that a 150W power supply (30V, 5A) can be utilized; this enables standard current-regulating integrated circuitry to be used. At maximum power input, the coils must dissipate the generated heat without being force-cooled.

A.1.4 DESIGN CALCULATIONS

A.1.4.1 MAGNETIC CIRCUITS

The magneto-static equations discussed in section 5.1 are applicable. The continuity of the magnetic field across boundaries leads to the following expression:

$$B_i A_i = B_j A_j \qquad [A1]$$

or equivalently:

$$\Phi_i = \Phi_j = \Phi \qquad [A2]$$

where Φ is the magnetic flux and the subscripts i and j refer to the discontinuity at the boundary (for example in a magnetic circuit). In the electric circuit analogy, the magnetic flux is equivalent to current. By use of Ampere's law [5.10] in integral form, and by converting the integral into a summation, the magnetic flux can be written:

$$\Phi = (N\ I)_{tot} / \sum_i R_i \qquad [A3]$$

where R_i is called the reluctance of part i of the circuit. Equation [A3] resembles Ohm's law and, in analogy, the reluctance is the resistance of the part i and the product of N and I, called magnetomotance, is the voltage. N represents the number of closed current loops and I is the current flowing through these. The reluctance can therefore be written:

$$R_i = l_i \ / \ \mu_r \ \mu_0 \ A_i \qquad [A4]$$

where l_i is the length of part i of the magnetic circuit, μ_r is the relative permeability of this part, and A_i is its cross-sectional area. With these equations a magnetic circuit comprising i individual parts may be calculated. In this process use can be made of tabulated values, numerical

methods, or graphical methods to account for non-linearities in the B versus H relationship.

The contribution to overall magnetic resistance from joints can be large. Ewing (1894) suggests that this resistance is due in part to a decrease in permeability in interfacial regions and also depends on surface roughness. It was found (Ewing, 1894) that under compression stress the magnetic resistance of a smooth joint decreases much more than that for a rough joint. This result suggests that the number of parts forming the yoke should be kept to a minimum and that their surfaces should be faced precisely. In the present case, joints are modelled as equivalent air gaps and values given by Ewing (1894) have been used.

The magnetic circuit representation of the electromagnet is shown in Figure A2. The gap in the center is depicted as a parallel circuit; this is necessary to account for fringe losses in the gap region. This particular circuit representation does not take into account losses which occur elsewhere. The total magnetic flux generated must be partitioned into useful- and fringe flux fractions. In the next step of the design procedure, the fringe flux must be evaluated. This is a difficult problem and only estimates can be obtained using the geometric properties in the gap region and by determining the most probable flux paths (Roters, 1941). The idealized gap geometry is depicted in a cross-sectional view in Figure A3.

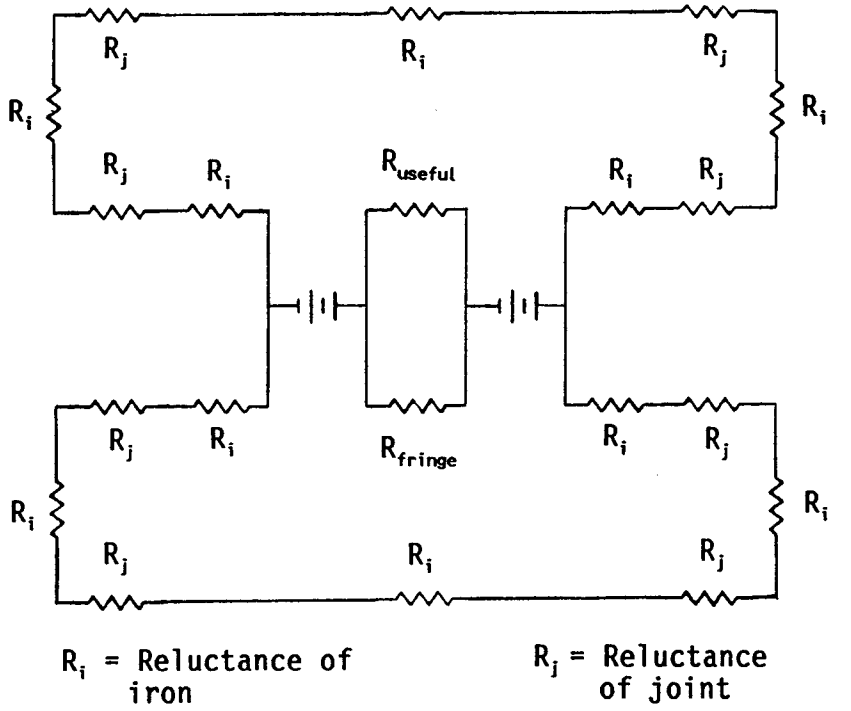

Figure A2 Magnetic circuit representation of the constructed H-yoke electromagnet.

Region 1 in Figure A3 indicates the volume of useful flux, while regions 2 and 3 indicate the volumes of the fringe flux; the broken lines are the mean path of the magnetic flux.

With these relations, an effectiveness factor ϵ, can be calculated:

$$\epsilon = P_{useful} / (P_{useful} + P_{fringe}) \qquad [A5]$$

where P stands for permeance which is the inverse of the

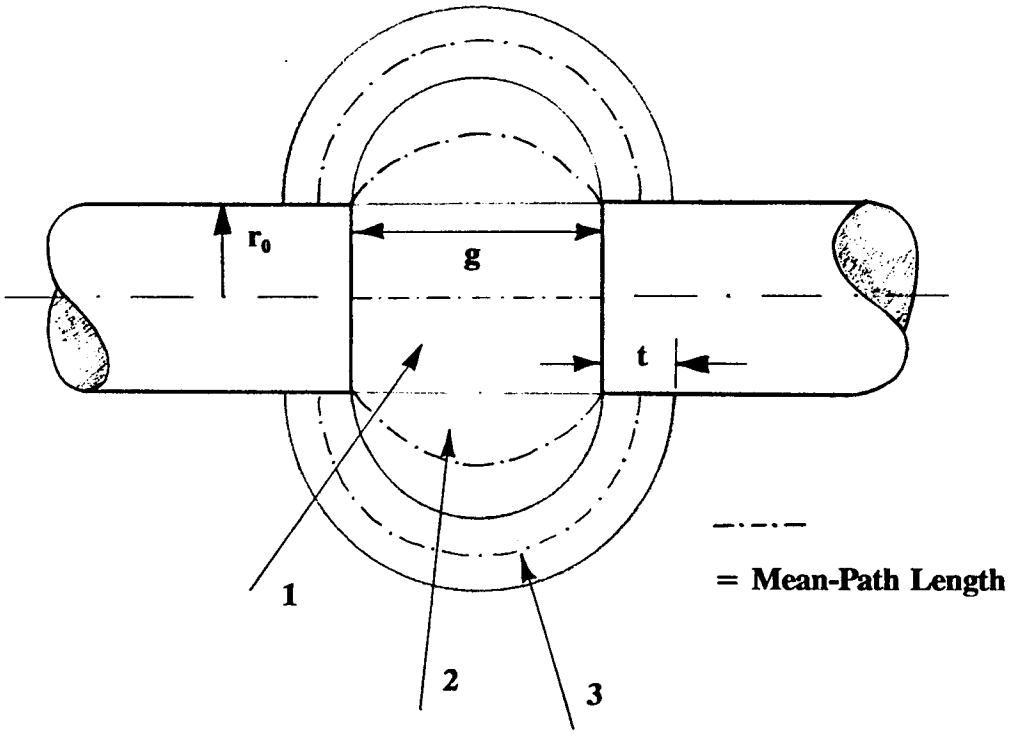

Figure A3 Idealized gap geometry, two dimensional view (the mean path of the magnetic flux is indicated by dashed lines in each region).

reluctance. The following relation was found for the effectiveness factor:

$$\epsilon = r_0 / (r_0 + 0.168\ \pi\ g + (4\ t\ g\ /\ (g + t)\ \pi)) \qquad [A6]$$

where r_0 is the radius of the pole piece and t and g are defined as in Figure A3.

An effectiveness factor of 0.30 has been determined for the present design, meaning that only 30% of the total

generated flux is useful at maximum gap width. The total magnetomotance to sustain a specified useful magnetic flux in the air gap is the sum of the magnetomotance necessary for the yoke and for the air gap, including the contribution necessary for the fringe flux. The contribution of the yoke to the magnetomotance is generally small when compared with that required for the air gap and, to a first approximation, can be neglected in the coil design. For the physical layout (Figure A4), a total magnetomotance of 8300 Ampere Turns has been calculated.

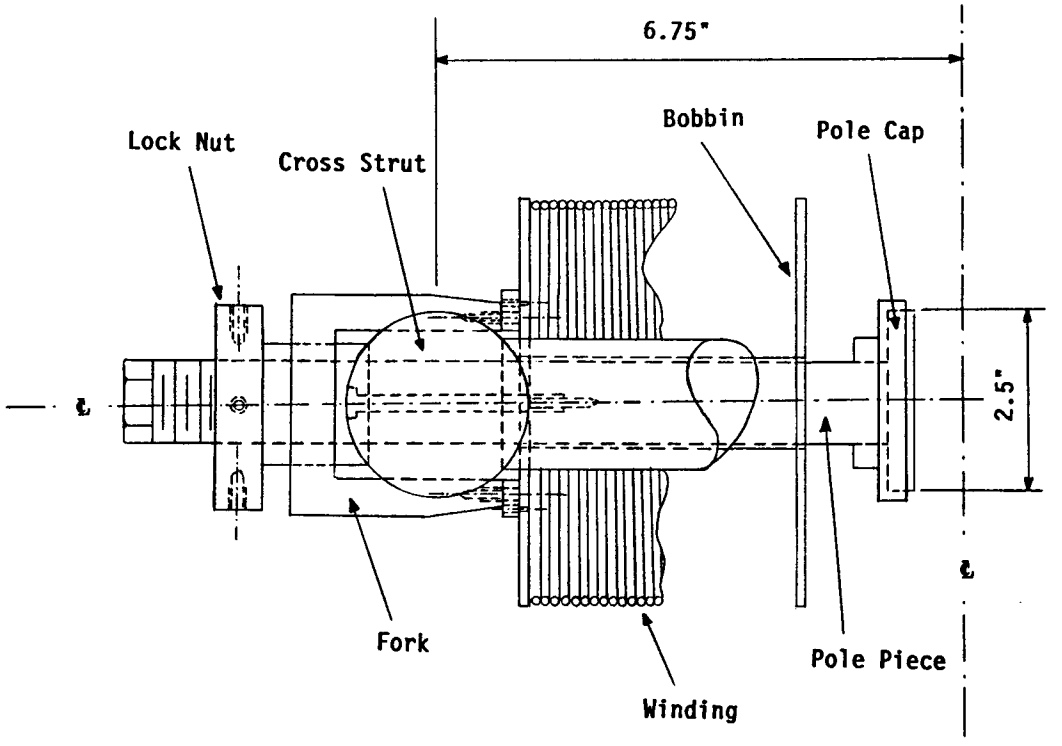

Figure A4 Cross sectional view of the electromagnet (not to scale).

A.1.4.2 COIL CALCULATIONS

The windings of an electromagnet have to be designed so as to meet the required magnetomotance in light of available power, winding space and heating effects. In many cases the coils of electromagnets are bobbin-wound and, depending on their size, sectioned and force cooled by liquids. Several relations pertaining to bobbin geometry, wire size, insulation thickness and winding mode can be established (Roters, 1941). Factors are applied to allow for embedding of the windings as well as losses due to reversal of winding direction (layer loss).

With respect to field homogeneity and coil efficiency, orthocyclic winding of the coils is favorable. In this method of winding, the plane of the turns is exactly perpendicular to the coil axis - - the transition from one turn to the next is made by a short jump. The coil is wound by layers and each wire turn lies in the groove of the wires forming the previous layer (Zijlstra, 1967a) (Figure A5). The high packing density of the copper winding which is attained with this approach improves heat transfer throughout the coil. But, compared with the thermal conductivity of copper (400W/ m K), the effective thermal conductivity of the assemblage is still low, at about 1W/ m K (Zijlstra, 1967a).

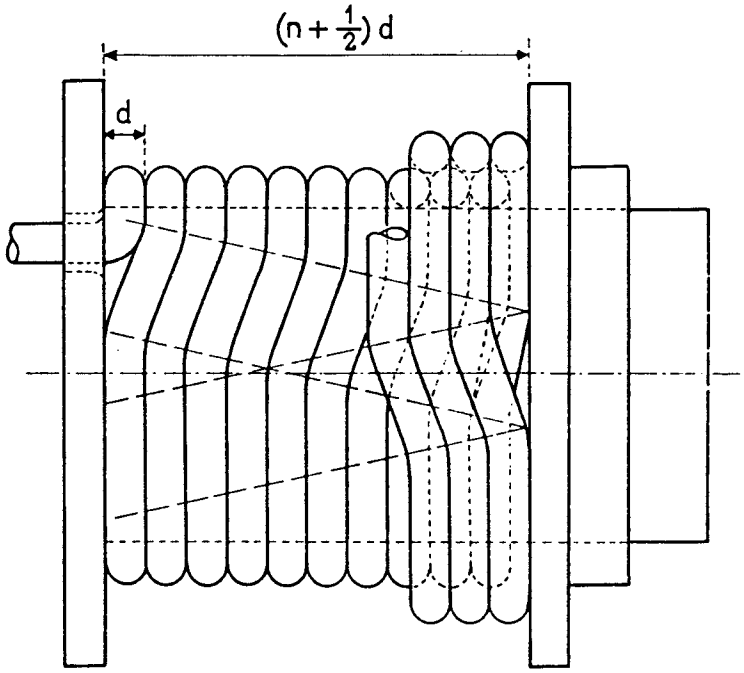

Figure A5 Orthocyclic winding of coils. The turns of each layer lie in the grooves between the turns of the previous layer (in Zijlstra, 1967a; after Lenders, 1961).

It may be shown that for a given wire size and a constant average length of a turn, the achievable magnetomotance of a coil is unaffected by the number of turns or the length of the winding. This is reflected in equation [A7] for a circular coil cross-section:

$$(N\ I) = V/\ \rho_T\ \pi\ d_{avg} \qquad [A7]$$

where V is the applied voltage, ρ_T is the temperature

dependent specific resistance of the wire and d_{avg} is the mean diameter of the winding. As already suggested, heating effects, especially towards the innermost layers of the winding, can be considerable and adequate means of cooling have to be provided. The total energy input, after the field has become stable, is used to maintain the current at a constant value and this energy is dissipated as heat because of the ohmic resistance of the winding. Zijlstra (1967a) suggests that a current density of $3x10^6 A/m^2$ at room temperature, which is equivalent to about $2x10^5 W/m^3$, can be considered a safe design value at which cooling by natural convection is sufficient. In this design a value of $2.8x10^6 A/m^2$ has been used.

To estimate heating effects, under the assumption of heat dissipation by natural convection from the cylindrical coil surface only, a worst case situation was modeled. Transient heating effects were calculated using a conservation of energy equation (Roters, 1941; Bird et al., 1960). The volume fraction of copper in the coil and the surface heat-transfer coefficient (needed in the calculations) were assumed to be 85% (Roters, 1941; Zijlstra, 1967a) and 25W/m K respectively.

The radial temperature distribution in the coil at steady state is obtained using a 1-D shell balance approach where it is assumed that the surface temperature is equal to the temperature at steady-state (Bird et al., 1960).

However, the restrictive conditions above lead to a conservative estimate; in reality, additional heat transfer through the center of the coil into the pole piece will result in less severe heat build up at the inner-most layers of the windings; this will lower the steady-state temperature. To enhance this mode of heat transfer, the center of the coil bobbin can be made from copper and thermal contact between bobbin and pole piece maximized. A computer program has been written by the author which helps in the design of the coils.

A.1.5 DESIGN REALIZATION

The yoke consists of four round ferromagnetic iron rods which are bolted together to form a square frame (Figures A1 and A4). The pole pieces can slide in accurately machined and aligned bores in the two cross struts. Fixtures made from aluminum are bolted to the cross struts and the pole pieces are fitted in their partially threaded bore. This arrangement allows for adjustment of the gap width by turning the pole pieces while aluminium lock nuts maintain the positioning. Four aluminium forks, two for each coil, slide in recesses in the cross strut; these are connected to the coil bobbin. Secure fastening of the coils is

important since considerable attractive magnetic forces can occur between them. To minimize losses, care was taken to maximize contact at joint interfaces.

A.1.5.1 MATERIAL CONSIDERATIONS

The ferromagnetic material used for yoke and pole pieces must have high permeability and low coercivity and these properties are generally provided by magnetically soft materials. Internal stresses, introduced by cold working and machining, decrease softness and must therefore be minimized. Furthermore, the amount of non-magnetic inclusions must be kept as low as possible and inclusions of the size of the domain walls must be avoided altogether (Boll, 1979; Habermehl et al., 1985).

The increased coercivity found in ferromagnetic steels is linked to the increased number of Fe_3C pinning sites which result from an increased carbon content of the steel (Habermehl et al., 1985). These pinning sites impede the motion of the domain walls under the influence of a magnetic field and, furthermore, reduce the grain size.

Besides the choice of very pure raw material, a heat annealing process after final machining is almost always necessary to release internal stresses. By reaction with the annealing atmosphere, a number of impurities can also be

eliminated. Furthermore, finely divided particles can be coalesced to produce larger, less disturbing ones (Boll, 1979). In carrying out the annealing of soft magnetic materials annealing time, temperature and cooling conditions must be accurately controlled. Reducing, or at least non-oxidizing, atmospheres are necessary. Many materials undergo a metallurgical phase transition upon cooling and the cooling rate determines which structure is taken on by the material. It is therefore very important to chose the cooling rate so as to allow for the formation of the magnetically advantageous phase.

High purity iron is the best material for yoke and pole pieces for magnets designed to produce field strengths up to about 2T (M_s(Fe): 2.15T). If higher magnetic fields are desired, special iron-cobalt alloys have to be chosen for pole pieces and pole caps.

In the present work, cold drawn iron rod (0.01% carbon), produced by Connecticut Metals Inc., was selected for yoke and pole pieces. This material is processed with a critical strain to insure high uniformity in the grain structure and the easy axis of magnetization is parallel with the rod length axis. Several magnetic material properties are listed in Table A1. The final machined parts were subjected to heat annealing (1hr dwell at 800°C; cooling rate: 50°C/hr down to 600°C) in a reducing atmosphere of 95% nitrogen and 5% hydrogen.

Table A1 Magnetic properties of CMI-C cold drawn iron rod (1/2" diameter; annealed).

Magnetization [T]	H(max) [A/m]	Remanence [T]	Coercivity [A/m]
1.0	207	0.44	51
1.5	756	0.66	58

A.1.6 PERFORMANCE OF THE MAGNET

A.1.6.1 MAGNETIC FIELD STRENGTH AS A FUNCTION OF GAP WIDTH AND COIL CURRENT

The projected field strength of 0.2T, at the power constraints mentioned above, is achievable at gap widths below 35mm and not, as intended, below 50mm (Figure A6). A leakage flux about twice as big as anticipated is partly responsible for this. This result is obtained by comparing measured with calculated field values for 31.75mm diameter pole pieces. However, considering the strongly sheared magnetization curve (Figure A8 , discussed below), saturation effects must also occur in the yoke and pole

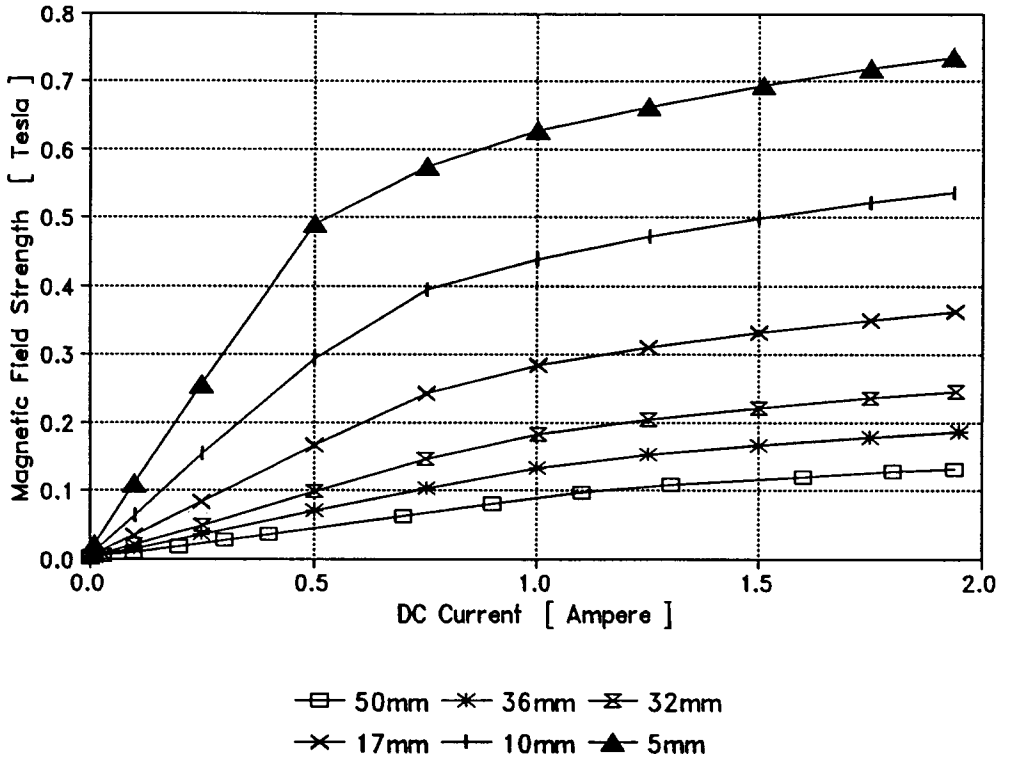

Figure A6 Measured magnetic field strength as a function of current and gapwidth (31.8mm pole piece diameter).

pieces. The use of overall larger dimensions and field focusing pole pieces would have yielded higher field values (Zijlstra, 1967a).

A.1.6.2 MEASURED MAGNETIZATION, HYSTERESIS AND APPARENT REMANENCE

The initial magnetization curve for a gap-width of 29.62 mm and 63.5 mm diameter pole caps (as used in the particle rotation experiments) is presented in Figure A7.

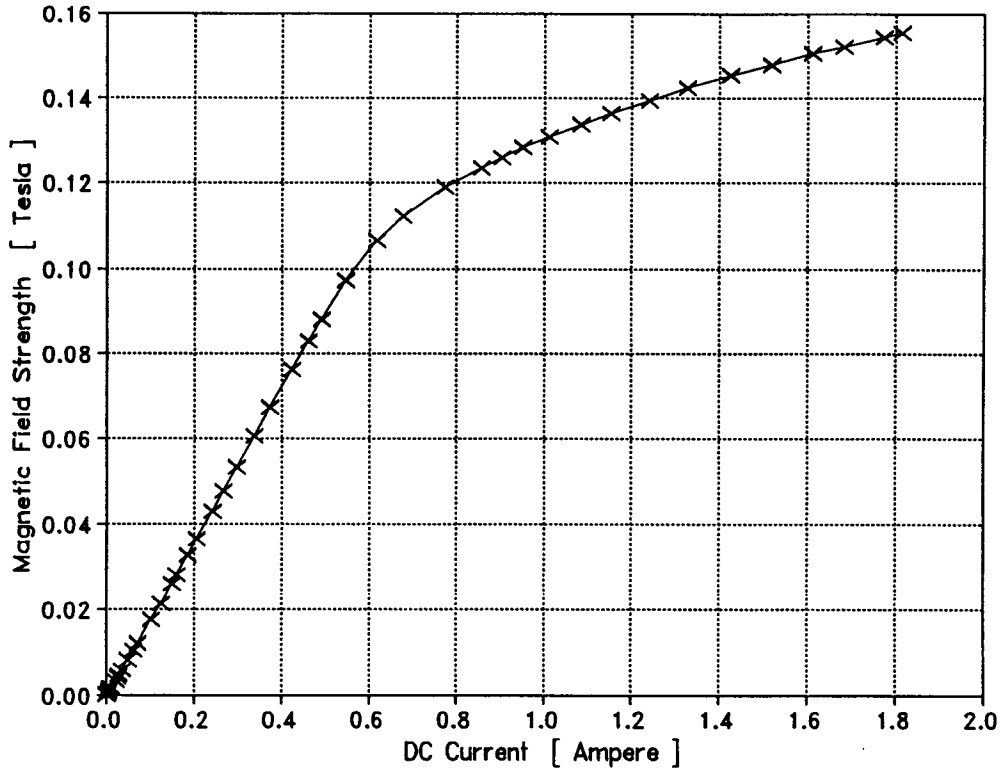

Figure A7 Magnetic field strength as a function of current; initial magnetization (29.6mm gap width; 63.5mm pole cap diameter).

The hysteresis loop in Figure A8 shows the typical shape found for sheared magnetic circuits. Shearing occurs in open magnetic circuits where sloping and flattening of the loop increases with increasing air gap. The coercivity is preserved but the remanence can change considerably (Boll, 1979). The width of the loop at the origin is indicative of the coercivity of the material.

The following data have been obtained by linear interpolation of data points in the descending branch of the hysteresis loop. To achieve zero remanent field strength a

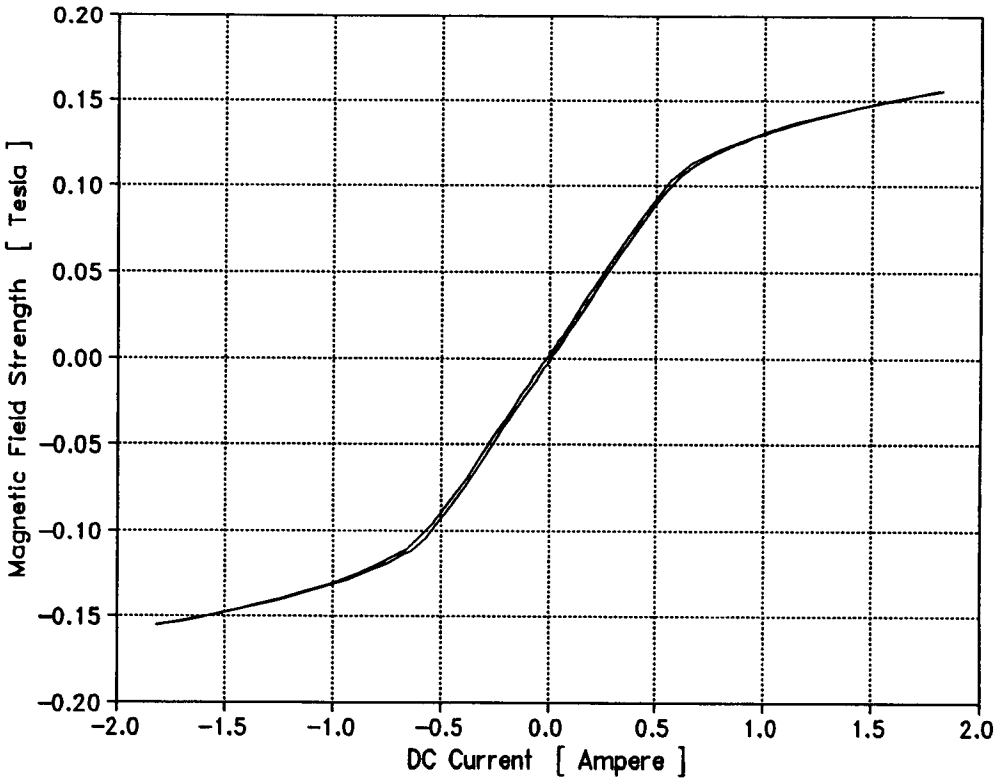

Figure A8 Magnetic field strength as a function of coil current; hysteresis loop (29.6mm gap width; 63.5mm pole cap diameter).

coil current of about -12mA is required. This translates, using the calculated number of turns and the average length per turn, to about 215A/m. A coercivity in this order of magnitude is considered small; however, the above value is about four times larger than that stated for the material at 1T excitation (Table A1).

The 63.5mm dia. pole caps, used to increase the field homogeneity, were not heat treated and this may account for the discrepancy. An apparent remanence, which is dependent

on the particular magnetic circuit and on the magnetic field strength of about $22*10^{-4}$T was found. Field strengths used in the experiments are about two orders of magnitude larger.

A.1.6.3 FIELD HOMOGENEITY

The original design with 31.75mm dia. pole pieces had a strongly inhomogeneous field. Figure A9 shows the percent change in field strength for two pole diameters as a function of distance from the center of the field at a gap width of 30.3mm. The upward sloping curves represent deviations in the axial direction, while downward sloping curves reflect changes in the transverse direction. The transverse field can be assumed to be rotationally symmetric and this has been confirmed through measurement; no difference in the location of the field center and the geometric center was found at a resolution of ±0.1mm.

Field homogeneity can be improved by increasing the ratio of pole-face diameter to gap width (Zijlstra, 1967a). In order to achieve this, two 63.5mm diameter pole caps were manufactured. These polished discs, made from the same material as pole pieces and yoke, are centered in aluminium rings which have a flange and a bore so that they slide exactly onto the 31.75mm pole pieces. The attractive magnetic forces which develop between pole piece and its

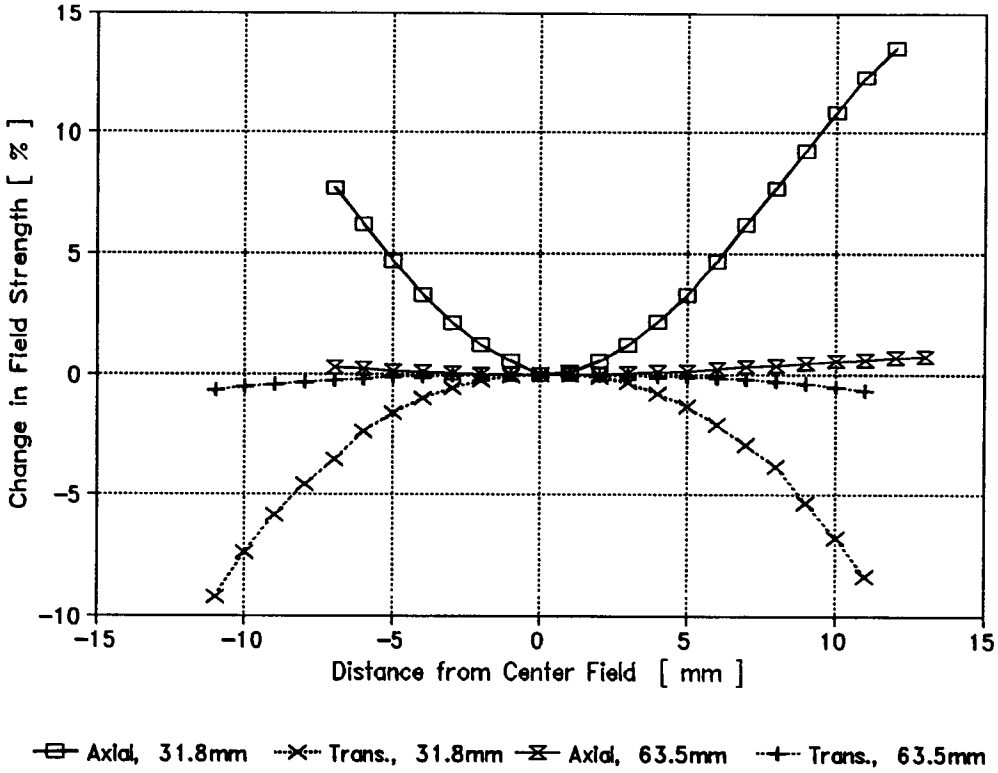

Figure A9 Change in magnetic field strength as a function of axial position and transverse position and pole diameter (relative to the field strength at geometric center).

pole cap, when the magnet is powered, insure intimate contact between the two. This approach of attachment has been chosen to avoid fasteners and machining of the previously annealed pole pieces.

The essentially flat curves in Figure A9 demonstrate the successful increase in field homogeneity achieved with the larger caps. Measurements at fields of 0.091 T and 0.019 T revealed no difference in the relative change of the field strength. In a rotationally symmetric volume of

$6.28*10^{-6}m^3$, centered in the gap, the largest relative change in the magnetic field is 0.55%, occurring in the middle of the cylindrical faces. However, the increased pole face area affected a loss in field strength; this is understood considering equation [A1].

A.1.6.4 COIL PERFORMANCE

Results for the projected coils and the actual manufactured coils are compared in Table A2.

Table A2 Coil performance (assuming 3.5% embedding and 7.5% layer loss).

	Design Calculation	Calculation for Manufactured Coil
Magnetomotance [A - Turns]	9756	9782
Resistance [Ohm]	14.51	Measured 15.92
Number of Turns [-]	4719	5192
Conductor Length [m]	1371.2	1504.6
Temperature Rise above Ambient [K]	42.4	40.6
Temperature Rise Time [hrs]	4.5	4.5

The measured resistance and the actual winding space are input to a program which calculates parameters of the manufactured coils. The calculation shows that about 9% more turns were obtained than originally anticipated. This result suggests that the factors used to account for embedding (+3.5%) and loss per layer (-7.5%) have been chosen conservatively in the design process. The magnetomotance is, however, little affected by this, which indicates that there is no difference in the ultimate performance of the designed and manufactured coil.

The calculated time of 4.5hrs for a temperature rise from ambient conditions to 98% of the steady state temperature is confirmed by experiment. However, the actual rise in temperature is about 35% less than that calculated; this is attributable to the additional heat transfer through the pole pieces which leads to a disadvantageous gap temperature increase.

A.2 POWER SUPPLY DESIGN

Many experiments require the magnetic field to be stable over an extended period of time. Field stability is mainly influenced by the current passing through the windings of the electromagnet. The power supply must therefore provide a stable output current and accommodate changes in output voltage due to the thermally induced changes in resistance of the windings. Batteries could perform this function but they are quite inconvenient to use (Bloom and Packard, 1955). High voltage, high current power supplies connected to the alternating-current mains are generally preferred.

A.2.1 DESIGN APPROACH AND REQUIREMENTS

Two different design strategies can be distinguished:

(1) High stability current regulation without feedback. This approach, well suited for short term stability, is generally simple, but requires good temperature stabilization of the supply. Magnet and power supply have no connection other than through the current leads.

(2) Current regulation with feedback from the magnetic field. For long term field stability, this approach is favored (Bloom and Packard, 1955). However, the feedback regulation can be subject to oscillation and requires a sensor in the magnetic field.

The supply must deliver 2A at 30V, which is necessary to achieve the stated magnetomotance (Table A2) and must have a current regulation better than 10ppm at coil currents larger than 1A.

A.2.2 DESIGN REALIZATION

For the present work a high stability supply without feedback has been constructed. It achieves current regulation by means of a LM138 5A adjustable power regulator. The current regulator design was based on application guidelines provided by the manufacturer (Anonym., 1971).

Because of the high degree of stability required, some unusual problems were encountered. In particular, thermal gradients within the instrument had to be kept to a minimum in order to retain stability of the reference voltage. Short wire lengths and heavy wire gages helped to reduce

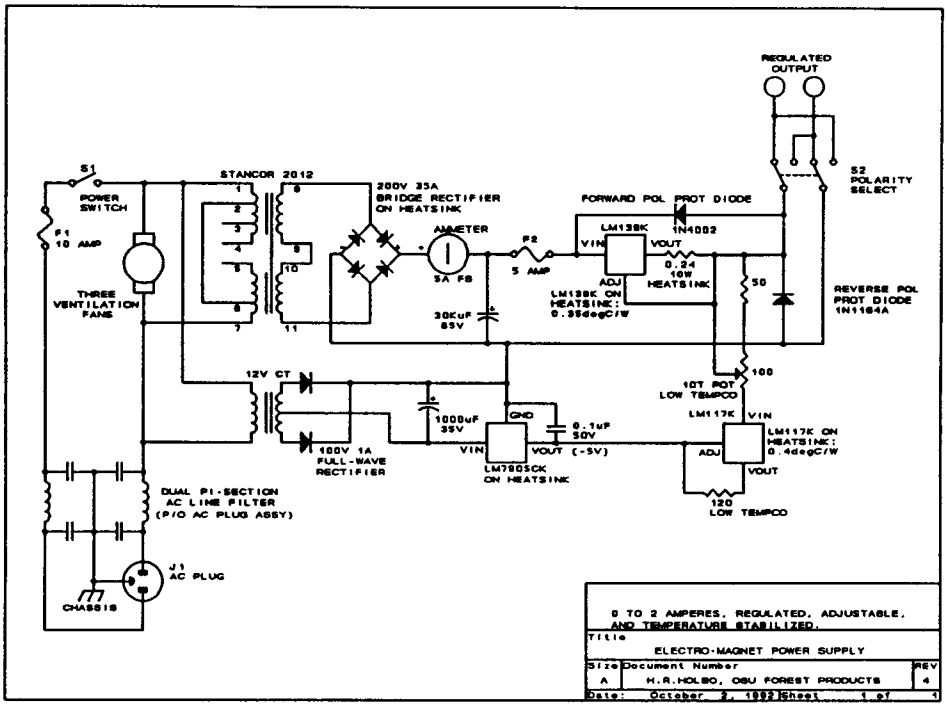

Figure A10 Schematic and parts composition for the high stability, constant current power supply.

lead drops. Single point grounding was used to diminish the risk of ground loops. The schematic and parts composition of the supply is presented in Figure A10.

Heatsink calculations for the regulator and supporting circuitry were made based upon estimated heat generation and thermal resistances. Thermal resistances of about 0.4°C/W were calculated for the heatsinks. To reduce these values further the complete supply was assembled in a fan ventilated enclosure where air flow over the heatsinks and constant air exchange were ensured. Stability of power regulation thus became dependent on the room temperature.

A.2.3 PERFORMANCE OF THE POWER SUPPLY

A.2.3.1 CURRENT REGULATION

(1) Short Term Stability

Over a period of several minutes the output current measurements with the supply set to deliver about 1A and 1.8A was monitored. During these tests current variability was $\pm 1*10^{-5}$A (the resolution limit of the meter) which suggests a stability of at least ±10ppm, ($1*10^{-5}$A/1.8A < $5.6*10^{-6}$).

(2) Long Term Stability

Measurements at about 1A over a period of 10 hrs revealed the current to be stable within ±90ppm, the resolution of the meter. No long term drift was observed. At 1A the power dissipation of the LM138 is higher than at 1.8A. In another test over a period of 7hrs at a current of about 1.8A, a drift of -560ppm was registered. It is more likely that this drift was due to a temperature change in the environment than due to self heating effects in the supply. These tests suggest that the supply's external environment is the limiting source of instability.

A.2.3.2 INFLUENCE OF POWER SUPPLY QUALITY ON MAGNETIC FIELD STABILITY

(1) Short Term Stability

The ±10ppm uncertainty in current regulation imposes a comparable limit upon the stability of the field at a current of 1A. This value was calculated using the linear regression equation established for the determination of the remanence (Section A.1.6.2). This equation links coil current with magnetic field strength. In the region were this equation is valid, the gradient of the hysteresis loop is largest and the instability estimate due to current changes is therefore conservative. Measurement of the field strength with a Hall probe determined a variation of about ±60ppm at 0.135T and 1.1A. This compares with the resolution limit of this method, which has been calculated by propagation of error.

(2) Long Term Field Stability

Over a period of 9 hrs the Hall voltage cycled in a regular fashion ±300ppm (0.135T, 1.1A). This can be explained if a cyclic temperature variation of the environment of ±0.7°C is assumed, considering that the Hall-sensor has a temperature coefficient of -0.1%/°C. The assumed temperature variation compares well with the actual cyclic temperature variation of about ±0.6°C. The short

term stability was again within the resolution limit of the Hall-effect measurement.

(3) Accuracy of Field Measurements

A propagation of error analysis for a field strength of 0.135T showed that the Hall-effect measurement had an accuracy of ±275ppm; this value does not include the non-linearity error estimated to be ±2% of the measurement. A comparison shows that this latter error is considerably larger than any uncertainty introduced by measurement (refer to Section 7.1).

A.3 CONCLUSIONS

An electromagnet and a constant current power supply have been designed and constructed. Although the desired field strength of 0.2T at 50mm gap width could not be achieved, the obtainable field strengths of 0.15T proved to be adequate for the fiber rotation experiments. Field homogeneity was improved by the addition of pole caps having a diameter larger than that of the pole pieces. Field homogeneity of ±0.5% over a volume of $6*10^{-6}m^3$ is considered to be excellent. Field stability over periods of minutes was high because of the very stable output current of the power supply.

APPENDIX B

DESIGN OF A SPRAY COATING SYSTEM

B.1 REQUIREMENTS FOR THE SPRAY COATING SYSTEM

(1) LC particles must remain separated throughout the coating process to avoid nonuniform treatment.

(2) System should allow spraying of other magnetic suspensions, for example PF resin modified with iron powder.

(3) Batch treatment should be possible for sample masses up to 15g.

B.2 DESIGN AND CONSTRUCTION

The underlying principle of the chosen approach is that of particle fluidization. Fluidization suggests suspension of particles where the suspension behaves like a dense fluid. A schematic of the system is presented in Figure B1, a photograph in Figure B2.

Fluidization is achieved by introducing a high velocity air stream in a rotating tank in which the particles are free to move about. This air stream creates a circulatory motion of the LC particles along the length axis of the

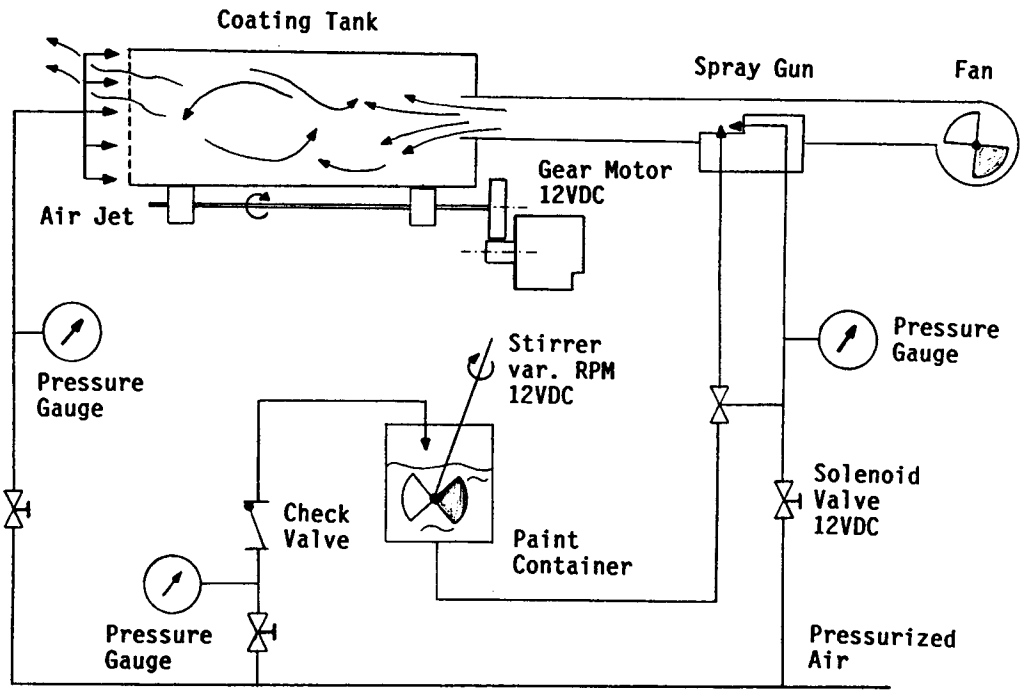

Figure B1 Schematic showing the spray coating system.

cylindrical tank. Excess air is vented through a fine wire screen which forms one end of the tank. Tank rotation about the stationary axial air jet is necessary to minimize particle build-up on the screen. A blower, attached to a pipe in opposite position to the air jet, creates enough airflow to prevent particles leaving the tank through that pipe. An external-mix, single action air spray gun is mounted in the pipe and introduces the ferromagnetic coating as a fine mist into the tank where it subsequently impinges on the LC-particles.

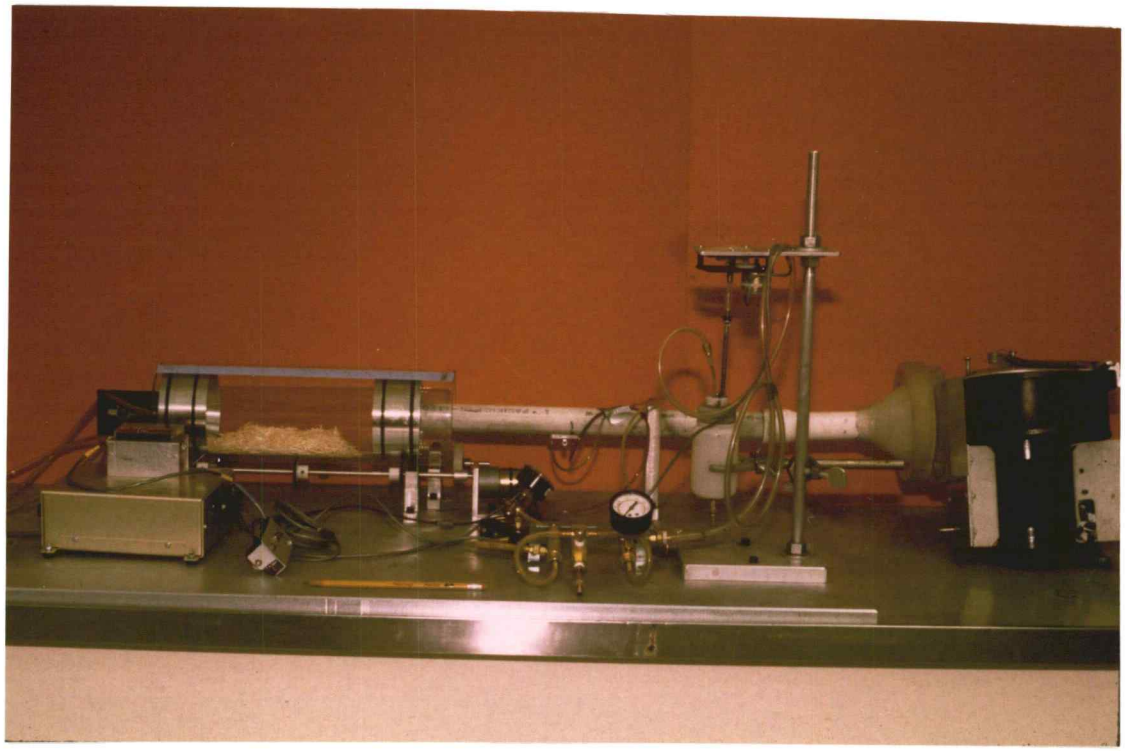

Figure B2 Photograph of the spray coating system.

The cylindrical tank, made from pyrex glass, has a length of 0.4m and a diameter of 0.1m; its volume is variable by moving the conic aluminium inserts. Rotation from 0 to 25RPM is achieved with a geared 12VDC motor and variable power supply. The contra-flow air jet is mounted in fixed position just in front of the fine wire screen and its air stream is distributed across the full diameter of this screen. Air pressures of up to 0.7MPa were used in the coating experiments. The blower delivers air velocities at 5 to 20m/sec, variable by its air-inlet aperture. The Ni-

coating is kept in a slightly pressurized container and is continuously stirred to avoid sedimentation. Air pressure at the spray gun and a slave valve in the feed line for the coating are both activated simultaneously by a solenoid pilot valve.

The main variable influencing the amount of coating injected is the period of time during which the spray gun is operating. Air pressures of 0.28MPa at the spray gun were used in the coating experiments. Figure B3 shows a photograph of the spray gun assembly built from parts of a commercial airbrush (Type: Badger Mod. 250).

B.3 PERFORMANCE

Two different types of wood particles were treated successfully: thermo-mechanical pulp (TMP), and the highly engineered wood strips used in the main experiments of the present work. It was found that with increasing particle size, tank volume, as well as sample mass, had to be reduced to assure fluidization. Batch masses of up to 15g TMP and 5g wood strips could be treated.

A suspension of Ni filamentary powder in an acrylic binder system (Electrodag® 440) was used in the present research. Variables influencing the spray mist (spray nozzle settings, air pressures, coating viscosity) were

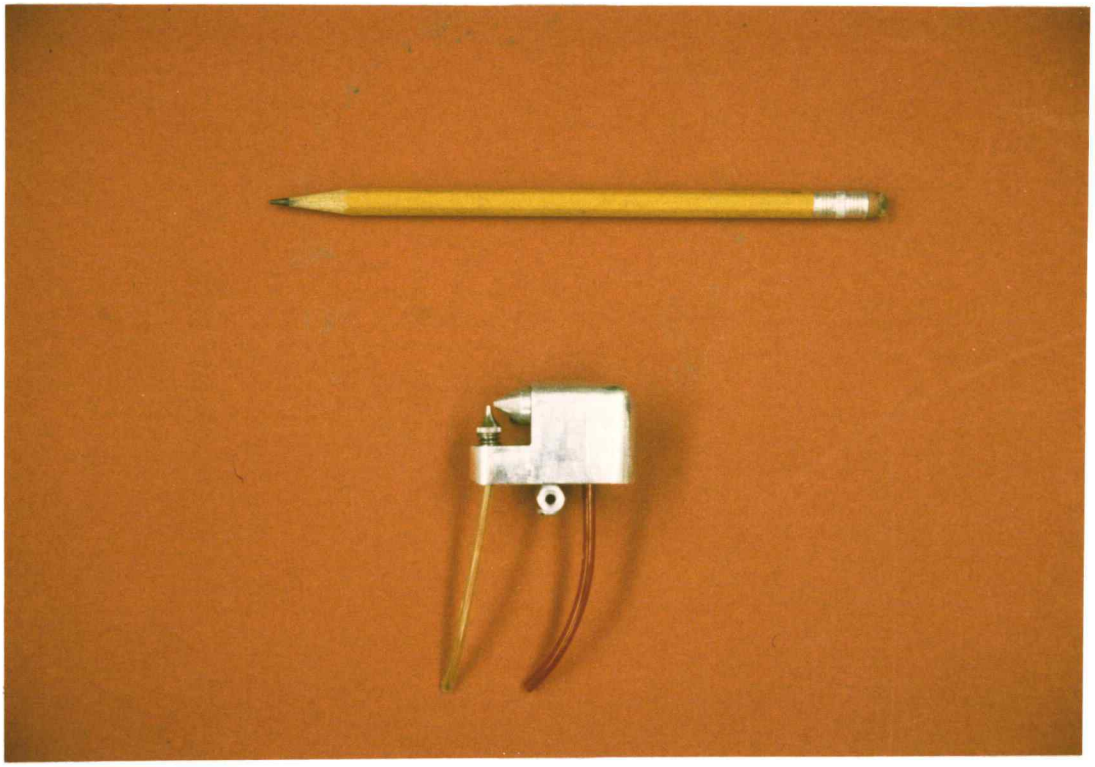

Figure B3 External mix, single action spray gun.

optimized experimentally to yield the finest spray mist possible and to avoid sputtering. Thinning of the coating in a 1/1 ratio by volume was necessary and resulted in a viscosity of about $45*10^{-3}$Pa sec.

Coating of wood particles is most probable while they are pinned to the wire screen because residence time there is much longer than at any other position in the tank. Experiments were conducted to investigate the dependency of spray mist intensity and consistency on position in the tank. It was found that a fanning effect results in more

even coating distribution further away from the pipe orifice. Even at the position farthest away from this orifice, dry spray was not noticed.

Intermittent operation of the spray gun results in dry out of the coating liquid at the gun. It was noticed that under such conditions, sputtering, as well as diminished coating volume, occurred. After treatment of several batches, cleaning of the spray gun was therefore usually necessary. A discussion of treatment uniformity and treatment levels may be found in the main body of this thesis (Section 9.1).